UNIVERSIDADE FEDERAL DE MINAS GERAIS
Instituto de Ciências Biológicas
Programa de Pós-Graduação em Fisiologia e Farmacologia

Thais Tunes Santos

INNOVATIVE FORMULATIONS CO-INCORPORATING AMPHOTERICIN B AND RETINOIC ACID IN LIPOSOMES FOR CUTANEOUS LEISHMANIASIS TREATMENT

Belo Horizonte
2025

Thais Tunes Santos

INNOVATIVE FORMULATIONS CO-INCORPORATING AMPHOTERICIN B AND RETINOIC ACID IN LIPOSOMES FOR CUTANEOUS LEISHMANIASIS TREATMENT

Thesis presented to the Postgraduate Program in Biological Sciences: Physiology and Pharmacology of the Biological Sciences Institute of the Federal University of Minas Gerais (UFMG) as a partial requirement for obtaining the Doctorate.

Field of concentration: Pharmacology

Supervisor: Frédéric Jean Georges Frézard, UFMG (Brazil)
Co-supervisor: Sébastien Pomel, UP-Saclay (France)
Co-supervisor: Marta Marques Gontijo de Aguiar, UFMG (Brazil)

Belo Horizonte
2025

043 Santos, Thais Tunes.
Innovative formulations co-incorporating amphotericin B and retinoic acid in liposomes for cutaneous leishmaniasis treatment [manuscrito] / Thais Tunes Santos. – 2025.
150 f. : il. ; 29,5 cm.

Orientador: Frédéric Jean Georges Frézard. Coorientadores: Sébastien Pomel; Marta Marques Gontijo de Aguiar.
Tese (doutorado) – Universidade Federal de Minas Gerais, Instituto de Ciências Biológicas. Programa de Pós-Graduação em Fisiologia e Farmacologia.

1. Farmacologia. 2. Anfotericina B. 3. Tretinoína. 4. Imunomodulação. 5. Leishmaniose Cutânea. 6. Farmacocinética. I. Frézard, Frédéric Jean Georges. II. Pomel, Sébastien. III. Aguiar, Marta Marques Gontijo de. IV. Universidade Federal de Minas Gerais. Instituto de Ciências Biológicas. V. Título.

CDU: 612:615

Ficha catalográfica elaborada pela bibliotecária Fabiane C M Reis – CRB 6 – 2680

UNIVERSIDADE FEDERAL DE MINAS GERAIS

ICB - COLEGIADO DE PÓS-GRADUAÇÃO EM FISIOLOGIA E FARMACOLOGIA - SECRETARIA

FOLHA DE APROVAÇÃO DA DEFESA DA TESE DE DOUTORADO

" INNOVATIVE FORMULATIONS CO-INCORPORATING AMPHOTERICIN B AND RETINOIC ACID IN LIPOSOMES FOR CUTANEOUS LEISHMANIASIS TREATMENT "

N° 400 DE THAIS TUNES SANTOS

ORIENTADOR: FRÉDÉRIC JEAN GEORGES FRÉZARD

Tese de Doutorado defendida e aprovada, no dia **27 de junho de 2025**, pela Banca Examinadora constituída pelos seguintes professores:

Profa. Dra. Eliana Martins Lima - UFG

Profa. Dra. Elaine Amaral Leite - FaFar/UFMG

Prof. Dr. Elias Fattal - UNIVERSITÉ PARIS-SACLAY

Dr. Rubens Lima do Monte Neto - CPqRR/FIOCRUZ-MG

Prof. Dr. Frédéric Jean Georges Frézard – Orientador - ICB/UFMG

Profa. Dra. Nadine Azas - INSTITUT HOSPITALO-UNIVERSITAIRE, AIX-MA

Profa. Dra. Marta Marques Gontijo de Aguiar – Coorientadora - FaFar/UFMG

Belo Horizonte, 27 de junho de 2025

Documento assinado eletronicamente por **Frederic Jean Georges Frezard**, **Professor do Magistério Superior**, em 10/07/2025, às 16:41, conforme horário oficial de Brasília, com fundamento no art. 5º do Decreto nº 10.543, de 13 de novembro de 2020.

Documento assinado eletronicamente por **Marta Marques Gontijo de Aguiar**, **Professora do Magistério Superior**, em 10/07/2025, às 17:48, conforme horário oficial de Brasília, com fundamento no art. 5º do Decreto nº 10.543, de 13 de novembro de 2020.

Documento assinado eletronicamente por **Elias Fattal**, **Usuário Externo**, em 23/07/2025, às 15:10, conforme horário oficial de Brasília, com fundamento no art. 5º do Decreto nº 10.543, de 13 de novembro de 2020.

Documento assinado eletronicamente por **Elaine Amaral Leite**, **Professora do Magistério Superior**, em 25/07/2025, às 08:02, conforme horário oficial de Brasília, com fundamento no art. 5º do Decreto nº 10.543, de 13 de novembro de 2020.

Documento assinado eletronicamente por **Rubens Lima do Monte Neto**, **Usuário Externo**, em 28/07/2025, às 09:22, conforme horário oficial de Brasília, com fundamento no art. 5º do Decreto nº 10.543, de 13 de novembro de 2020.

Documento assinado eletronicamente por **Eliana Martins Lima**, **Usuária Externa**, em 04/08/2025, às 10:26, conforme horário oficial de Brasília, com fundamento no art. 5º do Decreto nº 10.543, de 13 de novembro de 2020.

Documento assinado eletronicamente por **Nadine Anne Marie Azas**, **Usuário Externo**, em 03/09/2025, às 11:37, conforme horário oficial de Brasília, com fundamento no art. 5º do Decreto nº 10.543, de 13 de novembro de 2020.

A autenticidade deste documento pode ser conferida no site https://sei.ufmg.br/sei/controlador_externo.php?acao=documento_conferir&id_orgao_acesso_externo=0, informando o código verificador **4356447** e o código CRC **EE52BC0B**.

ACKNOWLEDGMENTS

I remember that, at my first enrollment in the PhD program, I thought four years would be long. Today, as the countdown to my defense begins, it feels like they have passed in the blink of an eye. Looking more closely, I realize that the PhD journey began even before my enrollment: it started as a small seed planted during my master's degree. First, by my mother, who always encouraged me to continue in research and who has been my most faithful supporter at every step of my life. This seed was also nurtured by people I deeply admire: Professor Lucas Ferreira, who during my master's encouraged me to pursue a Master 2 at Université Paris-Saclay, where I met Professor Philippe Loiseau, who, from our very first meeting, encouraged me to pursue a cotutelle PhD. Thank you so much, Lucas and Philippe, for believing in this journey even before I crossed the starting line. As I often say, by a coincidence of fate, they knew Professor Frédéric Frézard, who became my thesis supervisor in Brazil, and Sébastien Pomel, my supervisor in France — and they helped build the bridge that brought us together.

I want to thank Frédéric Frézard for his scientific contributions and the discussions — even late hours — for always responding patiently to my endless questions. Thank you for guiding me through these four years with understanding and attentiveness, with the politesse of a good French and the flexibility of an almost Brazilian. My sincere gratitude for your mentorship.

I am also grateful to Sébastien Pomel for his availability every time (and there were many) that I knocked on his door, for sharing his expertise in animal experiments, and for welcoming me into the laboratory during my time in France. Thank you so much for accepting to be part of this stage of my life.

This work also benefited greatly from the essential contribution of Professor Marta Aguiar, my co-supervisor. It has been almost six years since I have had the privilege of working under your guidance. Thank you for being so patient, always answering my questions, and offering a second look at my many formulation vials whenever I doubted what my eyes were seeing. Thank you for your assistance with the *in vivo* studies and for teaching me to see the glass half full. Thank you so much for trusting and supporting me throughout the PhD journey.

I also thank the Federal University of Minas Gerais and Université Paris-Saclay for the opportunity and infrastructure provided during this work. I am grateful for the funding support from CNPq, CAPES, and COST Action OneHealthDrugs. I am deeply aware that each line written here was made possible by the Brazilian and French citizens who sustain public universities and fund scientific research.

Over these four years, I had the opportunity to work in three different laboratories. I want to thank the LabNano, LTF, and BioCIS teams for the moments we shared — whether at the lab bench or over a coffee. Special thanks to my colleagues and friends: Ana Carolina, Carol, Gabriel, Jaqueline, Larissa, Letícia, Luiza, Lukas, Makiath, Mathew, Sabrina, Thais Cristina, Thais Mendes, and to the technicians Ernani, Marie-Nadine, and Nazaré.

This journey was lighter and brighter thanks to friends who were shoulders to lean on and true support. A heartfelt thank you to my friend and housemate Paty; to the friends I have carried with me since CEFET — Bella, Bina, Carol, Emília, Jojo, and Mara — and to the friends that France gifted me: Déborah, Erick, Ícaro, Marco, Marília, and Tiago.

I thank my uncles, aunts, and cousins, who always cheered me on, even while wondering how someone could study for so many years. A special thanks to my cousins Rafa and May for countless life conversations and to my dear cousins Gabriel, Gui, João, and Rafael.

I would also like to thank my fiancé Elvys, who has been present all these years — offering comfort at the end of exhausting days, preparing meals on the (many) days I was completely swamped, helping with some Excel tools, or simply being there. Thank you for being a steady support, with lightness and affection. I also thank your family for their constant encouragement and support.

I am grateful to my sister Amanda, who will always be my little one. Thank you for being sweet and strong in the right measure, for your comforting gestures, and for teaching me the importance of hugs. I also thank my brother Rodolfo for being present even from afar, sharing his entrepreneurial vision of life, and supporting me at every step.

To my grandparents — Eunice and Nuno, Nerilda and Milton — my heartfelt thanks for being the foundation of our family and the warmth of my childhood.

I want to end these acknowledgments with my beginning: my parents, Renata and Hilton. Thank you so much, Mom, for supporting my choices, for the love you expressed through lunches and homemade treats, for checking in with me every day, and for asking if everything was alright if I was drinking enough water or had taken a jacket. Thank you for reminding me that I am always loved and supported and for being an example of a strong, inspiring woman. I also thank my father. I am sure you would smile broadly today, celebrating my achievement as if it were yours. I love you both with all my heart.

My deepest gratitude goes to everyone I mentioned here and those who may have slipped my memory but who contributed to this work somehow.

Doing a thesis is truly a journey. We seek answers, but, in the end, we find many more questions. I am grateful to divine providence for allowing me to reach this point and continuing to guide my path!

"The important thing is to not stop questioning. Curiosity has its own reason for existing. One cannot help but be in awe when he contemplates the mysteries of eternity, of life, of the marvelous structure of reality. It is enough if one tries merely to comprehend a little of this mystery each day".

(Albert Einstein)

COLLABORATIONS

This work was supported by collaborators who contributed directly or indirectly through valuable technical and intellectual insights. This thesis, initiated four years ago, was brought to fruition through the combined expertise of teams in Brazil and France. For this reason, I would like to give special thanks to:

ACTAGen Platform (especially Claudine Deloménie and Pauline Tran), for their support in parasite load evaluation in the *L. major* infection model;

AnimEx Platform (particularly Ayma Aziza, Julie Burlot and Valérie Domergue), for their contribution to animal experimentation and for their kindness in helping whenever necessary;

Celso Martins Queiroz-Junior, for the careful histopathological evaluation of the kidneys following mice treatment;

Doumet Georges Helou, for kindly sharing his expertise and assisting with cytokine analysis from the liver;

Eduardo Burgarelli Lages, for his willingness to help whenever necessary, his assistance in validating the chromatography method (HPLC/DAD), and for his technical insights and enriching discussions—whether at the lab bench or over a coffee;

François-Xavier Legrand, for his availability and for making it possible to prepare the formulations at Institut Galien Paris-Saclay;

Leandro Gonzaga De Oliveira and Tiago Nery Queiroga Ricotta, for conducting the cytokine analysis from the spleen and generously sharing their knowledge;

Pierre Chaminade and Sonia Abreu, for their valuable insights into method validation using Liquid Chromatography coupled with Mass Spectrometry (LC/MS), as well as for their patience, kindness, and availability during my learning of this technique;

Raquel Martins de Almeida, for kindly providing us with the hamsters infected with *L. amazonensis*;

SAMM Platform (in particular Audrey Solgadi and Bastien Prost), for generously sharing their knowledge of the Orbitrap Exploris 120 and mass spectrometry;

Virgínia Vallejos, for performing parasite load evaluation in the *L. amazonensis* infection model and Guilherme Ramos, for previous knowledge in the preparation of liposomal formulations carrying AmB.

RESUMO

A leishmaniose é uma doença negligenciada que atinge principalmente as populações vulneráveis e imunodeprimidas, resultando em importantes desafios terapêuticos. A doença é causada por diferentes espécies de *Leishmania*, sendo observadas duas formas clínicas principais: cutânea (LC) e visceral (LV). Em 2022, 205.986 casos de LC e 12.842 casos de LV foram registrados, ressaltando a necessidade urgente de estratégias terapêuticas eficazes. A Anfotericina B (AmB), um dos agentes antileishmania mais potentes, apresenta limitações como baixa solubilidade, tendência à autoagregação e alta toxicidade. Embora a AmB lipossomal (AmBisome®) apresente um perfil melhor, ela é cara e menos eficaz nas formas complicadas da doença. Este trabalho estudou a quimioterapia clássica (AmB) combinada a um imunomodulador com o objetivo de superar essa limitação. O ácido retinoico todo-trans (RA) parece promissor, pois estudos recentes demonstraram efeitos tanto imunomoduladores quanto antileishmania. Mais especificamente, os objetivos desta tese foram: (i) desenvolver e caracterizar um lipossoma rígido PEGuilado para tratamento parenteral (LAmB-RA), assim como um lipossoma deformável (DLAmB-RA) para aplicação tópica; (ii) avaliar a estabilidade das formulações; (iii) estudar a atividade hemolítica *in vitro* do LAmB-RA; (iv) realizar um estudo farmacocinético do LAmB-RA em camundongos; e (v) avaliar a eficácia do LAmB-RA em modelos murinos de LC. Os lipossomas rígidos foram preparados seguindo um método simples e inovador permitindo a coencapsulação dos dois fármacos, explorando sua solubilidade dependente do pH e o efeito da temperatura sobre a fluidez da membrana. Enquanto o RA e a AmB são muito solúveis em meio alcalino, sua solubilidade diminui em pH neutro, o que favorece sua incorporação na membrana lipossomal. O LAmB-RA apresentou um diâmetro hidrodinâmico de 123,3 ± 6,5 nm e um índice de polidispersão (PdI) baixo de 0,11 ± 0,02, adequado para administração parenteral. Com uma taxa de encapsulação elevada de 97,1 ± 4,4 % para a AmB e de 94,7 ± 5,2 % para o RA, o LAmB-RA manteve-se estável em solução por 30 dias a 4 ºC. Essa formulação demonstrou uma atividade hemolítica reduzida em comparação com a formulação comercial Anforicin B® ($p < 0,0001$). A análise farmacocinética por LC-MS revelou concentrações plasmáticas mais elevadas e prolongadas da AmB a partir da formulação PEGuilada LAmB-RA, em comparação com o AmBisome® (lipossoma convencional), o que provavelmente contribuiu para a eficácia significativa do LAmB-RA em modelos murinos de infecção por *L. major* e *L. amazonensis*. No modelo utilizando *L. major*, o LAmB-RA reduziu o crescimento das lesões (−1,1 ± 2,1 mm contra 3,5 ± 1,4 mm) e a carga parasitária em relação ao grupo controle ($p < 0,05$). No modelo empregando *L. amazonensis*, o LAmB-RA reduziu o crescimento das lesões (1,1 ± 0,7 mm) em comparação aos grupos não tratados (3,3 ± 1,4 mm) e tratados com AmBisome® (2,5 ± 0,8 mm), bem como a carga parasitária esplênica ($p < 0,05$). Um aumento na razão IFN-γ/IL-10 também foi observado na cultura de esplenócitos estimulada com antígenos de *Leishmania*, indicando uma resposta imune favorável. O DLAmB-RA, por sua vez, foi formulado solubilizando o RA em etanol e a AmB em desoxicolato de sódio, tensoativo utilizado para formar vesículas deformáveis. Este lipossoma apresentou tamanho de 101,4 ± 1,3 nm, um PdI de 0,20 ± 0,01, com eficiência de encapsulação superior a 90 % para a AmB e para o RA, além de estabilidade por pelo menos 20 dias a 25 °C. Esses resultados apoiam o potencial das formulações LAmB-RA e DLAmB-RA como abordagens terapêuticas promissoras contra a LC, e justificam estudos complementares.

Palavras-chave: anfotericina B; ácido retinoico; imunomodulação; leishmaniose cutânea; farmacocinética; eficácia pré-clínica.

ABSTRACT

Leishmaniasis is a neglected disease that primarily affects socially vulnerable populations and immunocompromised individuals, posing significant treatment challenges. This disease is caused by different species of *Leishmania*, leading to two primary clinical forms: cutaneous (CL) and visceral (VL). In 2022 alone, 205,986 new CL cases and 12,842 new VL cases were reported, highlighting the urgent need for effective treatment strategies. Amphotericin B (AmB), one of the most potent antileishmanial drugs, faces obstacles such as low solubility, self-aggregation, and high toxicity. Although the liposomal AmB (AmBisome®) presents an improved profile, it is expensive, and its efficacy remains limited in complicated disease cases. This work investigated the classical chemotherapy (AmB) combined with an immunomodulator to address this limitation. All-trans-retinoic acid (RA) appears promising in this context, as recent studies showed both immunomodulatory and antileishmanial effects. Thus, this thesis aimed to evaluate an innovative approach based on liposomal formulations co-incorporating AmB and RA. The specific objectives were to (i) develop and characterize a rigid PEGylated liposome for parenteral treatment (LAmB-RA) and a deformable liposome (DLAmB-RA) for topical application; (ii) evaluate the stability of AmB-RA formulations; (iii) investigate LAmB-RA hemolytic activity *in vitro*; (iv) perform a pharmacokinetic study of LAmB-RA in mice; and (v) assess LAmB-RA antileishmanial efficacy in murine models of CL. Rigid liposomes were prepared using a simple and innovative method to co-encapsulate both drugs, exploiting their pH-dependent solubilities and the effect of temperature on membrane fluidity. While RA and AmB are highly soluble in alkaline solutions, their solubility decreases at neutral pH, favoring their incorporation into the liposomal membrane. LAmB-RA formulation exhibited a hydrodynamic diameter of 123.3 ± 6.5 nm and a low polydispersity index (PdI) of 0.11 ± 0.02, making it suitable for parenteral administration. With a high encapsulation efficiency of 97.1 ± 4.4% for AmB and 94.7 ± 5.2% for RA, LAmB-RA remained stable in solution for 30 days at 4 ºC. Moreover, LAmB-RA demonstrated reduced hemolytic activity compared to the commercial formulation Anforicin B® (p <0.0001). Pharmacokinetic analysis by LC-MS showed greater and more prolonged plasma concentrations of AmB from the PEGylated LAmB-RA formulation compared to AmBisome® (conventional liposome). These pharmacokinetic improvements likely contributed to the significant efficacy of LAmB-RA in murine models of *L. major* and *L. amazonensis* infections. In the *L. major* model, LAmB-RA treatment significantly reduced lesion growth (-1.1 ± 2.1 mm versus 3.5 ± 1.4 mm) and parasite load compared to the Control group (p < 0.05). In the *L. amazonensis* model, LAmB-RA significantly reduced lesion growth (1.1 ± 0.7 mm) compared to both untreated (3.3 ± 1.4 mm) and AmBisome®-treated groups (2.5 ± 0.8 mm), as well as the parasite burden in the spleen (p < 0.05). Additionally, LAmB-RA treatment enhanced the IFN-γ/IL-10 ratio in splenocyte cultures stimulated with *Leishmania* antigens, indicating a favorable immunomodulatory response. DLAmB-RA, in turn, was achieved by RA solubilization in ethanol and AmB solubilization in sodium deoxycholate, surfactant used to obtain deformable vesicles. This liposome showed a vesicle size of 101.4 ± 1.3 nm, a PdI of 0.20 ± 0.01, and encapsulation efficiency higher than 90% for both AmB and RA, being stable at least 20 days at 25 ºC. These findings support LAmB-RA and DLAmB-RA as promising alternatives for CL treatment, warranting further investigations.

Keywords: amphotericin B; retinoic acid; immunomodulation; cutaneous leishmaniasis; pharmacokinetics; preclinical efficacy.

LIST OF FIGURES

LIST OF TABLES

LIST OF ABBREVIATIONS

ADHs	Alcohol Dehydrogenases
ALDHs	Aldehyde Dehydrogenases
ALP	Alkaline Phosphatase
ALT	Alanine aminotransferase
AmB	Amphotericin B
ANOVA	Analysis of Variance
APL	Acute Promyelocytic Leukemia
ARAT	Acyl-CoA: Retinol Acyltransferase
AST	Aspartate aminotransferase
AUC	Areas under the concentration-time curve
BCO1	β-Carotene 15,15'-Oxygenase
BHA	Butylated Hydroxyanisole
BHT	Butylated Hydroxytoluene
BOD	Biochemical Oxygen Demand
CAC	Critical Aggregation Concentration
CD	Circular dichroism
CDCA	Chenodeoxycholic Acid
CHOL	Cholesterol
CL	Cutaneous leishmaniasis
ConA	Concanavalin A
CQAs	Critical Quality Attributes
DCL	Diffuse cutaneous leishmaniasis
DLAmB	Deformable liposome encapsulating AmB
DLAmB-RA	Deformable liposome co-delivering AmB and RA
DLEmpty	Deformable liposome without any drug
DLRA	Deformable liposome encapsulating RA
DLS	Dynamic light scattering
DMF	Dimethylformamide
DMPC	Dimyristoyl Phosphatidylcholine
DMSO	Dimethyl Sulfoxide
DNDi	Drugs for Neglected Diseases Initiative
DOC	Sodium Deoxycholate

DSPC	Distearoyl Phosphatidylcholine
DSPE-PEG2000	1,2-distearoyl-sn-glycero-3-phosphoethanolamine-N-[methoxy (polyethylene glycol)-2000]
DSPG	Distearoylphosphatidylglycerol
EA	Edge activator
EE(%)	Encapsulation efficiency
EMA	European Medicines Agency
EPR	Enhanced Permeability and Retention
FDA	Food and Drug Administration
G-CSF	Granulocyte colony-stimulation factor
H&E	Hematoxylin and eosin
HCD	High collision energy dissociation
HESI-II	Heated electrospray ion source
HIV	HIV (human immunodeficiency virus)
HPLC/DAD	High-performance liquid chromatography coupled to a diode array detector
HRQoL	Health-Related Quality of Life
HSPC	Hydrogenated soybean phosphatidylcholine
IFN-γ	Interferon-gamma
IL	Interleukin
IL	Intralesional
IM	Intramuscular
iNOS	Inducible Nitric Oxide Synthase
IP	Intraperitoneal
IS	Internal standard
IV	Intravenous injection
kDNA	Kinetoplast DNA
LAmB	Liposomes encapsulating AmB
LAmB-RA	Liposome co-delivering AmB and RA
LC-MS/MS	Liquid chromatography coupled with tandem mass spectrometry
LDL	Low-density lipoprotein
LEmpty	Liposomes without any drug
LRA	Liposomes encapsulating RA
LRAT	Lecithin: Retinol Acyltransferase

LS	Lesion size
LST	*Leishmania* skin test
MCL	Mucocutaneous leishmaniasis
MLV	Multilamellar Vesicle
Mo-DCs	Monocyte-Derived Dendritic Cells
MPS	Mononuclear phagocytic system
N-CoAs	Nuclear Co-Activators
N-CoRs	Nuclear Co-Repressors
NET	Neutrophil Extracellular Trap
NK	Natural Killer
NLC	Nanostructured Lipid Carrier
NO	Nitric Oxide
NPC1	Niemann-Pick Type C1
NPC2	Niemann-Pick Type C2
PAHO	Pan American Health Organization
PBS	Phosphate-buffered saline
PCR	Polymerase Chain Reaction
PdI	Polydispersity index
PKC	Protein Kinase C
PKDL	Post-Kala-Azar Dermal Leishmaniasis
PM	Paromomycin
PSG	Promastigote Secretory Gel
PVDF	Polyvinylidene fluoride
RA	All-Trans-Retinoic Acid
RAEs	Retinol Activity Equivalents
RALDHs	Retinaldehyde Dehydrogenases
RAR	Retinoic Acid Receptor
RBC	Red blood cells
RDA	Recommended Dietary Allowance
RDHs	Retinol Dehydrogenases
RE	Retinyl Ester
REHs	Retinyl Ester Hydrolases
ROS	Reactive Oxygen Species

RXR	Retinoid X Receptor
SC	Stratum Corneum
SD	Standard deviation
SEM	Standard error of the mean
SLA	Soluble *Leishmania* Antigen
SMT	Sterol 24-C-Methyltransferase
SSG	Sodium Stibogluconate
SUV	Small Unilamellar Vesicle
$t_1/2\alpha$	Early elimination phase half-life
$t_1/2\beta$	Terminal phase half-life
TACO	Tryptophan–aspartate-containing coat
TGF-β1	Transforming growth factor-β
Th1	T helper 1
Th2	T helper 2
TLR	Toll-Like Receptor
t-MS^2	Targeted-tandem mass spectrometry
TNF-α	Tumor necrosis factor-alpha
Tregs	Regulatory T cells
UV-Vis	Ultraviolet-visible
VAD	Vitamin A Deficiency
VL	Visceral leishmaniasis
WHO	World Health Organization
ZP	Zeta potential

CONTENTS

1. INTRODUCTION

Leishmaniasis represents a group of neglected tropical and subtropical diseases affecting socially vulnerable and unassisted populations. Different clinical manifestations depending on the *Leishmania* species and the host's immune status can be observed, with the most common clinical forms being cutaneous leishmaniasis (CL), usually manifested as skin ulcers, mainly on exposed parts of the body; mucocutaneous leishmaniasis (MCL) when mucous membranes are affected, primarily oropharyngeal; and visceral leishmaniasis (VL), the most severe form which is lethal in absence of treatment (Abu Ammar et al., 2019; PAHO/WHO, 2017).

The parasite is transmitted by phlebotomine sandflies during blood meal. Once introduced in the dermis, they can be lodged in the skin for CL and MCL or internal organs such as the liver, spleen, and bone marrow for VL. More than 20 species are already known to be infectious to humans (PAHO/WHO, 2017). In mammals, *Leishmania* is an intracellular parasite that resides inside immune cells, i.e., Mononuclear Phagocytic System (MPS) cells, especially in macrophages (Lipoldová & Demant, 2006).

In this sense, MPS cells can usually eliminate infectious agents, but the parasite *Leishmania* manages to circumvent the host cell's defense. The literature describes different mechanisms used by parasites, such as delaying the lysosome to the phagosome fusion, protection from lysis by the complement through the coating protein (lipophosphoglycan), and oxidative stress inhibition (Brasil, 2017; Rossi & Fasel, 2018). In this scenario, a competent immune system is essential for infection control. It has been proposed that a predominant cellular immune response with T helper 1 (Th1) characteristics involving CD4+ and CD8+ T lymphocytes, and cytokines such as interleukin (IL)-12, interferon-gamma (IFN-γ) and tumor necrosis factor-alpha (TNF-α), are necessary for a resolving response. This pro-inflammatory response activates macrophages, producing reactive oxygen and nitrogen species for parasite elimination (Brasil, 2017).

On the other hand, T helper 2 (Th2) responses, characterized by the production of anti-inflammatory cytokines such as IL-4 and IL10, are related to disease progression. However, there is a delicate balance between Th1/Th2 responses. Although the predominance of Th1-type responses is related to leishmaniasis control, its exacerbation has been associated with more severe symptoms. Therefore, introducing immunomodulators in leishmaniasis treatment could represent an interesting approach to influence this balance (Rossi & Fasel, 2018).

For more than 70 years, pentavalent antimonials (meglumine antimoniate, Glucantime®, and sodium stibogluconate, Pentostam®) have been the mainstay for leishmaniasis treatment despite their high cardiac, hepatic, and renal toxicity, as well as increasing resistance reports (Reguera et al., 2019). Patients can also be treated with amphotericin B (AmB) in deoxycholate or liposomal form, paromomycin (PM), pentamidine isethionate, or miltefosine (Brasil, 2017, 2020, 2024). It should be noted that these drugs have several limitations, such as toxicity, high cost, long treatment period, and the need for hospitalization (Abu Ammar et al., 2019; Gogulamudi et al., 2019). Furthermore, low efficacy was observed in certain complicated CL and VL cases, especially in immunocompromised patients (Guery et al., 2017; Mueller et al., 2007; Ritmeijer et al., 2011). For this reason, there has been an intense search for new treatment strategies in recent years.

One strategy has consisted of modifying the surface of liposomal AmB with 1,2-distearoyl-sn-glycero-3-phosphoethanolamine-N-[methoxy (polyethylene glycol)-2000] (DSPE-PEG_{2000}), allowing greater efficacy in a CL mouse model after parenteral and oral administrations (Ramos et al., 2022). Another recent strategy is the classical chemotherapy in association with an immunomodulator (Lanza et al., 2019; Thacker et al., 2020). In this context, retinoic acid (RA), a micronutrient obtained from retinol (vitamin A), seems promising. Recent studies evaluating vitamin D_3/RA and chenodeoxycholic acid/RA treatment combinations showed downregulation of the tryptophan–aspartate-containing coat (TACO) gene and parasite load reduction *in vitro* and *in vivo*. A marked Th2 immune response inhibition was also detected, with an increase in the Th1 response (Gogulamudi et al., 2015; Gogulamudi et al., 2019; Maciel et al., 2014; Verma et al., 2019). Moreover, vitamin A (RA precursor) deficiency has been reported in patients with leishmaniasis, suggesting an impact on the disease's clinical course (Luz et al., 2001).

In addition to an immunomodulatory effect, RA anti-leishmanial activity was reported *in vitro* (Prakash et al., 2022; Prakash & Kumar Rai, 2022; Prakash & Rai, 2022, 2023). RA has also been investigated for its potential to promote healing and stimulate fibroblast proliferation, with reduced skin reactions and irritation by encapsulation in nanosystems (Arantes et al., 2020).

Even though RA has a therapeutic interest, retinoids in their natural form are unstable and highly lipophilic (logP = 6.3), and have low bioavailability (Borges et al., 2021). To address these issues, nanocarriers can be used to improve RA physicochemical characteristics, protecting it from early degradation and favoring its delivery to target cells (MPS cells, particularly macrophages in the dermis). It is also worth highlighting that co-incorporating

different drugs within a single nanosystem can enhance treatment effectiveness through a synergistic effect while also helping to delay the development of drug resistance (Lanza et al., 2019).

From this perspective, while cross-sectional studies have reported that AmB alone is the most potent antileishmanial agent and that RA possesses both immunomodulatory and antileishmanial properties, this thesis introduces the innovative combination of these two drugs into a single formulation, leveraging their synergistic potential for a more effective CL therapy. Specifically, this research aims to (i) develop and characterize two AmB-RA formulations, using a rigid liposome for parenteral administration (LAmB-RA) and a deformable liposome (DLAmB-RA) for topical application; (ii) evaluate the stability of AmB-RA formulations under storage; (iii) investigate LAmB-RA hemolytic activity *in vitro*; (iv) perform a pharmacokinetic study of LAmB-RA in mice; and (v) assess LAmB-RA antileishmanial efficacy in murine models of New World and Old World CL.

2. THEORETICAL BACKGROUND

2.1. Leishmaniasis

2.1.1. *Etiology and epidemiology*

Neglected and tropical disease leishmaniasis is a public health problem in many developing countries. The World Health Organization (WHO) reported 205,986 new CL cases and 12,842 new VL cases in 2022. Many cases are misdiagnosed or not reported, underestimating the global burden (Ruiz-Postigo et al., 2023; Scorza et al., 2017). Leishmaniasis figures in the top 10 neglected tropical diseases, endemic in more than 90 countries, with more than 12 million people infected worldwide (PAHO/WHO, 2020).

It is believed that leishmaniasis has a long history, dating to 2,500 B.C., with early descriptions of the disease discovered in ancient texts and supported by recent molecular evidence from archaeological material (Akhoundi et al., 2016). The presence of leishmaniasis in the Americas also dates to ancient times, with the earliest evidence appearing between 400 and 900 A.D. in pottery from Peru, Ecuador, and Colombia, depicting nasal disfigurements similar to those caused by modern mucosal lesions. The parasite was identified in the early 20th century and named *Leishmania* in 1903. Subsequently, the various clinical forms of the disease became collectively known as leishmaniasis (PAHO, 2020).

In humans, infections range from asymptomatic to many clinical manifestations that can affect the skin, mucous membranes, and internal organs, depending on the parasite tropism, as seen in Table 1. Cutaneous forms are the most prevalent and are characterized by skin lesions. There may also be mucosal involvement, leading to MCL. VL, in turn, is less prevalent worldwide but can be fatal in untreated patients (PAHO, 2024).

These diseases are caused by more than 20 species of protozoa parasites belonging to the Trypanosomatidae family and *Leishmania* genus. Figure 1 shows *Leishmania* species grouped into the *Leishmania* and *Viannia* subgenera, but its classification continues to evolve. These subgenera were defined according to the site where the parasite is attached and develops in the vector's alimentary tract (pylorus). When parasite adheres and develops in the peripylarian region (behind), they belong to the *Viannia* subgenera; when it occurs in the suprapylarian (in front and the middle), they belong to the *Leishmania* subgenera (PAHO, 2020).

Table 1 – *Leishmania* species identified in humans and their tropisms in the Americas.

Subgenera			
Leishmania	***Leishmania***	***Viannia***	***Viannia***
Leishmania infantum[a]	*L. infantum* *L. mexicana* *L. pifanoia* *L. venezuelensis* *L. garnhami*[b] *L. amazonensis*	*L. braziliensis* *L. guyanensis* *L. panamensis* *L. shawi* *L. naiffi* *L. lainsoni* *L. lindenbergi* *L. peruviana* *L. colombiensis*[c]	*L. braziliensis* *L. panamensis* *L. guyanensis*
Tropism			
Visceral	**Cutaneous**	**Cutaneous**	**Mucosal**

Notes: [a] In the Region of the Americas, *L. chagasi* is the species that is also known as *L. infantum*; [b] The status of these species is under discussion; [c] The taxonomic position is under discussion. Source: WHO, 2010, *apud* PAHO, 2024.

Figure 1 – Taxonomy of the genus *Leishmania*

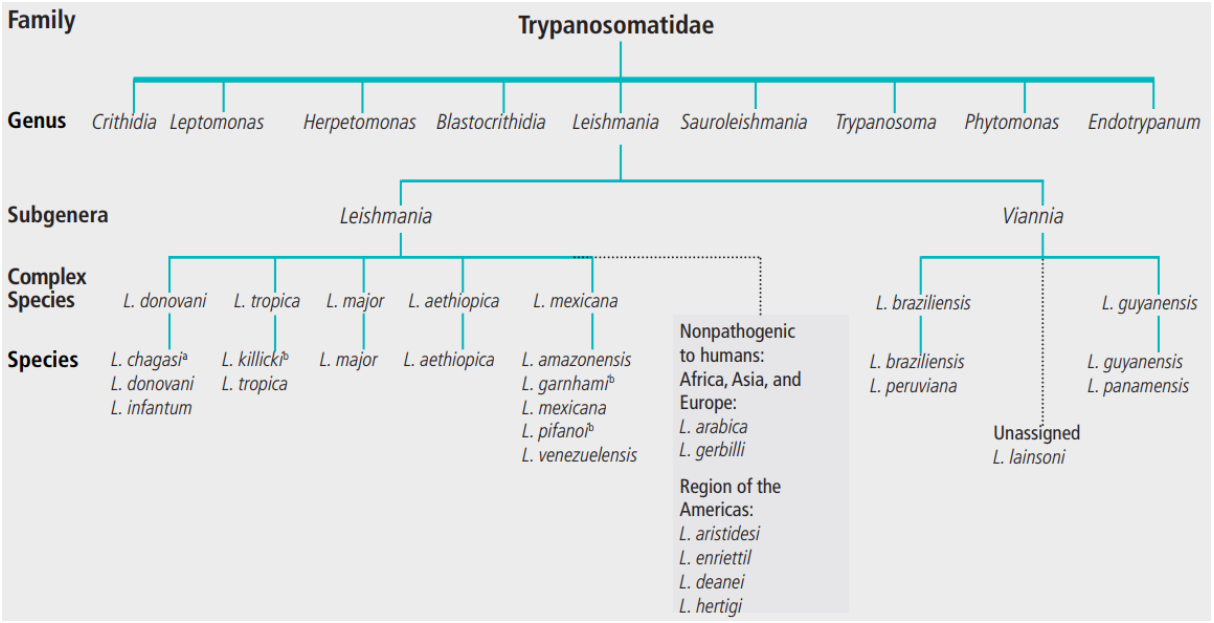

Notes: [a] In the Region of the Americas, *L. chagasi* is the species that is also known as *L. infantum*; [b] The status of these species is under discussion. Source: WHO, 2010, *apud* PAHO, 2024.

Leishmaniasis forms have been divided into New World and Old World depending on the geographical region where they are found. New World refers to Central and South America, where *Leishmania braziliensis*, *Leishmania guyanensis*, and *Leishmania mexicana* are the main species complex for CL. In the Old World, which includes Europe, Africa, Central Asia, and the Middle East, *Leishmania major* and *Leishmania tropica* are the main species complex. VL

is typically associated with the *Leishmania donovani* species complex in the New and Old World (Dorlo et al., 2012).

Besides the parasite species, other factors are linked with disease establishment, such as population displacement, poor housing, lack of financial resources, malnutrition, and a weak immune system. Most people who become infected with the parasite are asymptomatic during their lifetime. Only 10–25% of infected individuals will develop disease symptoms. Therefore, leishmaniasis refers to becoming sick due to a *Leishmani*a infection, not to being infected (WHO, 2020).

Human immunodeficiency virus (HIV) infection can also be considered a risk factor for developing a full-blown disease. Such patients usually present atypical clinical manifestations since the immunodepression caused by this virus facilitates parasite progression and vice versa. These patients have no defined clinical profile, but more serious or unusual clinical manifestations have been observed, like CL dissemination. In addition, patients with *Leishmania*-HIV coinfection have refractoriness to the usual chemotherapy regimens, high relapse and mortality rates. Coinfection has been reported in 45 countries, with a significant increase in recent years due to the geographical expansion of both diseases (Reguera et al., 2019; Roatt et al., 2020; WHO, 2025).

2.1.2. *Leishmania life cycle*

During the life cycle, parasites have two primary morphologies: promastigote, with a mobile flagellum that lives extracellularly within the phlebotomine digestive tract, or the amastigote form, without an apparent flagellum, living inside vertebrate-host MPS cells, mainly macrophages, as illustrated in Figure 2 (Brasil, 2017; PAHO, 2020). Depending on their species, *Leishmania* parasites are sustained in nature by different reservoirs, meaning domestic and sylvatic mammals, like marsupials, rodents, and primates, showing visible clinical signs or not (PAHO, 2024).

Figure 2 – *Leishmania* morphologies (a) promastigote (b) amastigote

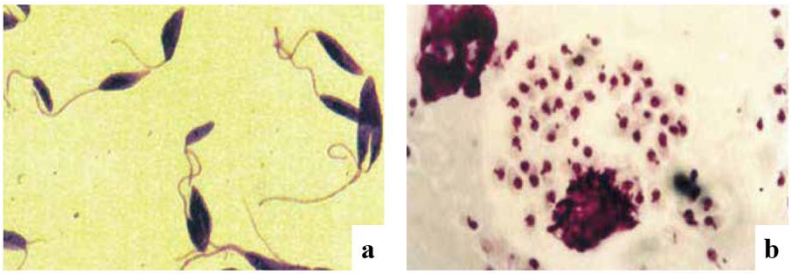

Source: Brasil (2017).

Leishmania is transmitted to mammals, including humans, by the bite of small insects called phlebotomine sandflies, also known as *mosquito palha*, *tatuquira*, *birigui*, and *chiclera*, among other names depending on the region (PAHO, 2024). These insects belong to the *Psychodidae* family, from the *Phlebotomus* genus in the Old World and *Lutzomyia* in the New World. Around 98 species of phlebotomine sandflies are found in *Leishmania* parasite transmission. Due to their hematophagous nature, females need blood for their egg development, infecting mammals during the blood meal (Volpedo et al., 2021; WHO, 2025).

As shown in Figure 3, the disease cycle starts when the insect introduces promastigotes parasites into the host's dermis and saliva, which have pro-inflammatory properties. After inoculation, *Leishmania* is phagocytosed by MPS cells, i.e., neutrophils, monocytes, dendritic cells, and macrophages (Lipoldová & Demant, 2006; PAHO, 2024). Once inside these cells, *Leishmania* lodges in the parasitophorous vacuole (phagolysosome), an organelle that derives from the phagosome fusion with the lysosome, then differentiate into amastigotes which multiply intracellularly, leading to cell rupture, new infections, and disease progression (Brasil, 2017; Lipoldová & Demant, 2006). The disease cycle continues when the insect bites an infected mammal and ingests macrophages parasitized by *Leishmania*.

In the insect vector, the parasite undergoes different transformations: parasite amastigotes are released in the anterior digestive tract of phlebotomine sandflies after macrophages rupture. In the phlebotomine gut, *Leishmania* differentiates back into promastigote flagellated forms. After this stage, the promastigotes settle in the vector esophagus and pharynx, adhering to the epithelium by the flagella. At this point, they differentiate into infective forms - metacyclic promastigotes, in a process known as metacyclogenesis (Brasil, 2017).

During metacyclogenesis, the parasites enter the stationary phase (they stop dividing) and become infective, undergoing biochemical changes that confer resistance to the host's immune response and a loss in the ability to adhere to the vector's intestinal epithelium. As a result, parasites migrate to the vector's proboscis (mouthpart) and become ready to be transmitted in the next phlebotomine blood meal (Brasil, 2017).

Figure 3 – Schematic representation of the leishmaniasis infection cycle

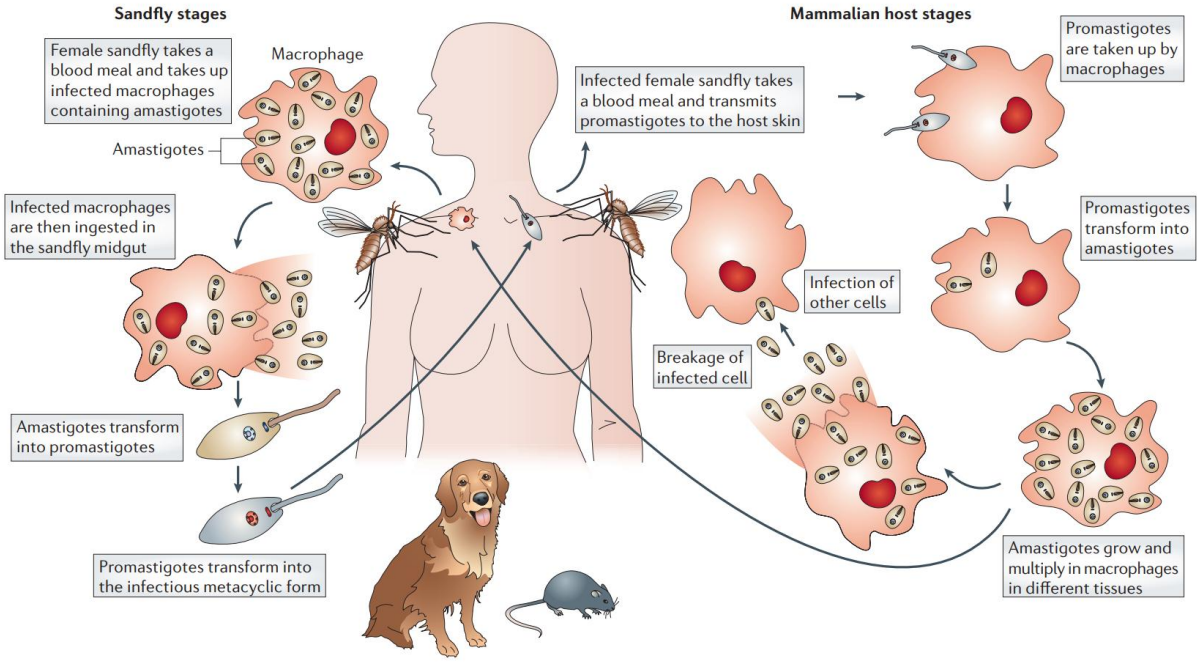

Source: Lipoldová & Demant (2006)

2.1.3. *Leishmaniasis diagnosis and prevention*

Early diagnosis and proper treatment are essential to avoid disease complications. Clinical signs suggestive of leishmaniasis in people from endemic areas must be combined with parasitological or serological tests. The parasitological analysis is helpful because it allows parasite visualization and remains the gold standard. In CL, skin scraping, aspirate, or biopsies can be used for direct detection using microscope visualization, parasite culture, histopathological analysis, and polymerase chain reaction (PCR). In MCL, direct detection can be performed by scraping mucous membranes or biopsies. Also, indirect detection via anti-*Leishmania* antibodies in serum using indirect immunofluorescence is an option for MCL diagnosis. In VL, an aspirate, preferably from the bone marrow, can be used for direct detection. Another option is the rapid diagnostic test (rK39-based), a serological test producing results in less than 30 minutes from patient serum or whole blood (PAHO, 2024; PAHO/WHO, 2020; WHO, 2025).

In addition to treating infected people, prevention strategies are essential. The strategies include avoiding outdoor activities from dusk to dawn; using mosquito nets, even in kennels; protective clothing and insect repellents; periodic cleaning of yards and grounds; and proper disposal of organic waste. In some regions, such as the Americas or the Mediterranean Basin, dogs are important VL reservoirs, so it is important to use insecticide-impregnated dog collars

and serological surveys in the canine population (PAHO/WHO, 2020). It is worth noting that the vector's resistance to the insecticides used to prevent the disease is a current concern. That is why the WHO conducted a multi-center laboratory study in 2020–2022 to determine discriminating concentrations of selected insecticides and published two guides for phlebotomine sandflies control programs (WHO, 2023a, 2023b).

Climatic models predict an increase in the geographical regions suitable for the survival of sandfly populations due to climate changes, especially warming temperatures. A gradual expansion of leishmaniasis across Europe into more northern regions and higher altitudes is observed (Paz, 2024). In addition, deforestation or human incursion into forest areas increases the contact with the vector (Reguera et al., 2019; WHO, 2025). Changes in the disease's global burden can be expected in the near future.

2.1.4. *Visceral leishmaniasis*

VL, known as kala-azar, is characterized by infection of MPS tissues (like liver, spleen, and bone marrow). Infected macrophage multiplication causes hepatosplenomegaly (enlargement of the liver and spleen) and systemic injury (PAHO, 2024). In addition to hepatosplenomegaly, the main symptoms are weight loss, severe anemia, fever, leucopenia, and thrombocytopenia (PAHO/WHO, 2020). The incubation period is usually two weeks to two months, affecting both sexes and mainly children under 5 years old (PAHO, 2024). A representative image of this clinical manifestation can be seen in Figure 4.

Figure 4 – Representative image of a child with VL, presenting hepatosplenomegaly and cutaneous pallor

Source: PAHO (2020).

If the patient receives no treatment within two years, the fatality rate can be as high as 100%, usually due to bacterial infections and/or bleeding (Brasil, 2014; WHO, 2025). Brazil, Ethiopia, Eritrea, India, Kenya, and Sudan account for 80% of VL cases globally. Considering only the Americas, Brazil accounts for 96% of cases, with an average of 3268 cases per year

from 2001–2020 (PAHO, 2024). It is important to note that Brazil has the highest case fatality rates, reaching 9.8% in 2022 (Ruiz-Postigo et al., 2023). Figure 5 shows VL endemicity worldwide in 2022.

In some regions, such as Africa, Asia, and Europe, man is a relevant reservoir for *L. donovani*. This is not the case in the Americas, where *L. infantum* is the causative VL species and leishmaniasis is a zoonosis, with dogs as the main reservoir in urban areas (PAHO, 2024).

Figure 5 – Status of endemicity of VL worldwide, 2022 (as reported by November 2023)

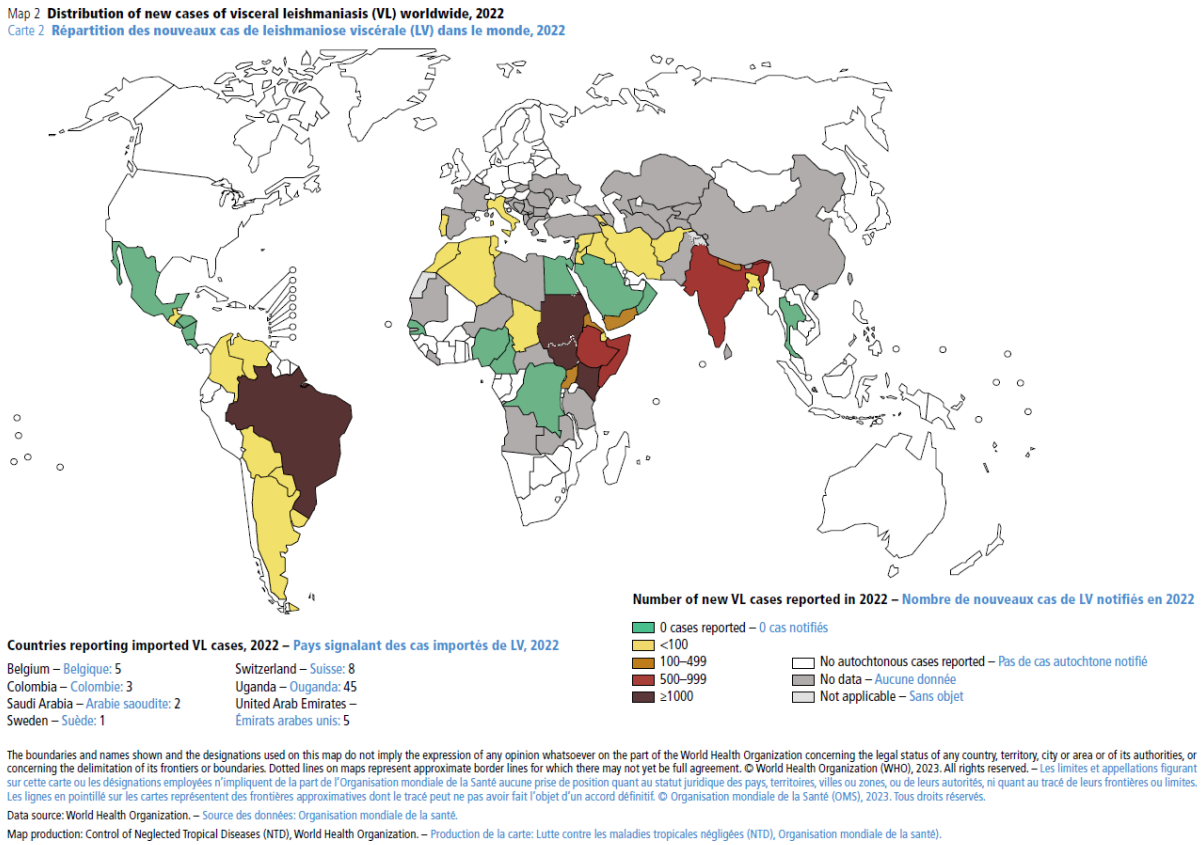

Source: Ruiz-Postigo et al., 2023.

After months or years of apparent VL cure, another clinical form of the disease known as Post-kala-azar Dermal Leishmaniasis (PKDL) can occur after *L. donovani* infection. PKDL is considered a complication of VL and is mainly seen in East Africa and Southeast Asia. However, it can also occur concomitantly or without VL history. The patient presents rashes in macules, papules, or nodules on the body (WHO, 2025). Mucous membrane involvement and lesion ulceration are uncommon, although they may occur. This manifestation in India and Sudan contributes to anthroponotic transmission (PAHO, 2020).

2.1.5. *Cutaneous leishmaniasis*

CL can occur in both sexes and all age groups, with an incubation period of two weeks to two months. Among the cutaneous forms, localized CL is the primary manifestation, characterized by unique or few cutaneous lesions, affecting exclusively the skin with a tendency to heal (Brasil, 2017; PAHO, 2024).

Classical lesions begin with parasites in the skin tissue, causing a chronic inflammatory reaction. This process causes edema and local induration due to cells and fluid extravasation from the blood vessels to the infection site. A macule initially appears at the bite location, which evolves into a papule. Then, it grows and develops into a nodule. Nodule formation is characterized by a dermal mass containing macrophages with abundant parasites and a lymphocytic infiltrate. This nodule grows in size and ulcerates due to necrosis at the center of the granulomatous reaction induced by the immune response (Brasil, 2017; PAHO, 2024).

Regional lymphadenopathy and nodular lymphangitis can also be observed since the parasites can invade the vessels and lymph nodes. Usually, lesions are rounded with raised margins, granular background, surrounding induration, and painlessness. Secondary infection with other microbial agents can occur, causing pain and, sometimes, purulent secretion (Brasil, 2017; PAHO, 2024). CL lesions usually appear in body-exposed areas, such as the face, arms, and legs. In many cases, they evolve to self-healing. However, resolution can take several months to years, resulting in a depressed, hypopigmented scar, which can lead to stigmatization (Scorza et al., 2017). The spontaneous cure rate in the Americas is low, making treatment even more necessary (Cota et al., 2016).

More complex manifestations include the disseminated form, mainly caused by *L. braziliensis* and characterized by the appearance of multiple papular and acneiform lesions affecting different body segments, with mucosal involvement in some cases and the recidiva cutis form, when new lesions are activated after the initial lesion heal (Brasil, 2017). An atypical CL has been described in some countries, such as Costa Rica, El Salvador, Honduras, Nicaragua, and Venezuela. The disease is caused by *L. infantum* and manifests with chronic circumscribed, non-ulcerated lesions (PAHO, 2024). Representative images of these clinical manifestations can be seen in Figure 6.

Figure 6 – Representative images of clinical manifestations: (a) Localized cutaneous leishmaniasis, (b) Disseminated cutaneous leishmaniasis, (c) Recidiva cutis, (d) Atypical cutaneous leishmaniasis

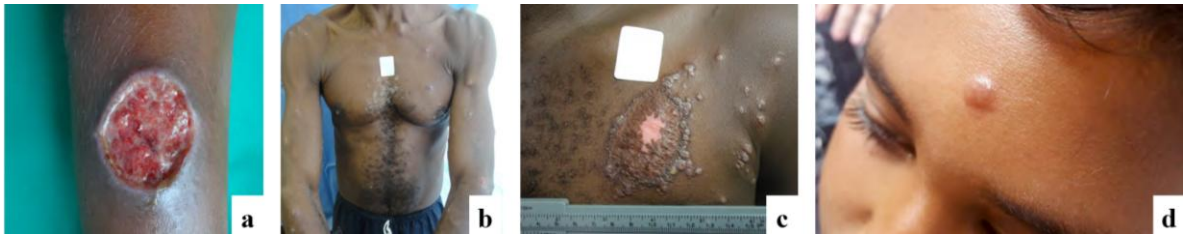

Source: Adapted from PAHO (2020).

CL can also evolve into one of the two more severe forms of the spectrum: the anergic pole, known as diffuse cutaneous leishmaniasis (DCL). In Brazil, DCL is associated exclusively with *L. amazonensis* infection, but *L. mexicana*, *L. venezuelensis*, *L. pifanoi*, and *L. braziliensis* can also cause it (PAHO, 2024). DCL manifestation leads to a lack of specific cellular response to the parasite's antigens, refractoriness, and relapses to treatment. In DCL, numerous parasite-rich lesions are observed. On the other hand, there is the hyperergic pole, MCL. MCL is characterized by an exacerbation of antileishmanial cellular responses, a shortage of parasites, and tissue destruction, with the primary etiological agent being *L. braziliensis* (Brasil, 2017; PAHO, 2024).

In most MCL cases, the disease is a consequence of metastasis through a hematogenous or lymphatic route from the skin lesion. More rarely, it can be an extension of skin lesions to contiguous mucosa or due to the direct vector bite on the mucous membrane. The most commonly affected site is the nasal septum. MCL cases mainly occur in the Americas, where Bolivia, Brazil, and Peru contribute the highest reports. Even though the immune response can contain parasite multiplication, relapses are usually frequent (Brasil, 2017; PAHO, 2024).

Representative images of these clinical manifestations can be seen in Figure 7. It should be noted that in all the manifestations mentioned, there is considerable tissue damage, severe impairment of the skin barrier, and the formation of an inflammatory infiltrate in the dermis, containing mainly macrophages, lymphocytes, neutrophils, and mast cells (Wijnant et al., 2018a).

CL infections have also been described in various species of wild animals, such as rodents, marsupials, edentates, and wild canids, which are considered hosts and possible natural reservoirs, depending on the *Leishmania* species considered. Infection records in domestic animals (canids, felids, and equids) are also high. However, no evidence proves their role as reservoirs for CL species (Brasil, 2017).

Figure 7 – Representative images of clinical manifestations: (a) Mucocutaneous leishmaniasis, (b) Diffuse cutaneous leishmaniasis

Source: Adapted from PAHO (2020).

It is worth noting that more than 80% of the new CL cases worldwide are reported in only seven countries (Afghanistan, Algeria, Brazil, Colombia, Iraq, Pakistan, and the Syrian Arab Republic). Of these, two countries are in the Americas, Brazil and Colombia. During the 2001–2020 period, 1 067 759 cases of CL and MCL were recorded, with an annual average of 53 387 cases in the Americas (PAHO, 2024). Figure 8 shows CL endemicity worldwide in 2022.

Figure 8 – Status of endemicity of CL worldwide, 2022 (as reported by November 2023)

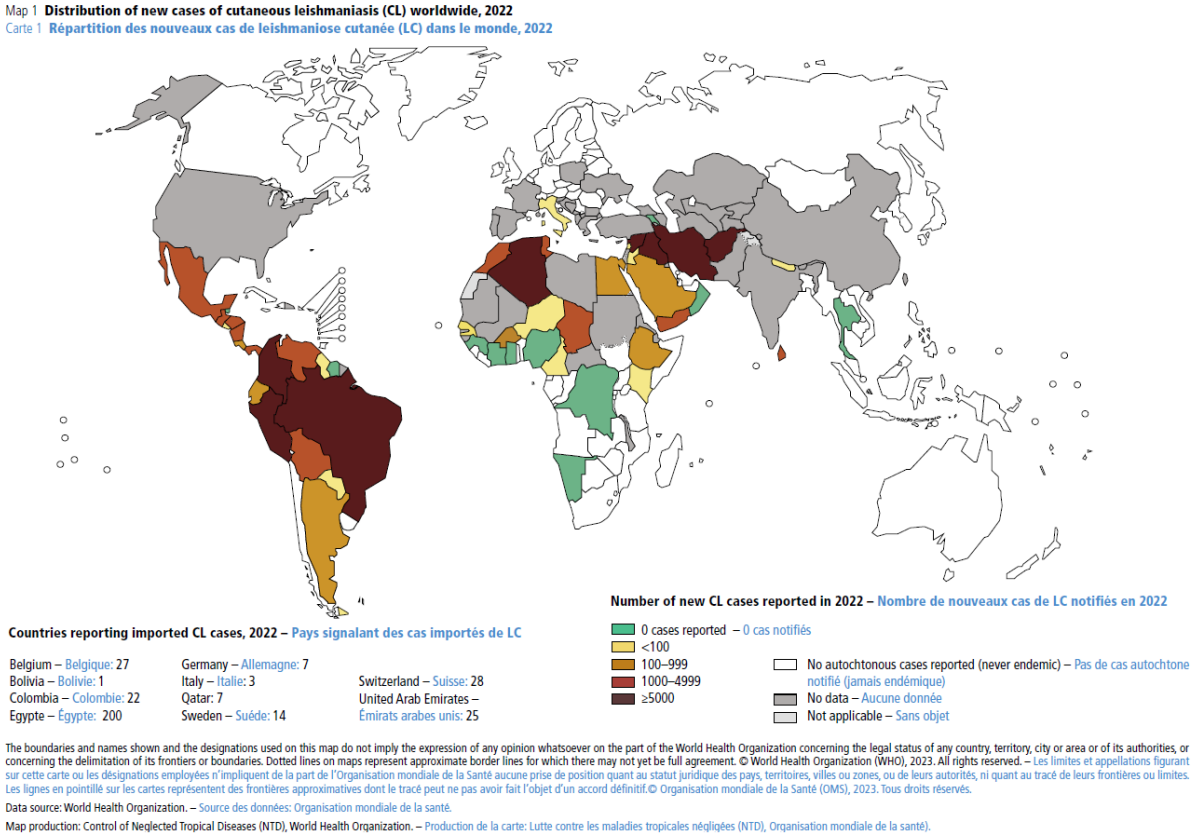

Source: Ruiz-Postigo et al., 2023.

CL impairs patients' quality of life regarding social relationships and self-esteem (Alvar et al., 2006). Recent studies in Ethiopia and Morocco confirm this disease's impact. In Ethiopia, 302 patients with active CL were evaluated. Patients diagnosed with DCL reported a lower health-related quality of life (HRQoL) than those with other forms. In addition, those with lesions on their head and neck regions and younger than 50 years (20-49 years age group) had significantly lower HRQoL. Notably, almost half of the participants reported markedly reduced HRQoL (Doni et al., 2023). In Morocco, 87 patients were evaluated, with 26.4% reporting a mild impact on HRQoL and 73.6% reporting a moderate impact (Ali et al., 2025). Significant social stigma and psychological distress can profoundly affect patients, confirming the need for affordable new treatments to improve outcomes.

2.2. Cutaneous and mucocutaneous leishmaniasis treatment

2.2.1. *Medicines in clinical use and limitations*

CL and MCL are difficult diseases to treat, especially since most drugs require parenteral administration, hospitalization, and close monitoring. Treatment is only indicated if the patient shows the clinical signs of the disease and must be adapted to the clinical form, with laboratory diagnosis support (Brasil, 2024).

The cure criterion for CL is clinical and is defined by the epithelialization of ulcerated lesions and inflammatory infiltrate regression. It is expected that complete epithelialization will occur within 90 days of completing the first treatment regimen (Brasil, 2017). Signs of infiltration and erythema should disappear within 6 months. However, it may not be accompanied by a sterile cure. Viable *Leishmania* or their DNA have been found in the scars of cured patients, even years after treatment, justifying late relapses and also disease resurgence in immunosuppressed patients (Brasil, 2017; Scorza et al., 2017). For MCL, regression of all clinical signs is the criterion for cure. This should be confirmed by ear, nose, and throat examination six months after treatment. The patient's clinical progress should be monitored for 12 months because, in therapeutic failure or relapse, a second treatment regimen must be implemented (Brasil, 2017, 2024).

It is important to note that no vaccine or prophylactic drug is available to prevent infection, and treatments are far from ideal (Reguera et al., 2019). Therapeutic options include pentavalent antimonials, miltefosine, pentamidine isethionate, PM, and AmB (conventional liposome or deoxycholate formulations). According to the Cochrane review, intramuscular meglumine antimoniate and oral miltefosine may offer improved therapeutic outcomes among

immunocompetent patients with CL and MCL in the Americas. However, the evidence quality is moderate to low (Pinart et al., 2020). The Cochrane review assessing interventions for Old World CL found the evidence inconclusive (Heras-Mosteiro et al., 2017).

Recently, Pan American Health Organization (PAHO) published the Guidelines for the Treatment of Leishmaniasis in the Americas, developed following the WHO Handbook for Guideline Development and the GRADE (Grading of Recommendations Assessment, Development, and Evaluation) methodology, which takes into account the quality of the evidence for each outcome (PAHO, 2022). The dosage for adult patients with CL described in this topic follows the recommendations in this guide and are summarized in Table 2.

The first treatment against leishmaniasis was with a trivalent antimonial (Sb^{3+}), introduced by Gaspar de Oliveira Vianna in 1913. Nowadays, pentavalent antimonials (Sb^{5+}) are commercialized as meglumine antimoniate (Glucantime®) and sodium stibogluconate (SSG, Pentostam®) and continue to be the treatment mainstay (PAHO, 2020; Reguera et al., 2019). They act as a prodrug, as Sb^{5+} is reduced in the body to their active form, Sb^{3+}, a metal ion with a high affinity for nitrogen- and sulfhydryl-containing compounds. Consequently, their mechanism of action is thought to result from interactions with endogenous parasite molecules, such as proteins and enzymes. Limitations are associated with high cardiac and hepatic toxicity and increasing resistance reports (Roatt et al., 2020).

Pentavalent antimonials administered intralesionally (IL) are strongly recommended for CL patients with 1 to 3 lesions up to 900 mm^2 and immunocompetent. It can be administered with 3–5 infiltrations of 1–5 mL per lesion. Its systemic administration is usually with 20 mg Sb^{5+}/kg/day for 10 to 20 days via intramuscular (IM) or intravenous (IV), having conditional recommendations with moderate to low evidence (Table 2) (PAHO, 2024). MCL patients, in turn, have strong recommendations to be treated with pentavalent antimonials, with or without oral pentoxifylline, for any species of *Leishmania*. The evidence is low to very low. Despite being used for a long time as Brazil's first line of leishmaniasis treatment, the product Glucantime® recently had its registration canceled and will no longer be marketed by Sanofi in Brazil (ANVISA, 2025).

Miltefosine is the only orally administered drug in the leishmaniasis treatment arsenal. It belongs to the alkylphosphocholine family and was initially developed for topical use in treating breast cancer cutaneous metastases. Its mechanism of action is still not completely clear. However, it is associated with parasite death through programed cell death, as it disrupts lipid metabolism in the parasite, affects membrane permeability, and interferes with cellular signaling (Brasil, 2020). Adult treatment with oral miltefosine is strongly recommended, with

low evidence. The treatment regimen consists of 2.5 mg/kg/day, administered 2 to 3 times per day, with a maximum dose of 150 mg/day (3 capsules/day) for 28 days (Table 2). The most common adverse effects are related to the gastrointestinal tract; however, miltefosine is teratogenic, requiring caution when prescribed to women of childbearing age (Brasil, 2020; PAHO, 2024). Additionally, its efficacy has declined over the past decade, and the number of relapses following treatment has increased (Dorlo et al., 2012; Roatt et al., 2020). Also, miltefosine is an expensive drug manufactured by a single laboratory. There is also no agreement with WHO to reduce the cost and favor its inclusion in public health programs (PAHO, 2022).

Pentamidines are primarily used to treat CL caused by *L. guyanensis*. The drug is available as pentamidine isethionate. It has conditional recommendations with moderate to low evidence. Pentamidine can be administered by IV route at 2 mg/kg/day, divided into 3–4 doses on alternate days, or IM route at 4–7 mg/kg/day, in 3 doses applied every 72 hours (Table 2). Its mechanism of action is not yet fully understood, but studies suggest it acts as an inhibitor of active substance transport and mitochondrial replication in the parasite (Bruni et al., 2017; PAHO, 2024). Severe adverse reactions include cardiac arrhythmias, leukopenia, thrombocytopenia, acute kidney failure, and toxic effects on pancreatic beta cells, which may lead to hypoglycemia during treatment and late-onset diabetes *mellitus* (Brasil, 2017).

PM is an aminoglycoside antibiotic used to treat intestinal infections such as amebiasis and cryptosporidiosis, rediscovered as an antileishmanial drug in the 1980s. It has been effectively used as an injectable treatment for VL and, with less consistent results, as a topical therapy for CL (Bruni et al., 2017; Dorlo et al., 2012). PM's exact mechanism of action in *Leishmania* remains unclear, but it is believed to target the protein synthesis machinery. The main adverse reactions reported are nephrotoxicity, ototoxicity, and hepatoxicity (Bruni et al., 2017). The current PM recommendation is a topical cream of 15% applied in the affected area for 20 days, with very low evidence (Table 2) (PAHO, 2022).

AmB, in turn, is the only drug used to treat *Leishmania*-infected pregnant women and is the first choice for patients co-infected with HIV or immunosuppressed individuals (PAHO, 2024). Since AmB is the focus of this study, its characteristics and properties will be discussed in more detail in section 2.2.1.1.

Table 2 – Recommendations for local and systemic treatment of cutaneous leishmaniasis in adult patients.

Local treatments for adult patients with cutaneous leishmaniasis

The criteria for indication of local treatment are: 1 to 3 lesions up to 900 mm² (largest diameter: 3 cm); lesions located in any area (except the head and periarticular regions); absence of immunosuppression; and possibility of follow-up.

Recommendations	Strength of the recommendation and certainty of the evidence	Route of administration	Treatment scheme
It is recommended to apply **intralesional pentavalent antimonials** in patients with localized cutaneous leishmaniasis caused by *L. braziliensis* or *L. amazonensis*.	**Strong** recommendation **Low** certainty evidence	Subcutaneous injection	3–5 infiltrations of 1–5 ml per lesion (depending on the size of the lesion; in the amount needed to cover each lesion). Interval of 3–7 days between sessions. Traditionally, the infiltration technique described requires the volume necessary to achieve the saturation of the lesion, which is understood as complete swelling of the lesion. It is suggested not to exceed the total volume of 15 ml infiltrated per day across all lesions.
It is suggested to apply **thermotherapy** in patients with localized cutaneous leishmaniasis caused by *L. braziliensis*, *L. panamensis*, and *L. mexicana*.	**Conditional** recommendation **Very low** certainty evidence	Application of local heat with an electromagnetic device that generates high frequency waves	Following local anesthesia, the electrode is applied at 50 °C for periods of 30 seconds, in the center and at the margin of the lesion. One session with the number of applications needed to cover the entire lesion.
It is suggested to use **paromomycin** in patients with cutaneous leishmaniasis caused by *L. panamensis*, *L. braziliensis*, or *L. mexicana*.	**Conditional** recommendation **Very low** certainty evidence	Topical cream 15%	Apply to the affected area once a day for 20 days.

Systemic treatments for adult patients with cutaneous leishmaniasis

Recommendations	Strength of the recommendation and certainty of the evidence	Route of administration	Treatment scheme
It is recommended to use **miltefosine** in adult patients diagnosed with cutaneous leishmaniasis caused by *L. panamensis*, *L. mexicana*, *L. guyanensis*, or *L. braziliensis*.	**Strong** recommendation **Low** certainty evidence	Oral	2.5 mg/kg/day, with a maximum dose of 150 mg/day, for 28 days. It is suggested to divide the doses and to take the medication after meals to reduce gastrointestinal side effects.
It is suggested to administer **pentamidine isethionate** in patients diagnosed with cutaneous leishmaniasis caused by *L. guyanensis*.	**Conditional** recommendation **Low** certainty evidence	Intramuscular	Studies report the following doses: 4–7 mg/kg/day in 3 doses applied every 72 hours.
It is suggested to use **pentavalent antimonials** in adult patients diagnosed with cutaneous leishmaniasis caused by *L. braziliensis*, *L. panamensis*, *L. amazonensis*, *L. peruviana*, or *L. mexicana*.	**Conditional** recommendation **Moderate to low** certainty evidence	Intravenous or intramuscular	20 mg Sb^{+5}/kg/day as a single daily dose **for 20 days (moderate to low** certainty evidence): • Maximum dose of 1215 mg Sb^{+5}/kg/day or 3 ampoules of pentavalent antimonial to reduce adverse effects (expert opinion). • Indication of doses (5, 10, 15 mg Sb^{+5}/kg/day) should be based on the risk-benefit balance or local evidence. • The dose indication of 5 mg Sb^{+5}/kg is only for Rio de Janeiro (Brazil). • In areas with circulation of *L. braziliensis*, consider the local evidence, due to the different therapeutic responses observed for that species according to geographical location. 20 mg Sb^{+5}/kg/day as a single daily dose **for 10 days**, only for *L. braziliensis* and *L. panamensis* (**very low** certainty evidence): • Maximum dose of 1215 mg Sb^{+5}/kg/day or 3 ampoules of pentavalent antimonial to reduce side effects (expert opinion). • In areas with circulation of *L. braziliensis*, consider the local evidence due to the different therapeutic responses observed for that species according to geographical location.

Source: PAHO, 2022, *apud* PAHO, 2024.[1]

Concerning pediatric patients, topical PM, IV or IM pentavalent antimonials, or oral miltefosine can be used, the latter being strongly recommended. In special cases, such as pregnant or breastfeeding women, patients with electrocardiogram alterations, kidney and liver

[1] The original formatting of the table has been preserved for clarity, so it is included as an image in this document.

diseases, immunosuppression, disseminated, diffuse, or atypical CL, other protocols are suggested in the Guide, taking into account comorbidities and treatment toxicity (PAHO, 2024).

A document published by the WHO estimated that between US$ 7–8 million are necessary to treat approximately 150,000 new CL cases each year for medical supplies and devices (WHO, 2020), representing an important socio-economic impact. As explained, CL therapeutic choice must consider the patient's age, comorbidities, and contraindications. There are currently only few drug options, and inconveniences such as long treatment duration, which can increase parasite resistance, drug toxicity, and the need for parenteral administration for most treatments compromise patient compliance and drug effectiveness (Bruni et al., 2017). In addition, SSG, PM, and miltefosine rely on single manufacturers, making their supply chain vulnerable (van Griensven et al., 2024). This scenario corroborates the need to search for new alternatives.

2.2.1.1. *Amphotericin B*

AmB belongs to the class of polyene macrolides with amphipathic properties, characterized by a lactonized macrocyclic ring containing a heptaene chain and a polyhydroxylated region with seven hydroxyl groups. This ring also has a carboxylic acid group (pKa 3.72) and a side chain formed by a mycosamine moiety with a free amino group (pKa 8.12) (Figure 9), which together confer amphoteric character to AmB—a property that inspired its name. AmB's solubility in aqueous media is strongly pH-dependent: it increases under highly acidic or basic conditions (pH < 2 or pH > 10), where only one of the ionizable groups is charged (Barratt & Bretagne, 2007; Cavassin et al., 2021; Frézard et al., 2023).

However, at neutral pH (6–7), when both groups are ionized, AmB exhibits very low water solubility. Under these conditions, AmB tends to self-associate, initially forming dimers through hydrophobic interactions, particularly between the polyene regions of adjacent molecules. As the concentration exceeds the critical aggregation concentration (CAC) of approximately 0.001 mg/mL and/or the temperature increases, these dimers further assemble into higher-order aggregates. In addition, AmB is sparingly soluble in alcohols, and more readily soluble in dimethyl sulfoxide (DMSO) and dimethylformamide (DMF) (Cavassin et al., 2021; Frézard et al., 2023).

Figure 9 – Chemical structure of AmB

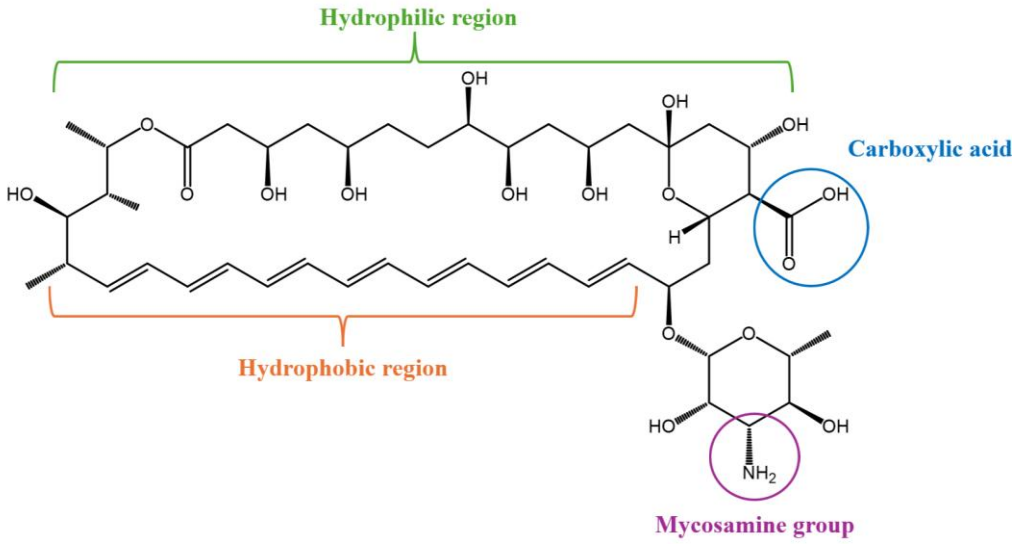

Source: Created with ChemDraw v. 23.1.2 (Revvity Signals, 2024).

AmB was discovered in 1956 and isolated from the actinomycete *Streptomyces nodosus*, a bacterium initially identified in a soil sample collected in Venezuela. Its commercial use began in 1960 with the introduction of Fungizone® (Bristol-Myers Squibb, USA), the conventional formulation of AmB, which is marketed in Brazil as Anforicin B® (Cristália, Brazil). In this formulation, the bile salt sodium deoxycholate is employed to solubilize AmB by forming micelles in solution (Cavassin et al., 2021).

AmB is classified under the pharmacotherapeutic group of systemic antimycotics (ATC code: J02AA01) and remains, to this day, the most common agent to treat invasive fungal infections in intensive care units (Cavassin et al., 2021; NIPH/WHO, [n.d.]). Additionally, it is considered as one of the most potent antileishmanial drugs. AmB's primary mechanism of action involves binding to ergosterol—the main sterol in fungal and *Leishmania* membranes—leading to pore formation. In this model, multiple AmB molecules insert into the membrane bilayer, with AmB hydrophobic polyene chains interacting with ergosterol, while the hydrophilic domains line the aqueous channel, leading to ion leakage and ultimately parasite death (Figure 10a) (Carolus et al., 2020; Cavassin et al., 2021).

Pore stability is maintained by three non-covalent interactions, as seen in Figure 10b: (i) hydrogen bonding between the sterol's hydroxyl group and AmB's carboxyl group (reinforced by its amino group), (ii) Van der Waals interactions between the polyene chain and sterol molecule, and (iii) π–π stacking between the polyene tail of AmB and the double bond at C-22 of ergosterol's side chain. This double bond maintains ergosterol in a flat conformation, favoring interaction with AmB. It could explain AmB's greater affinity for ergosterol over

cholesterol, as cholesterol's flexible side chain adopts less favorable conformations (Carolus et al., 2020; Herve et al., 1989).

Figure 10 – AmB mechanism of action (a) AmB interaction with the fungal membrane (i) and toxicity in a mammalian cell (ii); (b) Three-dimensional model of AmB (i) with the cylindrical ergosterol (ii) and sigmoidal cholesterol (iii)

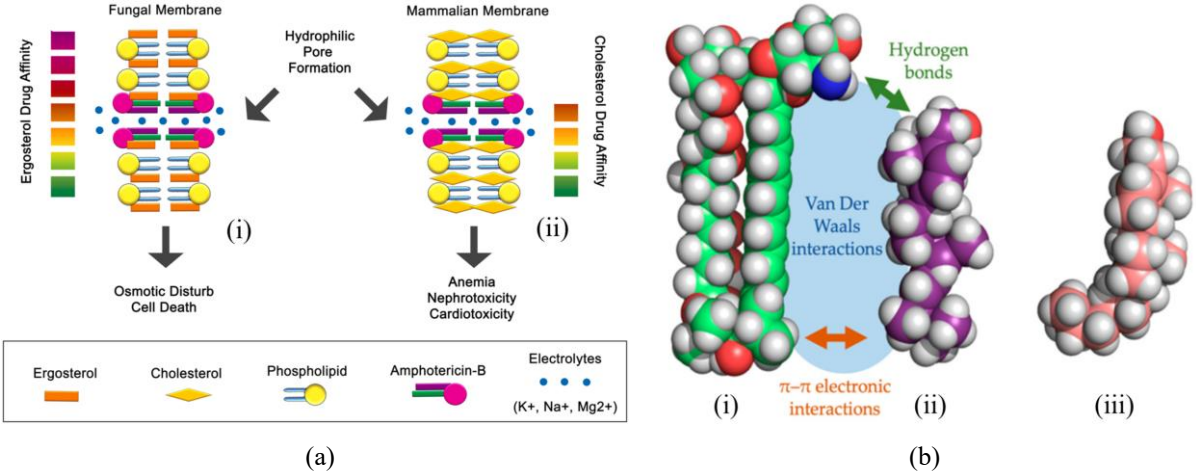

Source: Adapted from Cavassin et al. (2021) and Carolus et al. (2020).

In addition to the classical pore model, two alternative mechanisms have been proposed in which AmB destabilizes the membrane: the surface adsorption model, where AmB binds to ergosterol at the membrane surface without insertion, and the sterol sponge model, where extracellular AmB aggregates extract ergosterol from the membrane (Carolus et al., 2020). Furthermore, AmB can induce oxidative stress, increasing reactive oxygen species (ROS) and nitric oxide (NO), contributing to parasite death. Immunomodulatory effects have also been described, including the stimulation of cytokine release (e.g., TNF-α, IL-1β) by monocytes and macrophages (Carolus et al., 2020; Golenser & Domb, 2006).

Even though AmB has a greater affinity for ergosterol, it can also bind to cholesterol, which is present in the mammalian cells, leading to its toxicity. The toxic effects of AmB are typically categorized as either acute or subacute. Acute toxicity—characterized by symptoms such as fever, nausea, and headache—occurs in approximately 80% of patients and is associated with the innate immune recognition of AmB as a bacterial-derived molecule. This recognition is mediated by Toll-like (TLR) and CD14 receptors expressed on immune cells, triggering an inflammatory response (Carolus et al., 2020; Lemke et al., 2005). Subacute toxicity, notably nephrotoxicity, affects around 30% of patients and represents one of the most significant adverse reactions linked to AmB treatment (Lemke et al., 2005; Vyas & Gupta, 2006). The nephrotoxic mechanism is thought to involve the interaction of AmB with low density

lipoprotein (LDL) and its uptake by renal epithelial cells, exhibiting LDL-receptors (Barratt & Bretagne, 2007). This interaction may lead to renal vasoconstriction, resulting in decreased glomerular filtration rate and tubular dysfunction (Deray, 2002).

In the late 1990s, in an attempt to reduce AmB nephrotoxicity, three lipid formulations were developed: Abelcet®, Amphocil® and AmBisome® (Lemke et al., 2005). Abelcet® was the first lipid-based formulation of AmB approved by the FDA in 1995. This lipid complex consists of distearoyl phosphatidylcholine (DSPC) and distearoyl phosphatidylglycerol (DSPG) forming a multilamellar system characterized as "ribbon-like". One year later, Amphocil® was approved as a colloidal dispersion of AmB with sodium cholesteryl sulfate, resulting in disc-shaped particles. In 1997, AmBisome® was introduced as a liposomal formulation of AmB composed of small unilamellar vesicles made from hydrogenated soy phosphatidylcholine, cholesterol and DSPG (Torrado et al., 2008; Golenser & Domb, 2006).

The main advantage of AmB lipid-based formulations lies in their improved safety profile compared to the conventional micellar formulation, even during prolonged treatment regimens (Arruda et al., 2016; Torrado et al., 2008). Before the approval of these formulations, Fungizone® was mixed with lipid emulsions used in parenteral nutrition (e.g. Intralipid® and Lipofundin®) to reduce toxicity. The interaction of AmB with phospholipids on the surface of oil droplets helped lower toxicity compared to Fungizone® alone (Barratt & Bretagne, 2007). However, issues with stability limited the widespread use of these mixtures (Arruda et al., 2016; Torrado et al., 2008).

Lipid excipients offer well-known advantages in drug delivery, including improved bioavailability, therapeutic index, and biocompatibility—especially for poorly water-soluble compounds (Santiago et al., 2018). This improved safety profile is reflected in dosing: liposomal AmB is recommended at 2–5 mg/kg/day with no maximum daily dose, while conventional AmB is limited to 0.7–1.0 mg/kg/day and a maximum of 50 mg/day. Thus, liposomal AmB can be safely administered at doses up to five times higher than micellar AmB (Brasil, 2017). Up to now, AmB treatments are administered intravenously with mandatory hospitalization (Reguera et al., 2019), due to AmB low solubility in water, combined with high molecular weight (924.08 Da) and instability in extreme pH, leading to low oral and topical bioavailability (Bruni et al., 2017).

AmBisome® is currently considered the safest and the first-line treatment for VL. Nonetheless, its efficacy may be reduced in some CL cases and leishmaniasis-HIV co-infection (Guery et al., 2017; Mueller et al., 2007; Ritmeijer et al., 2011). Additionally, although rare,

reports of AmB-resistant *Leishmania* strains have emerged for both CL (Ferreira et al., 2024) and VL (Purkait et al., 2012; Srivastava et al., 2011).

Despite its therapeutic advantages, AmBisome® cost remains a major barrier to widespread use in endemic and low-income regions, where it is most needed. One milligram of AmB in the liposomal formulation costs approximately 35 times more than the conventional form (Arruda et al., 2016). In Brazil, AmBisome® is included in the National List of Essential Medicines (Rename) and is financed, procured, and distributed by the Ministry of Health. Since 2007, a partnership between the PAHO/WHO and Gilead Sciences, the drug supplier, has enabled significant price reductions—from USD 202 to USD 21 per vial—exclusively for the treatment of leishmaniasis. This agreement has facilitated access to AmBisome® within the Brazilian public health system and in other endemic countries (Brasil, 2021).

A three-year collaboration between WHO and Gilead (2023–2025), valued at USD 11.3 million was recently signed (WHO, 2023c). This context reveals a dubious situation: while the price subsidy allows access to the drug, it shows that the countries where it is most needed, i.e. developing countries, may experience a collapse if supply agreements are not renewed or production is interrupted. Given these limitations, the development of therapeutic alternatives remains essential.

2.3. New therapeutic strategies

In recent decades, only a limited number of new drugs, innovative formulations of existing drugs, or their combinations have received approval for the treatment of leishmaniasis. One of the reasons that may explain this fact is the low private investment. Neglected tropical diseases, such as leishmaniasis, affect mainly impoverished populations, which means low economic return to the pharma industry (Reguera et al., 2019). In the WHO road map for neglected tropical diseases 2021–2030, one of the critical actions for CL is to develop and scale up oral or topical treatment that could be used in health centers (WHO, 2020).

This part of the manuscript will discuss three new treatment strategies related to this thesis subject: combination therapy, immunomodulators, and nanotechnological approaches.

2.3.1. *Combination therapy*

Drug combinations have been encouraged by WHO and Drugs for Neglected Diseases Initiative (DNDi) to enhance efficacy and reduce the emergence of resistant strains (Reguera et al., 2019).

Various antileishmanial combinations have been clinically evaluated for VL, PKDL, and CL, particularly for patients unresponsive to antimonial monotherapy.

A four-year study in Bangladesh and India assessed the safety, efficacy, and adherence of three VL treatments: (i) single-dose liposomal AmB, (ii) PM-miltefosine, and (iii) single-dose liposomal AmB followed by miltefosine. All had cure rates above 95%, confirming their effectiveness. Based on this, WHO recommends single-dose intravenous AmBisome® as the first-line VL treatment in South Asia, with a 10-day PM-miltefosine regimen as an alternative (DNDi, 2025a). In India, combination therapy with a single dose of liposomal AmB and miltefosine (various durations) is more cost-effective than most monotherapies, costing $124–160 per averted death. When including indirect costs like productivity loss, the PM-miltefosine combination was the most cost-effective at $97 per averted death (Dorlo et al., 2012).

In East Africa, a study compared the efficacy and safety of PM alone (21 days), PM plus SSG (17 days), and SSG monotherapy (30 days). PM alone (84.3%) was significantly less effective than SSG (94.1%), while the SSG-PM combination (91.4%) was comparable to SSG. All regimens had similar safety profiles (Musa et al., 2012). Since 2010, WHO has recommended the 17-day SSG-PM regimen as the first-line VL treatment in East Africa (DNDi, 2021). However, a study in eastern Sudan found that 40% of patients were ineligible for SSG-PM treatment due to contraindications to one of the drugs. Additionally, with children comprising 83% of cases in this region, the need for two painful intramuscular injections daily for at least 17 days likely contributed to follow-up losses (Atia et al., 2015).

To improve safety and patient adherence, a Phase III study launched in 2018 evaluated miltefosine plus PM as an alternative to SSG-PM. The combination was as effective but required fewer injections, had a shorter duration, and avoided SSG-related cardiotoxicity. WHO is reviewing the results for potential guideline updates (DNDi, 2025b; Musa et al., 2023).

In Latin America, a study evaluated the efficacy and safety of different treatments for VL: AmB deoxycholate (1 mg/kg/day for 14 days), liposomal AmB (3 mg/kg/day for 7 days), and a combination of liposomal AmB (10 mg/kg single dose) with meglumine antimoniate (20 mg/kg for 10 days), compared to standard meglumine antimoniate (20 mg/kg for 20 days). AmB deoxycholate treatment was discontinued early, due to toxicity. At six months, cure rates were 77.5% for meglumine antimoniate, 87.2% for liposomal AmB, and 83.9% for the combination, with no significant differences between groups (Romero et al., 2017). Liposomal AmB had the fewest adverse events, leading to its adoption as the first-line treatment in Latin America (PAHO, 2022). These results, coupled with the low cure rates of miltefosine monotherapy, which discouraged trials in miltefosine combination for VL treatment, have meant that

combination therapy is still not adopted as first-line in Latin America (van Griensven et al., 2024).

In Ethiopia, a study compared AmBisome monotherapy, the WHO-recommended VL/HIV treatment at the time, with liposomal AmB plus oral miltefosine. The combination showed 88% efficacy after 58 days versus 55% for monotherapy. A similar study in India reported 96% efficacy for the combination after 210 days, compared to 88% for standard treatment. These findings led the WHO to update its guidelines in 2022, recommending this combination for VL/HIV patients in East Africa and Southeast Asia (DNDi, 2025c; WHO, 2022).

For PKDL, DNDi's Phase II studies in India and Bangladesh confirmed liposomal AmB monotherapy and its combination with short-course miltefosine as safe, effective alternatives to long-course miltefosine, reducing treatment duration from 12 to 3 weeks. Similarly, in Sudan, miltefosine plus PM and liposomal AmB plus miltefosine also proved to be shorter, effective treatments (DNDi, 2025d, 2025e).

In CL treatment, a Phase II study showed that combining thermotherapy with a shorter course of oral miltefosine was more effective than thermotherapy alone (80.3% *vs*. 57.8%) (López et al., 2022). Thermotherapy involves the application of heat using an electromagnetic device that generates high-frequency waves. The electrode is applied at 50 °C for 30-second intervals in both the lesion's center and edges (PAHO, 2022). In Phase III, this combination was non-inferior to standard miltefosine monotherapy after 90 days (65.5% *vs*. 75.0%). It also appeared more effective for lesions due to *L. braziliensis*. Most adverse events were mild and consistent with the expected safety profile (DNDi, 2025f).

Another combined treatment exploiting the thermosensitivity of *Leishmania* is cryotherapy associated with intralesional antimonials. Cryotherapy is a simple procedure that does not need anesthesia, produces rapid destruction of *Leishmania* due to the subzero temperature, is comparatively inexpensive (approximately $4.0 US per patient), and is not associated with serious complications, being effective in some CL cases. Although the exact mechanism of cryotherapy in CL healing remains unclear, it is hypothesized that the treatment destroys amastigotes, triggering cryonecrosis and an immune response through the release of antigenic substances (López-Carvajal et al., 2016; Panagiotopoulos et al., 2005). Intralesional antimonials combined with cryotherapy are more effective than either treatment alone. In combined therapy, intralesional injection of antimonials alternate with local applications of a cryogen, usually liquid nitrogen (−195 °C), for 30-second intervals. This therapy seems to be

more promising for small-sized lesions (< 3 cm) and in the early stages of disease (duration, ≤ 3 months) (Asilian et al., 2004; Salmanpour et al., 2006).

DNDi is evaluating a combination therapy for complicated CL and PKDL involving CpG-D35, an immunomodulator, and a short, low-dose antimonial (Sb^{5+}) regimen. CpG-D35, a TLR9 agonist, selectively activates plasmacytoid dendritic cells (pDCs), triggering IFN-α secretion, which promotes monocyte maturation into active DCs and enhances NK cell IFN-γ production. CpG-D35 was used as an adjuvant to Sb^{5+} in a non-human primate CL model, improving antimonial efficacy. In healthy volunteers, CpG-D35 was safe and stimulated an immune response linked to disease control. The multiple ascending dose study is being planned (DNDi, 2025g; Thacker et al., 2020).

Other combination therapies for CL have been reported, primarily associating antimonials with systemic or local treatments such as allopurinol, ketoconazole, 50% trichloroacetic acid, carbon dioxide laser, tamoxifen or PM. Miltefosine combined with intralesional pentamidine has also been studied. However, leishmaniasis treatment guidelines have not incorporated these combinations (ReBEC, 2020; Machado et al., 2018; Madusanka et al., 2022).

Combined therapy, especially with two drugs with different mechanisms of action, offers several advantages, including shorter treatment duration (improving compliance), lower drug doses (reducing toxicity and costs), and a lower risk of selecting drug-resistant parasites (Bruni et al., 2017). Despite various studies identifying effective combination therapies, they are not suitable for all patients, and resistance to some drugs has already been reported. Therefore, developing new combination therapies remains a priority.

2.3.2. *Immunomodulators*

Parasite-host interaction in leishmaniasis is very complex. It is not well understood what drives differences in clinical outcome, ranging from asymptomatic to flow blow disease, with anergic and hyperergic poles. It is known that the parasite strain, along with the host's immune response, genetic or environmental factors all contribute (Scorza et al., 2017).

It has become evident that sandfly saliva contains components that modulate the host's immune response and hemostasis. When feeding, sandflies pierce the host's skin, triggering a hemostatic response to prevent blood loss. To counteract this host response, sandflies produce bioactive salivary compounds, such as protein maxadilan, with vasodilator and immunomodulatory properties (Abdeladhim et al., 2014). Furthermore, the parasite produces a

gelatinous plug called promastigote secretory gel (PSG), which contains filamentous proteophosphoglycan and occludes the sandfly's anterior midgut. Due to its occlusion, the sandfly must regurgitate this gel along with the parasite before successfully feeding blood. PSG acts synergistically with sandfly saliva to recruit macrophages to the bite site, exacerbating lesion development (Rogers et al., 2009). Although sandfly salivary molecules have been explored as potential exposure markers and vaccine candidates, no effective human vaccine has been developed to date (Abdeladhim et al., 2014).

Once inside the host, *Leishmania* employs multiple immune evasion strategies, including delaying lysosome-phagosome fusion, resisting complement-mediated lysis via lipophosphoglycan, and inhibiting oxidative stress responses (Brasil, 2017; Rossi & Fasel, 2018). A key survival mechanism involves manipulating macrophage L-arginine metabolism. Macrophages can either destroy or support intracellular amastigotes, depending on the balance between two enzymes: nitric oxide synthase 2 (iNOS) and arginase-1, both of which utilize L-arginine as a substrate. During the initial inflammatory phase (1–2 days), M1 phenotype macrophages, classically activated by Th1 cytokines (e.g., IFN-γ, TNF-α, IL-12, IL-2, IL-17), enhance iNOS activity, which converts L-arginine into nitric oxide (NO), a toxic molecule to *Leishmania* (Rabienia et al., 2024; Rogers et al., 2009).

However, these M1 cells are soon replaced by M2 phenotype macrophages via alternative activation driven by Th2 cytokines (e.g., IL-4, IL-10, IL-13, IL-21) and myeloid cells, which express arginase-1 to facilitate wound healing by promoting fibroblast proliferation and collagen deposition. Arginase-1 hydrolyzes L-arginine into ornithine, a precursor for polyamines, which are essential for cell growth and tissue repair. The interesting point is: polyamines are also essential molecules for parasite proliferation. It means that *Leishmania* has evolved to exploit the host-wound response for its survival (Rabienia et al., 2024; Rogers et al., 2009).

As mentioned, M1 or M2 polarization is highly important to disease resolution or establishment. Neutrophils are the first immune cells recruited to the skin following parasite inoculation. Neutrophils play divergent roles during infection, as they can kill the parasite with Neutrophil Extracellular Traps (NET) but also function as a Trojan horse (Mahor et al., 2023). In this case, they transfer the infection to macrophages. Macrophages can acquire the infection via efferocytosis when they engulf infected neutrophils and induce an anti-inflammatory macrophage state, triggering Mer Tyrosine Kinase (MERTK) signaling and increased TGF-β release, allowing parasite survival (Scorza et al., 2017). Macrophages can also internalize parasites via phagocytosis, as seen in Figure 11.

Following the initial neutrophil response, monocytes are recruited to the inoculation site and can differentiate locally into macrophages or monocyte-derived dendritic cells (Mo-DCs), modulated by epidermal cytokines. Inside the macrophage, *Leishmania* multiplies until the infected cells rupture, releasing parasites and antigenic particles. These antigens are captured by Mo-DCs and transported to lymph nodes, where they activate naive $CD4^+$ T cells and drive their differentiation into T helper 1 (Th1) or T helper 2 (Th2) cells (Brasil, 2017; Scorza et al., 2017). Th1 cells return to the infection site and can secrete IFN-γ, together with NK cells, which upregulate iNOS and contribute to parasite elimination. While Th1 responses promote disease resolution, Th2 favors persistence by suppressing NO synthesis and supporting macrophage differentiation into the M2 phenotype (Scorza et al., 2017).

Figure 11 – Monocytic cells in *Leishmania* control in murine skin

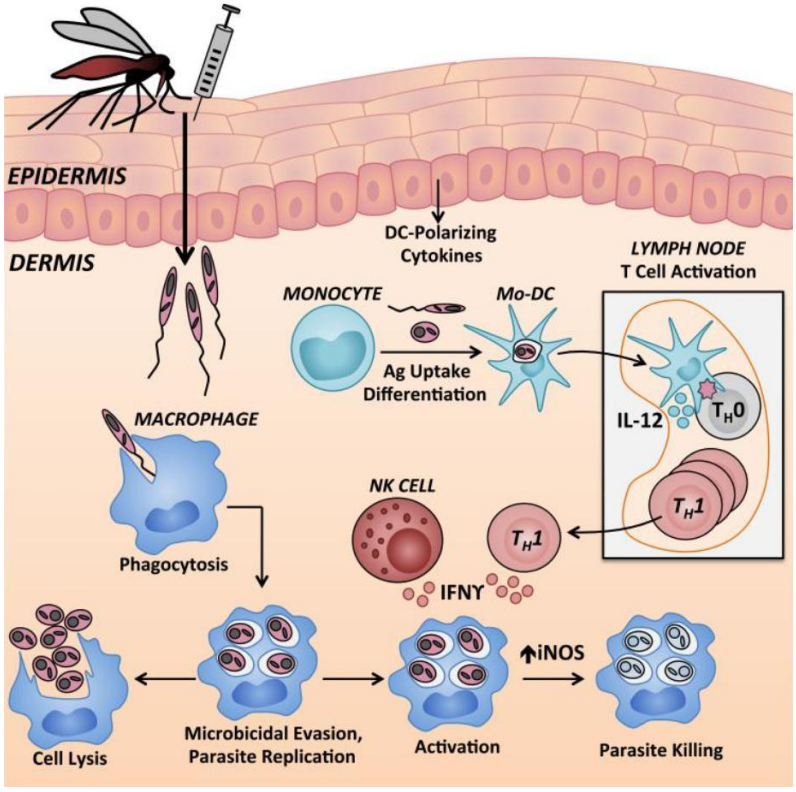

Source: Scorza et al. (2017).

Although the Th1/Th2 paradigm is central to *Leishmania* infection, increasing evidence suggests that host resistance is regulated by a broader interactive immune network rather than a simple linear model (Lipoldová & Demant, 2006). Studies in chimeric mice indicate that both T-cell-dependent and independent mechanisms contribute to parasite clearance. Resistant (C57BL/6) and susceptible (BALB/c) mice were reconstituted with naïve T cells from genetically different backgrounds. BALB/c mice receiving C57BL/6-derived T cells resolved

the CL infection, developing a protective Th1 response (high IFN-γ, low IL-4), while BALB/c controls succumbed with a Th2 profile (low IFN-γ, high IL-4, IL-10). Conversely, C57BL/6 chimeric mice receiving susceptible T cells from BALB/c mice still had a controlled infection, initially exhibiting a Th0 response before shifting to Th2 as they were cured. Moreover, T cells from a non-curing genotype can mediate parasite elimination in a curing environment, highlighting the complexity of host resistance mechanisms (Shankar & Titus, 1995).

A more severe imbalance of Th1/Th2 responses is observed in CL complex cases, as seen in Figure 12. Anergic diffuse cutaneous leishmaniasis presents a weak Th1 response and excessive Th2 activation, with high IL-4, IL-5, and IL-10 levels driving M2 polarization, TGF-β–induced T cell anergy, and treatment large inefficacy. In contrast, MCL is characterized by severe inflammation with high cytotoxicity, excessive IFN-γ and TNF-α production, and low IL-10 levels, causing disfigurement. MCL is treatment-refractory in up to 40% of cases (Lafleur et al., 2024). A balanced immune response is crucial in CL. While a Th1 response is essential for parasite clearance and clinical cure, excessive activation can lead to tissue damage. In contrast, a Th2 response, though linked to parasite persistence, also helps control inflammation and promote healing (Maspi et al., 2016).

Figure 12 – Representation of disease severity and Th1-Th2 balance across different CL and PKDL forms

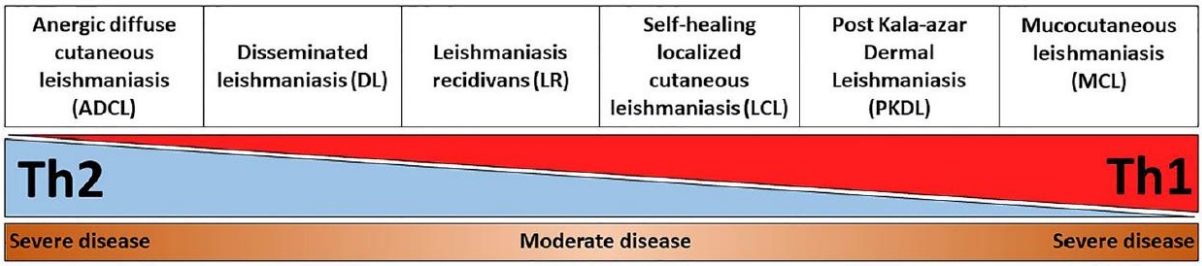

Source: Volpedo et al. (2021).

Immunotherapy is a treatment modality that modulates immune responses to help disease resolution. Immunotherapeutic strategies can include recombinant cytokines, cytokine antagonists, immune checkpoint inhibitors, TLR agonists, modulators of cellular receptors and signaling, enzyme inhibitors, anti-inflammatory and antioxidant agents, cellular therapy, and therapeutic vaccines (Lafleur et al., 2024).

The use of biological molecules to enhance cell-mediated immunity for therapeutic success has been evaluated in preclinical and clinical studies. For example, the phenolic compounds gallic acid or ellagic acid were combined with AmB in a topical gel (poloxamer 407 plus propylene glycol) due to their immunomodulatory properties. After 21 days of

treatment, the combined formulations proved to be more effective in an experimental model of CL (*L. major*), with a reduction in the size and parasite load in the lesion compared to the Control (Alves et al., 2020).

To assess IL-10's role in VL, this cytokine was neutralized in splenic aspirate cultures from 67 patients. IL-10 neutralization reduced parasite load in 73% of cases, with 30% achieving complete clearance, with enhanced TNF-α and IFN-γ secretion, indicating its immunosuppressive role in VL (Gautam et al., 2011). IL-12 also plays a key role in controlling *L. donovani,* as Murray et al. (2000) showed. Treatment with recombinant IL-12 and pentavalent antimony resulted in enhanced Sb^{5+} efficacy compared to animals treated with the drug alone. In contrast, IL-12 knockout mice failed to respond to pentavalent antimony (Murray et al., 2000).

In humans, a case report in Italy showed safety and efficacy using rHuGM-CSF (recombinant human granulocyte-macrophage colony-stimulating factor) with liposomal AmB in an HIV/VL co-infected patient (Mastroianni, 2004). There is also the CpG-D35, an immunomodulator for combination therapy with antimonials, described in the previous section and currently undergoing clinical trials by the DNDi (DNDi, 2025g). In addition, human recombinant IFN-γ has been successfully used with antimony treatment to accelerate antiparasitic and clinical responses (Haas et al., 2002, Sundar et al., 1995).

The potential application of immunotherapies in clinical practice is observed for pentoxifylline, a phosphodiesterase inhibitor that inhibits TNF-α and other proinflammatory mediators. Although it has not shown therapeutic benefit in some clinical studies, its efficacy in treating refractory MCL when combined with pentavalent antimony, shortening treatment duration, has been demonstrated (Lafleur et al., 2024). It is currently recommended by PAHO for the treatment of MCL combined with pentavalent antimonials (PAHO, 2022).

Another widely studied strategy is therapeutic vaccines. Interesting results have already been obtained in clinical trials (Mahor et al., 2023; Roatt et al., 2020), but the topic of vaccines will not be covered here.

The host's immune status is considered as a key point for treatment success. It could explain the greater risk of developing severe disease in patients with conditions impacting the immune system, such as malnutrition, age, HIV coinfection, bacterial infections, or bleeding (PAHO, 2020). Experiments using BALB/c mice immunosuppressed with anti-TNF or methotrexate and then treated with Glucantime® showed that these mice were unable to develop specific cellular immunity to *L. infantum* and produced low levels of pro-inflammatory

cytokines. This may explain the increased risk of VL relapse in immunosuppressed patients (Bernardo et al., 2023).

Immunological balance is crucial in determining natural resistance or susceptibility to leishmaniasis. Disruptions in this equilibrium can lead to the progression from asymptomatic to symptomatic leishmaniasis or trigger infection reactivation (PAHO, 2020). Therefore, introducing immunomodulators in leishmaniasis therapy is an interesting strategy.

2.3.2.1. *Retinoic acid*

Vitamin A (retinol) and retinoids, its natural and synthetic derivatives, have been described as responsible for a multitude of cellular effects in animals and humans, participating in growth, vision, reproduction, and immune response (Frankenburg et al., 1998; Reigada et al., 2017). Vitamin A is a fat-soluble essential micronutrient exclusively obtained from the diet. It can be obtained as retinyl esters directly from animal resources such as milk, eggs, and liver or through pro-vitamin A carotenoids in some fruits and vegetables (Lavudi et al., 2023; Polcz & Barbul, 2019). In animal-based foods, retinyl esters are hydrolyzed by retinyl ester hydrolases (REHs) in the intestinal lumen and brush border, releasing retinol. Retinol is later oxidized to retinaldehyde via retinol dehydrogenases (RDHs). In plant-based sources, carotenoids like β-carotene are absorbed through the SR-B1 transporter and cleaved by β-carotene 15,15'-oxygenase (BCO1) within enterocytes, producing retinaldehyde. Retinaldehyde can either be irreversibly oxidized into retinoic acids by aldehyde dehydrogenases (ALDHs) or reversibly reduced back to retinol by retinal reductase, allowing tight regulation of retinoic acids levels (Lavudi et al., 2023; Polcz & Barbul, 2019), as can be seen in Figure 13.

Once absorbed, retinol undergoes esterification via lecithin: retinol acyltransferase (LRAT) or acyl-CoA: retinol acyltransferase (ARAT), forming retinyl esters (RE). These are incorporated into chylomicrons and transported through the lymphatic system to the liver. RE can be hydrolyzed into retinol within hepatocytes, but the majority is transferred to hepatic stellate cells, where it is stored in intracellular lipid droplets (Lavudi et al., 2023; Polcz & Barbul, 2019).

When needed, retinol is mobilized and binds to retinol-binding protein 4 (RBP4), which is synthesized by hepatocytes. This retinol–RBP4 complex, stabilized by transthyretin (TTR) to prevent renal excretion, circulates in the bloodstream until it reaches target cells. Cellular uptake is facilitated by the Stimulated by Retinoic Acid 6 (STRA6) receptor. Inside the target cells, retinol is converted into retinaldehyde and subsequently oxidized into the major

biologically active isomers: all-trans-retinoic acid (RA; tretinoin) and 9-cis-retinoic acid (alitretinoin) (Lavudi et al., 2023; Polcz & Barbul, 2019). This conversion occurs through two consecutive oxidation steps: retinol is first oxidized to retinaldehyde by RDHs and alcohol dehydrogenases (ADHs). In the second step, retinaldehyde is further oxidized to retinoic acids by retinaldehyde dehydrogenases (RALDHs), including RALDH-1 and RALDH-2 (Wu et al., 2024).

Figure 13 – Schematic representation of the retinoid synthesis pathway

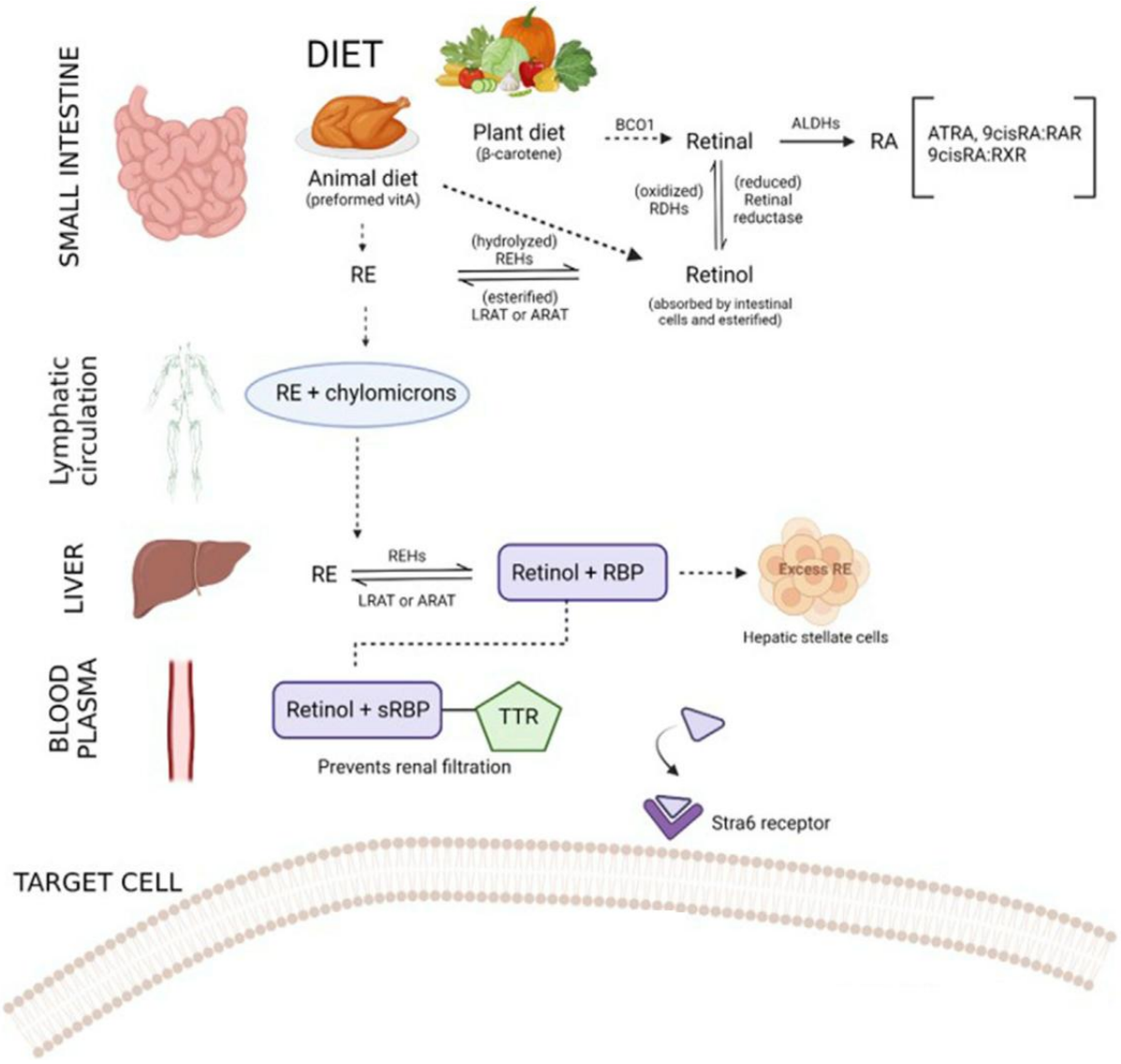

Note: RE – retinyl esters; REHs – retinyl ester hydrolases; LRAT – retinol acyltransferase; ARAT– retinol acyltransferase; RDHs – retinol dehydrogenases; BCO1 – β-carotene 15,15'-oxygenase; ALDHs – aldehyde dehydrogenases; RA – retinoic acid; ATRA – all-trans-retinoic acid; RBP – retinol-binding protein; sRBP – serum retinol-binding protein; TTR – transthyretin; STRA6 – stimulated by Retinoic Acid 6. Source: Adapted from Lavudi et al., 2023.

Verma et al. (2019) showed that *L. donovani*-infected macrophages exhibited lower expression of RALDH-1 and RALDH-2, leading to a shift from Th1 to Th2 immune response. Moreover, pre-treatment with an RALDH-2 inhibitor enhanced parasite survival and further suppressed iNOS, IFN-γ, and TNF-α while increasing Arginase-1 and IL-10, as shown in Figure 14.

Figure 14 – *L. donovani* Suppresses Retinoic Acid Synthesis to Favor Parasite Persistence

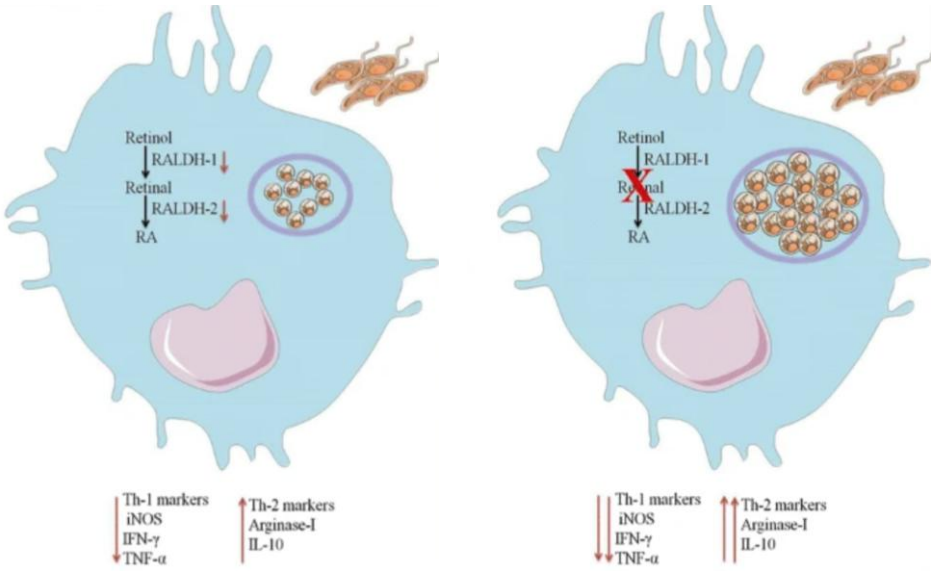

(a) (b)

Note: Impact of *L. donovani* infection on RA synthesis in macrophages: (a) Infected macrophages exhibit reduced expression of RALDH-1 and RALDH-2, leading to lower RA levels. This results in a shift from a Th1 to a Th2 immune response, characterized by decreased iNOS, IFN-γ, and TNF-α and increased Arginase-1 and IL-10 (b) When RALDH-2 is further inhibited, RA synthesis is completely blocked, exacerbating the Th2 response and increasing parasite burden. Source: Graphical abstract by Verma et al., (2019).

Retinoids levels are tightly controlled through cytochrome P450 enzymes, which mediate its degradation by oxidation into inactive metabolites (Ferreira et al., 2020). The chemical structures of retinoids are illustrated in Figure 15 for better understanding.

Figure 15 – Retinoid chemical structures

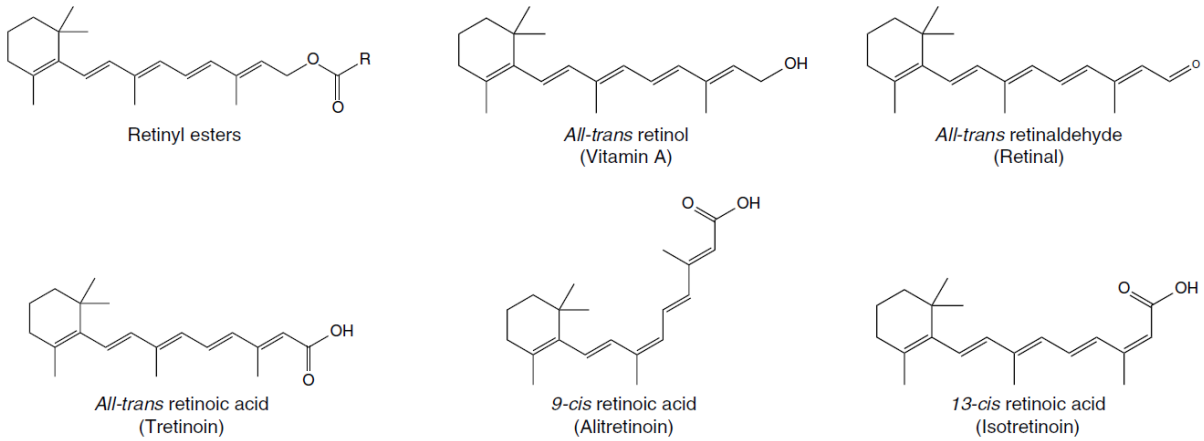

Source: Ferreira et al. (2020).

RA and its isomers exert their effects primarily by binding to nuclear receptors, specifically retinoic acid receptors (RARα, β, and γ) and retinoid X receptors (RXRα, β, and γ). These receptors regulate gene expression by forming RAR/RXR heterodimers or, in the case of RXR, also homodimers. Approximately 193 human genes are directly regulated by RAR and RXR (Lavudi et al., 2023). The resulting RAR-RXR complex is bound to specific DNA sequences known as retinoic acid response elements (RAREs) in the promoter regions of target genes. The transcriptional activity of this complex is dynamically regulated by the recruitment of either co-repressors or co-activators, as shown in Figure 16. In the absence of RA, RAR-RXR recruits nuclear receptor co-repressors (N-CoRs) and histone deacetylases (HDACs), maintaining chromatin in a condensed state, thereby repressing gene transcription. When RA binds to RAR, a conformational change leads to the release of co-repressors and the recruitment of co-activators (N-CoAs). These co-activators facilitate chromatin decompaction through histone acetylation, facilitating the access of the transcriptional machinery and enabling gene transcription (Lavudi et al., 2023; Wu et al., 2024).

RA also binds to other nuclear receptors, such as peroxisome proliferator-activated receptors (PPARs), which are predominantly expressed in adipose tissue, brain, skin, and muscle. This interaction regulates genes involved in energy homeostasis, insulin response, and cell proliferation (Polcz & Barbul, 2019). Although RA primarily functions through transcriptional regulation, it also exerts non-genomic actions, such as intracellular calcium influx modulation (Wu et al., 2024).

Figure 16 – RA signaling mechanism

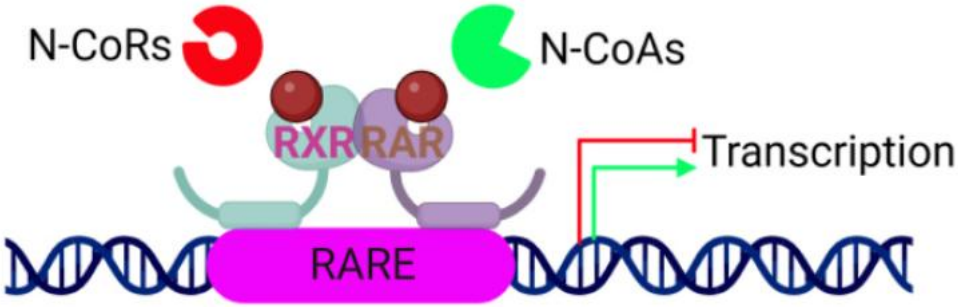

Source: Adapted from Wu et al. (2024).

The interest in using vitamin A and other retinoids for treating leishmaniasis resides in its immunomodulatory effect. Retinoids supplementation aims to increase the cell-mediated immune response, which is essential in combating intracellular pathogens (Ferreira et al., 2020). RA is the primary form in all tissues. In addition to natural ones, synthetic retinoids have been created, such as Tamibarotene, Palovarotene, or Adapalene, to improve the stability and reduce the toxicity of natural retinoids by targeting a specific retinoid receptor subtype. Another strategy to improve stability and decrease toxicity is RA encapsulation in nanosystems, which proved advantageous in various biomedical applications (Ferreira et al., 2020).

In the 1960s, the use of RA for treating skin disorders was awakened, and in the 1980s, their use was expanded in the treatment of cancers such as acute myeloid leukemia (AML) and cervical neoplasia. Interest in retinoids has grown over the past decades, as evidenced by more than 50 clinical trials (Ferreira et al., 2020). These trials primarily investigate retinoid's effects on cancer (28 trials), with a focus on hematologic malignancies (16 trials) and brain tumors (8 trials), as well as its role in skin conditions like acne, photoaging, and eczema (5 trials). Additionally, retinoids are being studied for inflammatory diseases, olfactory loss, and neuropsychiatric disorders (Ferreira et al., 2020).

Marketed formulations containing retinoids (Table 3) can be divided into two groups: topical, for the treatment of skin-related diseases, and oral, particularly for the treatment of skin diseases and cancer. Currently, formulations containing RA are marketed in the form of a gel, lotion, or cream for topical use in the treatment of acne and skin wrinkles under different brand names such as Altreno®, Renova®, and Retin-A®, ranging between 0.01 and 0.1% of RA (FDA, [n.d.]). It is also marketed as gelatin capsules (initially marketed under the brand name Vesanoid®) containing 10 mg of RA dispersed in soybean oil and adjuvants as the first line therapy in acute promyelocytic leukemia (APL) at the dose of 45 mg/m^2/day (Borges et al., 2021; Wu et al., 2024).

A liposomal formulation carrying RA intended to be delivered by IV route (Atragen® later renamed as ATRA-IV®) was also developed as a lyophilized powder containing RA and dimyristoyl phosphatidylcholine (DMPC) at a drug: lipid ratio of 1:10 and soybean oil (Wallace et al., 2000). Advantages of the liposomal-IV formulation were observed over the oral gelatin capsule, such as maintenance of RA plasma levels following ATRA-IV® administration, whereas a noticeable decline was observed with Vesanoid® (Ozpolat et al., 2003). Moreover, treatment with ATRA-IV® resulted in molecular remission in APL patients, an outcome not achieved with Vesanoid®. Additionally, ATRA-IV® was proven to be safe, with no significant adverse effects reported in patients. Nevertheless, the FDA declined to approve the drug due to the limited number of patients benefitting from this new formulation (Borges et al., 2021).

Table 3 – Marketed formulations containing retinoids.

Name/company	Composition	Indication	Year approved
9-cis RA (brand name: Panretin)/Eisai Inc.	Topical formulation; 0.05% or 0.1% gel containing alitretinoin	Cutaneous Kaposi's sarcoma; treatment of recalcitrant chronic hand dermatitis	2000
13-cis RA (brand name: Accutane)/Roche	Topical formulation; 0.05% and 0.1% cream	Photoaging and acne	1982
ATRA	Topical formulation; 0.05% cream	Photoaging and acne	1971
Gel microsphere formulation containing ATRA/Advanced Polymer Systems	Topical formulation; macroporous beads, 10–25 μm in diameter	Acne	1997
9-cis RA	Topical formulation; 0.1% gel	AIDS-related Kaposi's sarcoma	1999
Retinol	Topical formulation; 0.5–5% lotion, cream	Cosmetic	NA
Retinaldehyde	Topical formulation; 0.01, 0.015, 0.1% cream	Cosmetic	NA
ATRA (brand name: Vesanoid)/Roche	Oral formulation of tretinoin	Acute myeloid leukemia, in particular, acute promyelocytic leukemia	2000
Acitretin	Oral formulation	Psoriasis, disorders of keratinization	1997
13-cis RA	Oral formulation	Severe acne/related disorder	1982
Retinol	Oral formulation	Prevent/treat hypovitaminosis A	NA

Note: AIDS – acquired immunodeficiency syndrome; ATRA – all-trans retinoic acid; NA – not available.
Source: Adapted from Ferreira et al. (2020).

The high prevalence of poor diet and infectious disease regularly converges into a vicious cycle in socially vulnerable communities. Diets often fail to meet the recommended daily requirements, and significant losses caused by diarrhea, malabsorption, and parasitic infections can take place. In this sense nutritional deficiencies promote the progression of *Leishmania* infection, due to impacts on the host's immune state, and, in turn, it worsens malnutrition status (Custodio et al., 2018). The recommended dietary allowance (RDA) for adult men and women is 900 µg and 700 µg of retinol activity equivalents (RAEs) per day, respectively. During pregnancy and lactation, these values increase to 770 µg and 1300 µg RAE, respectively. Adults' tolerable upper intake is 3000 µg daily (NIH, 2025).

Retinoids related toxicity results in hypervitaminosis A, a condition caused by excessive retinoid exposure in humans and animals. Common signs include weight loss, alopecia, skin and mucosal dryness, lethargy, and bone fractures due to stimulated bone remodeling. Laboratory findings often show serum elevated alkaline phosphatase (ALP) and mild increases in liver enzymes (ALT and AST), though severe liver damage is uncommon. Mild anemia and slightly elevated blood triglycerides may also occur. Histologically, the bones and testes are the most frequently affected organs (Wallace et al., 2000).

Serum retinol concentration < 0.70 µmol/L indicates subclinical vitamin A deficiency (VAD) in children and adults, and a concentration of < 0.35 µmol/L indicates severe deficiency (WHO, 2009). Even though the global incidence of VAD decreased in the last decade, from 877,376,294.55 cases in 1990 to 489,662,708.61 cases in 2019, it remained high (Zhao et al., 2022). The main causes of VAD include inadequate intake of vitamin A-rich foods, poor intestinal absorption, and excessive excretion of the vitamin. Although malnutrition trends have shifted in recent years from undernutrition to excessive energy intake, the consumption of food rich in essential micronutrients, including vitamin A, especially in countries and territories with low socio-demographic index remains insufficient (Zhao et al., 2022).

Monteiro and colleagues (2021), in a cross-sectional study of 139 patients with VL performed in Piauí, Brazil, showed that VAD was linked to more severe cases of leishmaniasis and was prevalent among elderly populations. Additionally, VAD was associated with low hemoglobin levels and elevated C-reactive protein, contributing to anemia in affected individuals (Monteiro et al., 2021). Similar findings were made by Maciel et al. (2008) after the evaluation of 149 children divided into four groups: active VL cases (n = 20); patients recovered from VL (n = 33); asymptomatic patients (n = 40) and patients with no signs of VL (n = 56). Authors observed that patients with active VL had significantly lower vitamin A and highest C-reactive protein and alpha-1-acid glycoprotein levels (Maciel et al., 2008). Other

authors also observed that most VL patients had low serum vitamin A levels (Luz et al., 2001). Despite these findings, it is still difficult to establish whether low micronutrient levels are a risk factor for leishmaniasis or a consequence of the extended consumption process during the disease. Additionally, the impact of retinoids supplementation in therapeutic outcomes is still poorly understood (Custodio et al., 2018).

The supplementation in the active form, RA or derivatives, has been evaluated in different diseases, such as fungal infections, pneumocystis pneumonia, and Chagas disease. Pistoia et al. (2022) demonstrate that RA at 300 µg/mL acts as a fungicidal agent against *Candida albicans*, damaging the fungal membrane, while at 150 µg/mL, it has a fungistatic effect (Pistoia et al., 2022). Another interesting *in vitro* finding was RA fungistatic activity and synergistic effect with AmB against *Aspergillus Fumigatus* (Campione et al., 2016, 2021). In an invasive pulmonary aspergillosis model, RA treatment reduced mortality comparable to posaconazole, the current standard therapy. Mechanistically, the therapeutic benefit was explained via RA increase in macrophage phagocytic capacity and downregulation of heat shock protein 90 (Hsp90) expression, a key regulator of fungal stress response and drug resistance (Campione et al., 2021). RA also showed a beneficial effect on pneumonia, inducing myeloid-derived suppressor cell differentiation into alveolar macrophages and the clearance of *Pneumocystis* infection (Lei et al., 2013). In addition, 13-cis-retinoic acid, a RA analog, showed a trypanocidal effect against *Trypanosoma cruzi* by inhibiting polyamine transporter TcPAT12 (Reigada et al., 2017).

Few studies to date have investigated the use of retinoids in leishmaniasis therapy. Promising results were presented in a series of studies, showing that RA supplementation in *L. donovani*-infected macrophages restored macrophage cholesterol and reduced the parasite load. *Leishmania* parasites exploit the host's membrane cholesterol for the early infection establishment, impairing macrophage antigen-presenting ability. Authors proposed a mechanism to explain this effect based on RA increasing the mRNA expression of Niemann-Pick type C2 (npc2) and Niemann-Pick type C1 (npc1) genes involved in the uptake of extracellular cholesterol. NPC2 is a soluble protein that binds and mobilizes cholesterol within the lysosomal compartment. It subsequently transfers the sterol to NPC1, a transmembrane protein localized in the limiting membrane of lysosomes. NPC1 then facilitates the export of cholesterol from the lysosome to the cytoplasm, where it can be utilized for cellular functions. In *Leishmania donovani*-infected macrophages, RA-driven restoration of cholesterol primarily through the upregulation of this NPC2–NPC1-mediated pathway and is independent of

mammalian (or mechanistic) target of rapamycin complex 1 (mTORC1) signaling (Prakash et al., 2022; Prakash & Kumar Rai, 2022; Prakash & Rai, 2022, 2023).

On the other hand, the authors showed that RA inhibits the ergosterol synthesis pathway in parasites. Through computational and *in vitro* evaluations, they demonstrated that RA effectively inhibits sterol 24-C-methyltransferase (SMT), an essential enzyme required for zymosterol to ergosterol conversion. A dose-dependent decrease was observed following RA treatment (Prakash & Rai, 2023). Given these findings, authors pointed to a dual RA function: as an immunomodulator and a direct parasiticidal compound (Prakash et al., 2022; Prakash & Kumar Rai, 2022; Prakash & Rai, 2022, 2023).

Gogulamudi and collaborators demonstrated that vitamin D_3/RA and Chenodeoxycholic Acid (CDCA)/RA treatments reduce *L. donovani* infection by downregulating the tryptophan–aspartate containing coat (TACO) gene, which encodes the TACO phagosome coat protein. This inhibition prevented parasite entry and promoted early phagosome maturation in infected macrophages *in vitro* (Gogulamudi et al., 2015). In *L. donovani*-infected BALB/c mice, these treatments significantly reduced parasite load in the liver and spleen, particularly after 28 days of treatment. Additionally, they suppressed Th2 immune responses (IL-4, IL-5) while enhancing Th1 immunity (IL-2, IFN-γ, TNF-α) (Gogulamudi et al., 2019). In this sense, this study points to the RA mechanism of action illustrated in Figure 17.

Figure 17 – Potentially pathways involved in host immune modulation against *Leishmania* infection and parasite clearance with vitamin D_3/RA/CDCA molecules

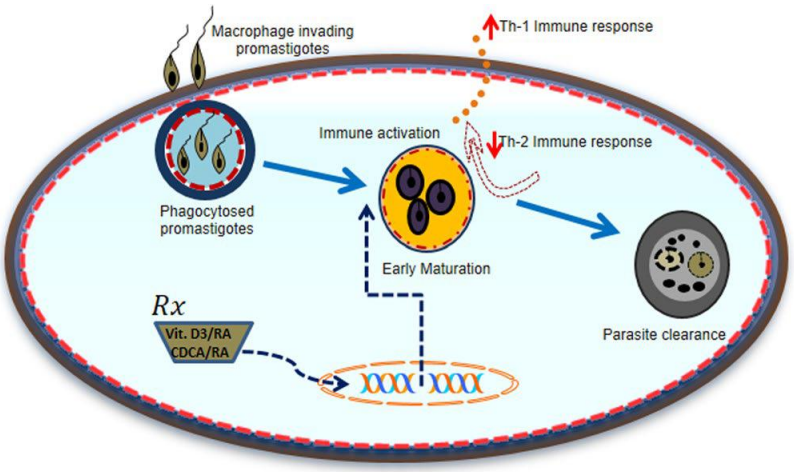

Note: *Leishmania* promastigotes bind to macrophages and are entered by phagocytosis. Vitamin D_3/RA and CDCA/RA treatment affect the early maturation of phagosomes by immune modulation towards the Th1 immune response and downregulation of the Th2 immune response, leading to parasite clearance. Source: Gogulamudi et al. (2019).

RA supplementation (0.5 nM) in a culture of splenocytes from dogs infected with *L. infantum* led to increased NO and ROS production after the addition of soluble *Leishmania* antigen. No change was observed in INF-γ levels, but there was an increase in TNF-α and a reduction in IL-10 levels, with a tendency to parasite load reduction (Hernandez et al., 2021). In another study, ornithine decarboxylase (ODC), a key enzyme in polyamine production, was reduced by RA treatment in *L. donovani* promastigote cultures. RA also inhibited parasite growth in a dose-dependent manner (Mukhopadhyay & Madhubala, 1994).

Contradictory results concerning RA influence on Th1 or Th2 immune response polarization have also been published. A research group showed M1-to-M2 transition in bone marrow-derived macrophages, after treatment with RA, leading to increased parasite survival (Pereira et al., 2011; Vellozo et al., 2017). Garg et al. (2004) evaluated the effects of vitamins A, B complex, C, E, and iron, alone or with SSG, in *L. donovani*-infected hamsters. Vitamin A (1 mg/kg) was tested as a prophylactic treatment for 15 days before infection, with some animals continuing supplementation for 30 days post-infection. Therapeutic effects were assessed by administering vitamin A (1mg/kg) and SSG (10 mg/kg) 30–35 days post-infection, following a similar protocol for other nutrients. Parasite burden was evaluated by spleen imprints. Results showed that only vitamin C, when used prophylactically, reduced parasite load, with or without SSG. In contrast, vitamin A worsened infection, whether given prophylactically or along with treatment, increasing spleen parasite levels. When combined with SSG, vitamin A reduced the treatment efficacy (Garg et al., 2004).

Cytokine levels were not assessed in this study, so it is not possible to correlate the response to the Th1/Th2 balance. It is important to note that vitamin A was administered orally and SSG intraperitoneally (IP) in this work. Thus, it is expected that the pharmacokinetics of these drugs were substantially different, as their arrival at the site of action, impacting the possible synergism of their combination (Borges et al., 2021).

In another study, authors found that vitamin A, when added to lymph node cells and T-cell lines derived from *L. major*-infected mice, selectively inhibited the secretion of type 1 cytokines (IFN-γ, GM-CSF, and IL-2) in a dose-dependent manner, while type 2 cytokines (IL-4 and IL-10) remained unaffected. This effect was associated with the inhibition of protein kinase C (PKC) activity. Notably, the inhibitory effect was observed in T cells but not in antigen-presenting cells (Frankenburg et al., 1998). On the other hand, Isakov showed that RA promoted PKC activation in T cells. The author demonstrated that inhibition, activation, or lack of effect can be observed depending on the retinoid (Isakov, 1988).

An interesting finding reveals a context-dependent role of vitamin A in leishmaniasis. *In vitro*, RA induced IL-10 production in T cells and monocytes from healthy children, but prevented its increase in cells from VL children when combined with Soluble *Leishmania* Antigen (SLA), suggesting that vitamin A modulates immune responses differently in infected and healthy individuals. In addition, serum retinol inversely correlated with IL-10 and TGF-β in Treg cells from VL children (Maciel et al., 2014).

Retinoids have also been investigated for their potential to promote healing, because they regulate cell growth and differentiation in the skin and stimulate fibroblast proliferation. Their deficiency results in abnormal epithelial keratinization (Polcz & Barbul, 2019). Enhanced RA tolerability, reduced skin reactions and irritation can be achieved by its encapsulation in nanosystems (Arantes et al., 2020), being an interesting agent in wound healing (Nazarnezhad et al., 2022), especially for topical application.

Drug repurposing is the favored approach to accelerate drug discovery in fields with limited funding and a pressing need for affordable treatments. This strategy involves identifying new therapeutic applications for approved drugs and mitigates the financial and developmental risks associated with traditional drug discovery (Reguera et al., 2019).

In summary, current data from studies on human and animal models regarding the role of vitamin A and retinoids in the outcome of *Leishmania spp*. infections are controversial. Few studies have focused on the relationship between nutritional state, immune system, and disease development. Meanwhile, malnutrition has been associated with severe disease due to poor immune status, contributing to the increased morbidity and mortality of leishmaniasis (Garg et al., 2004; Luz et al., 2001). In this context, the role of RA in the treatment of leishmaniasis deserves further investigation. This is the first study focusing on liposomal delivery of RA together with AmB.

2.3.3. *Nanotechnological approaches*

The concept of nanotechnology was introduced by Richard Feynman in 1959 (Salvioni et al., 2019) and is defined by the National Nanotechnology Initiative (NNI) as:

> the understanding and control of matter at the nanoscale, at dimensions between approximately 1 and 100 nanometers, where unique phenomena enable novel applications. Matter can exhibit unusual physical, chemical, and biological properties at the nanoscale, differing in important ways from the properties of bulk materials, single atoms, and molecules […] (NNI, [n.d.])

Despite its introduction in the 1950s, the application of nanotechnology to medicine was only successfully established in the 1990s. This interdisciplinary field of research is known as nanomedicine. It led to several biomedical applications, especially for disease treatment and diagnosis, as well as regenerative medicine and tissue engineering (Salvioni et al., 2019). The first nanomedicine was the PEGylated liposomal doxorubicin (Doxil® / Caelyx®), marketed in 1995 (Giordani et al., 2023).

For the preparation of nanosystems, various materials can be employed, such as lipids, natural or synthetic polymers, carbon, silica, or metals, but essential characteristics must be respected: non-toxicity, biocompatibility, stability, non-immunogenicity, non-thrombogenicity, and, if possible, biodegradability (Kopeckova et al., 2019). Based on these different materials, several types of nanosystems have been developed for biomedical applications, including lipid nanosystems (e.g., liposomes, emulsions, solid lipid nanoparticles, self-emulsifying drug delivery systems), inorganic nanosystems (e.g., carbon nanomaterials, gold nanoparticles), and polymeric nanosystems (e.g., dendrimers, micelles, nanofibers) (Kopeckova et al., 2019).

Following IV administration, nanosystems are immediately exposed to high concentrations of plasma proteins known as opsonins. Opsonization corresponds to the nanoparticle surface coating by antibodies and other plasma proteins, creating the protein corona that can modify their stability and surface properties and influence their metabolism. Opsonization triggers nanosystems recognition and clearance by MPS cells, one of the main players in eliminating nanoparticles (Salvioni et al., 2019; Wilhelm et al., 2016). As a result, opsonized nanosystems are passively targeted to the liver or spleen for metabolism and elimination, significantly reducing their circulation time.

One of the best-known strategies for increasing circulation time of nanocarriers is to graft hydrophilic polymers onto their surface, thereby reducing opsonin adsorption and, consequently, their capture by the MPS (Gatto et al., 2024). In this respect, the most widely used polymer is polyethylene glycol (PEG), formed by repeating ethylene oxide units produced in different configurations and molecular weights. PEG enables immunoevasion thanks to its hydrophilicity and steric repulsion effects, as seen in Figure 18 (Milton Harris et al., 2001).

Figure 18 – Liposome PEGylation prevents opsonization

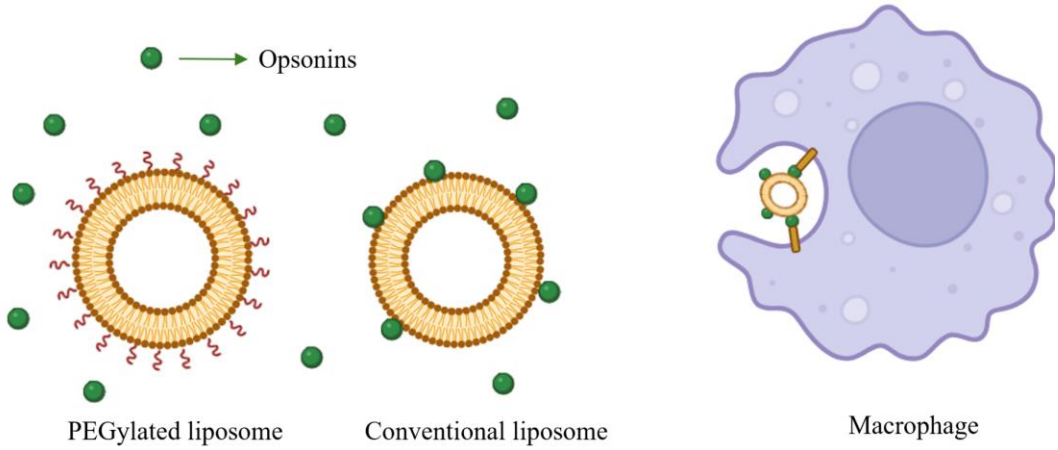

Source: Created with biorender.com.

The example of doxorubicin illustrates the PEG effect on drug pharmacokinetics. Free doxorubicin has a plasma half-life of 0.2 h, increasing to 2 – 3 h when encapsulated in non-PEGylated liposomes (Myocet™) and 41-70 h when encapsulated in PEGylated liposomes (Doxil®). In addition, plasma exposure is increased by 12 and 236 times for Myocet™ and Doxil®, respectively, compared with free drug (Hofheinz et al., 2005).

However, optimizing stealth nanoparticles is important to balance plasma half-life increase, bilayer packing and thermodynamic stability. For example, a dense layer of PEG can limit interaction with target cells and, in some patients, it is also responsible for complement activation and immune reactions (Hamad et al., 2008; Liu et al., 2022).

Nanocarriers face physical and biological barriers after administration that must be considered. Wilhelm et al. (2016) cite other barriers, such as diffusion, flow, shear, aggregation forces, phagocytic sequestration, and renal clearance, in addition to opsonization. So, all these factors can impact the percentage of nanoparticles reaching target cells. In addition, some physicochemical characteristics, shown in Figure 19, such as size, shape, charge, hydrophobicity, and nanocarriers targeting ligands, can influence particle absorption, distribution profile, and clearance. These properties can also affect nanocarriers' interaction with cells or proteins (Saleem et al., 2019; Salvioni et al., 2019).

Figure 19 – Tunable physical and chemical properties of nanocarriers

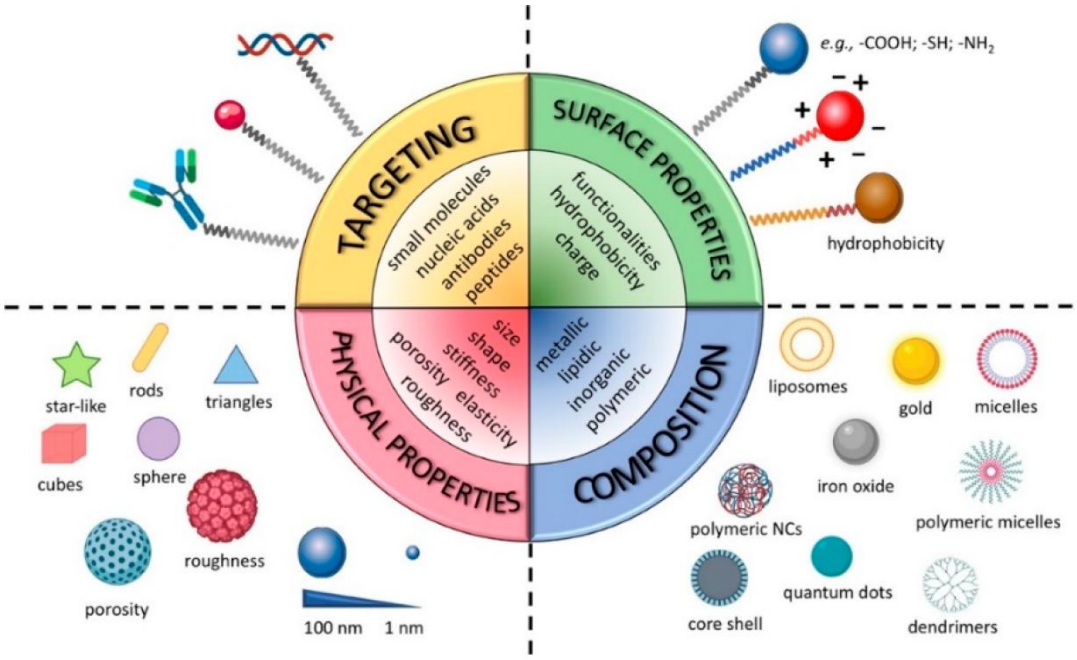

Source: Salvioni et al. (2019).

The use of nanostructured anti-*Leishmania* systems is an interesting strategy to deliver the necessary high drug concentration to MPS cells phagolysosome, where the parasite is hosted. As stated above, the body readily recognizes these colloidal systems as a natural immune process. Macrophages mainly internalize nanoparticles through phagocytosis, a type of endocytosis where particles larger than 0.75 µm in diameter are engulfed. Drug release inside the cell can favor a high local concentration and, ultimately, *Leishmania* death (Bruni et al., 2017; Saleem et al., 2019). This "passive targeting" is interesting, especially when the aim is to deliver the drug to the liver and spleen. However, the rapid clearance of nanoparticles from the bloodstream after IV administration may make it difficult to achieve adequate drug concentrations in organs such as the skin.

Advantages of drug nanocarriers approaches include the improvement in drug solubility, drug protection of the drug against degradation in biological fluids, and the possibility of drug administration via alternative routes to the parenteral route (Bruni et al., 2017). Several nanosystems have been developed in order to treat leishmaniasis, with special emphasis on liposomes, polymeric nanoparticles, solid lipid nanoparticles, nanoemulsion, and metallic nanoparticles, with chemotherapeutics currently used in the clinic or not (Saleem et al., 2019). Table 4 summarizes the advantages and limitations of each nanosystem.

Table 4 – Advantages and limitations of nanocarrier systems.

Nanocarrier	Advantages	Limitations
Liposomes	Ability to carry either hydrophilic or hydrophobic drugs, biocompatible, biodegradable, stable, possibility of surface functionalization	Toxicity because of drug leakage and displacement into the bloodstream; High production cost
Polymeric nanoparticles	Biocompatible, low toxicity, biodegradable, cost-effective, possible surface functionalization, avoids leakage of the drug	Difficult to scale up
Solid lipid nanoparticles (SLN)	Protect drug against harsh environmental conditions, easy scale-up, biocompatible	Low drug-loading efficacy due to its crystalline structure, there is a chance of drug expulsion during the storage of the crystalline structure and initial burst release can occur
Nanoemulsions	Stable, carry both hydrophobic and lipophilic drugs	Toxicity of surfactants
Metallic nanoparticles	Antibacterial, antifungal properties, stable, uniform structure	Toxicity

Source: Adapted from Saleem et al. (2019).

Numerous articles have been published in the literature evaluating nanosystems applied to leishmaniasis. A broad search on the PubMed platform, using the keywords ((nanoparticle OR nanocarrier OR nanosystem OR nanotechnology) AND (leishmaniasis OR leishmania OR "Leishmania infection" OR "Leishmania treatment" OR "anti-leishmanial")) returns 647 publications in the last decade (2015-2025). Although it represents robust research on the subject, just for comparison, a similar search, focusing on cancer and using the keywords ((nanoparticle OR nanocarrier OR nanosystem OR nanotechnology) AND (cancer OR neoplasm OR tumor OR carcinoma OR malignancy OR "oncologic treatment" OR "anticancer" OR "antitumor")) returns 87,213 results for the last 10 years (2015-2025). Of course, this is a direct and superficial comparison of two different domains with distinct impacts on public health, but it gives an idea of the investment in research in these domains.

Among the various systems already investigated in the treatment of leishmaniasis, liposomes are one of the most widely used due to their interesting properties (Saleem et al., 2019), which will be discussed in the next section.

2.3.3.1. *Liposomes as drug nanocarriers*

Liposomes are spherical nano vectors with a membrane morphology similar to human cell membranes, constituted of self-assembled natural and/or synthetic (phospho)lipids. The primary constituents are glycerophospholipids, amphiphilic lipids consisting of a glycerol backbone linked to a phosphate group, and two fatty acid chains, which can be either saturated or unsaturated. Additionally, the phosphate group may be attached to another organic molecule. Depending on this organic group, natural phospholipids are categorized into phosphatidic acid (PA), phosphatidylcholine (PC), phosphatidylethanolamine (PE), phosphatidylinositol (PI), phosphatidylglycerol (PG), and phosphatidylserine (PS) (Guimarães et al., 2021).

Due to their amphipathic character, these phospholipids can self-assemble to form stable bilayers in an aqueous environment, enclosing a central aqueous compartment. Within this vesicle, lipophilic, hydrophilic or amphiphilic agents can be trapped in the lipid membrane or the aqueous core, as illustrated in Figure 20 (Giordani et al., 2023). Liposomes can be divided into different types depending on their size or lamellarity. For example, Small Unilamellar Vesicles (SUV) have just one lamella and are 20 to 100 nm in size. Multilamellar vesicles (MLV), in turn, can have more than five lamellae and size > 500 nm (Liu et al., 2022).

Figure 20 – Configuration of a conventional liposome, encapsulating hydrophobic drugs in its lipid bilayer, hydrophilic drugs in its aqueous core, and amphiphilic drugs in both regions

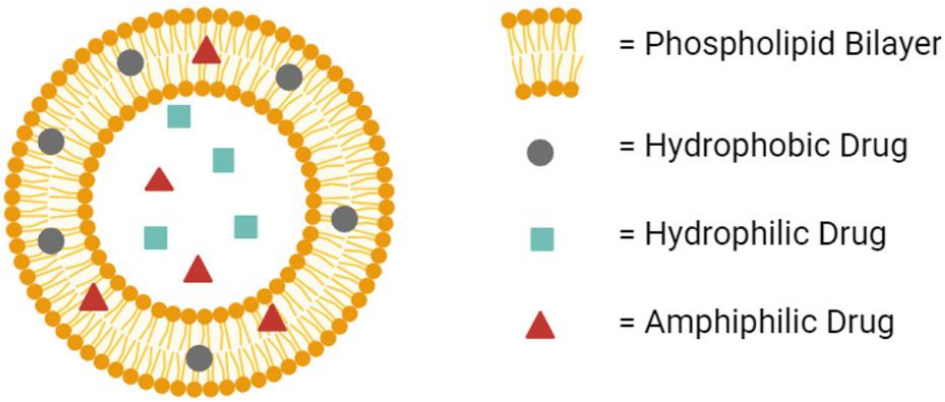

Source: Gatto et al. (2024).

In view of their attractive features, such as stability, biocompatibility, safety, drug protection from physiological degradation, and ability to carry several molecules with different physicochemical characteristics and prolong their half-life, liposomes have also been widely applied in the food and cosmetics industry (Liu et al., 2022). In the pharma industry, regarding the twenty liposomes-based formulations (Table 5) approved by the Food and Drug

Administration (FDA) and/or European Medicines Agency (EMA), the main application is in cancer therapy, but also involves infection, anesthesia, vaccine, lung disease, and photodynamic therapy (Giordani et al., 2023). According to a recent report, the global liposomal drugs market is predicted to reach USD 10.21 billion by 2032, nearly double that of 2024 (USD 5.31 billion) (Research, 2024).

Since their discovery by Bangham in the 1960s (Bangham et al., 1965) with the classical thin film hydration method, technologies in this field have evolved considerably, enabling the development of several preparation methods that include solvent injection techniques (ether/ethanol injection), reverse phase evaporation, detergent removal, supercritical fluid, dual asymmetric centrifugation, and microfluidics (Guimarães et al., 2021). A common step after liposome production is size-reduction techniques, as liposomes' size and size distribution are crucial factors for their performance and safety. Extrusion and high-pressure homogenization are among the most popular methods for this purpose (Liu et al., 2022). Thin film hydration and ethanol injection methods were used in this work as described in the next paragraph.

Table 5 – Summary of liposomal products approved by FDA and EMA, excluding lipid-drug complexes.

Type	Name	API	Approved year/area	Applications
Cancer therapy (Drug formulation)	Doxil®/Caely™	Doxorubicin	1995 (US) 1996 (EU)	Ovarian, breast cancer and Kaposi's sarcoma
	DaunoXome®	Daunorubicin	1996 (US, EU)	Kaposi's sarcoma
	Onivyde®	Irinotecan hydrochloride trihydrate	1996 (US) 2016	Pancreatic adenocarcinoma
	Myocet®	Doxorubicin	2000 (EU)	Breast cancer
	Mepact®	Mifamurtide	2009 (EU)	Osteosarcoma
	Marqibo®	Vincristine	2012 (US)	Leukemia
	Vyxeos®	Daunorubicin + cytarabine	2017 (US) 2018 (EU)	Leukemia
	Zolsketil®	Doxorubicin	2022 (EU)	Breast and ovarian cancer, multiple myeloma, Kaposi's sarcoma
Other application (Drug formulation)	AmBisome®	Amphotericin B	1997 (US, EU)	Fungal infections
	DepoCyt®	Cytarabine	1999 (US) 2001	Lymphomatous meningitis
	Visudyne®	Verteporfin	2000 (EU)	Age-related macular degeneration
	DepoDur®	Morphine sulfate	2004 (US)	Pain management
	Arikayce®	Amikacin	2018 (US, EU)	Lung infections
	Exparel®	Bupivacaine	2020 (EU)	Anesthesia
Vaccine	Epaxal®	Inactivated hepatitis A virus (RG-SB strain)	1994 (EU)	Hepatitis A
	Inflexal V®	Influenza virus surface antigens (haemagglutinin and neuraminidase), virosomal. 3 different strains.	1997 (EU)	Influenza
	Mosquiri™	Proteins found on the surface of the Plasmodium falciparum parasites and the hepatitis B virus	2015 (EU)	Malaria
	Shingrix®	Recombinant varicella-zoster virus glycoprotein E	2017 (US) 2018 (EU)	Shingles and post-herpetic neuralgia
	COMIRNATY™	mRNA	2021 (US, EU)	COVID-19
	SPIKEVAX™	mRNA	2022 (US, EU)	COVID-19

Source: Adapted from Giordani et al. (2023).

In the thin film hydration method, a thin film is obtained when the lipid–solvent solution evaporates during flask rotation under a vacuum. Then, an aqueous solution is added to hydrate the lipid film at a temperature above the lipids phase transition, forming a liposome suspension (Gatto et al., 2024; Liu et al., 2022). In the solvent-injection technique, the organic phase containing the lipids is injected into a large amount of aqueous buffer, leading to the spontaneous formation of liposomes as the solvent diffuses into the aqueous medium, generating interfacial turbulence. The organic solvent can then be eliminated through evaporation, lyophilization, dialysis, or diafiltration. Ethanol is often chosen as the organic solvent due to its safety profile (Liu et al., 2022).

During liposome preparation, drug loading can be done passively or actively. The passive loading method refers to the process where the drug is incorporated during liposome formation. Hydrophilic drugs are distributed within the aqueous phase, while hydrophobic drugs are located within the lipid bilayer. The active loading method, in turn, relies on generating a transmembrane pH or ion gradient that drives the drug through the lipid bilayer. This technique is performed after liposome formation (Guimarães et al., 2021).

Once prepared, some critical quality attributes (CQAs) should be assessed to ensure liposome safety and effectiveness. To candidate a liposome-based drug for market approval, the main CQAs include liposome composition, relative abundance of each compound, their degradation products, and impurities. Liposome morphology, size, polydispersity index (PdI), zeta potential (ZP), surface area, hydrophobicity, and surface coating must also be determined. Other important parameters are drug loading, drug release, and physicochemical stability (Liu et al., 2022). Regulatory documents for liposome market approval, offering an overview of the CQAs and the most common approaches used to assess these CQAs, have been published by international agencies, like the FDA in the United States (FDA, 2018) and EMA in Europe (EMA, 2013).

Different administration routes have been evaluated for liposomes delivery, such as parenteral, pulmonary, oral or transdermal. Furthermore, liposomes' passive and/or active targeting have been explored to deliver their payload more selectively (Liu et al., 2022). Passive targeting has mainly been applied in oncology, exploiting tumor environments. It relies on the preferential accumulation of liposomes ranging from 10 to 500 nm at the site of action due to inflamed tissues, leaky blood vessels and the lack of functional lymphatics. On the other hand, an integral vasculature in healthy tissues prevents the passage of these colloidal systems. This mechanism is known as the enhanced permeability and retention (EPR) effect. The passive targeting approach also takes advantage of liposomes' inherent properties, such as their surface

charge or size. However, the heterogeneity of the EPR effect within tumors and patients led to the search for active targeting. In active targeting, specific ligands are conjugated to the liposome's surface. Various targeting ligands have been used, including antibodies, nucleic acids, peptides, whole proteins, and small molecules like vitamins (Guimarães et al., 2021).

In the treatment of leishmaniasis, AmBisome® (conventional liposomal AmB) remains the only liposome currently approved for clinical use, while all other drugs encapsulated in this nanosystem are still in the experimental stages (Tuon et al., 2022). The primary target of antileishmanial therapy is amastigotes residing within macrophage phagolysosomes, but they are difficult to reach since drugs must cross significant structural barriers, such as the macrophage plasma membrane, the parasitophorous vacuole and the parasite plasma membrane, as illustrated in Figure 21 (Bruni et al., 2017).

Figure 21 – Liposome delivery of leishmanicidal drug to infected macrophages

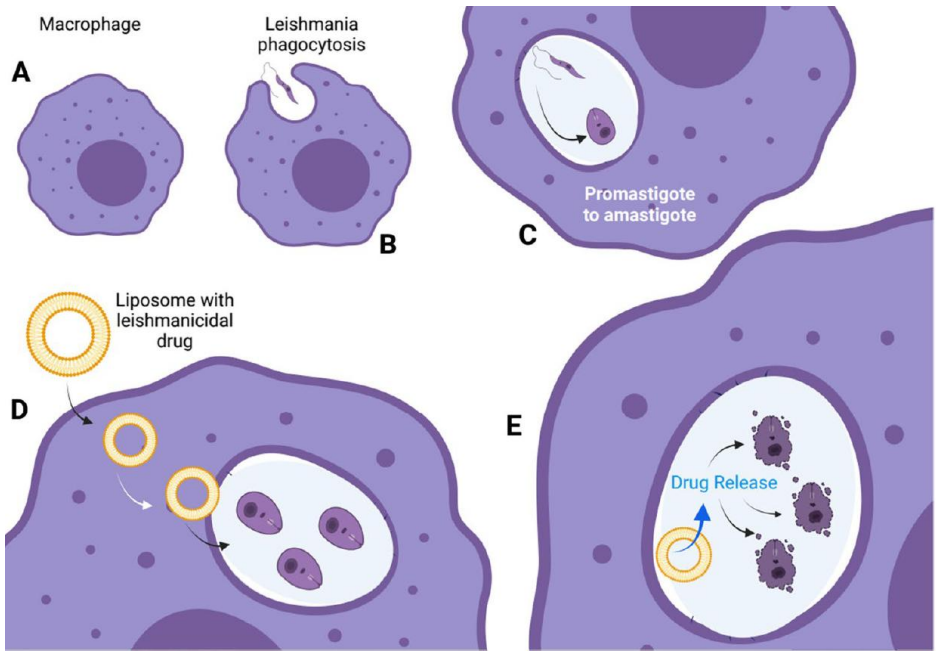

Note: In leishmaniasis, macrophages (A) are infected by the promastigote parasite form (B) that transforms inside the lysosome to the amastigote form (C). Liposome-encapsulated drugs with leishmanicidal activity are released in the lysosome (D) after the liposome enters the macrophage (E). Source: Tuon et al. (2022).

Since resident macrophages primarily clear conventional liposomes in the MPS system after systemic administration, they tend to accumulate mainly in key phagocytic organs such as the liver, spleen, bone marrow and lymph nodes (Bruni et al., 2017). These are the organs where parasites are commonly found in VL. Thus, this "passive delivery" could favor VL treatment.

Wijnant et al. (2018c), in a skin pharmacokinetic study, revealed that liposomal AmB (AmBisome®) can also accumulate more effectively at the lesion site in CL than micellar AmB

(Fungizone®). After a single IV dose of 1 mg AmB/kg, AmBisome® and Fungizone® had similar concentrations at the lesion site, but after five doses, AmBisome® levels were 3 times higher. In addition, infected mice's healthy back skin and lesion site (rump) showed AmB levels 5 times higher than those of uninfected ones for both formulations. In this study, the authors point out the important impact of CL infection on skin accumulation for liposomal and micellar AmB formulations. The increased drug accumulation is linked to inflammation, vascular leakage, and the migration of drug-carrying monocytes, resembling the EPR effect in cancer therapy.

Wijnant and colleagues (2018b, 2018c) also showed that liposome penetration into CL skin lesions may be influenced by the stage of the disease (papule > initial nodule > established nodule > healthy skin), by *Leishmania* species as a result of different local tissue inflammation, but also by liposome size, due to more prolonged circulation time of small-sized vesicles (Wijnant et al., 2018a, 2018b).

Our research group also hypothesized that long-circulating liposomal AmB may increase its efficacy against CL infections (Ramos et al., 2022). In this study, authors demonstrated that PEGylated liposomes can achieve greater efficacy than in-house AmB-conventional liposomes or AmBisome® by both parenteral and oral routes (Ramos et al., 2022). Despite the vesicle size being larger than the commercial formulation (~80 *vs* 130 nm), greater efficacy was achieved and attributed to the PEG-mediated long-circulation properties, which promote increased extravasation through the leaky capillaries within inflamed skin lesions (Ramos et al., 2022).

Given these interesting results, we sought to evaluate PEGylated liposomes carrying AmB, associated with RA, as an immunomodulator, to further enhance efficacy of CL therapy.

2.3.3.2. *Deformable liposomes*

Conventional liposomes struggle to traverse the stratum corneum (SC) in their intact form when topically applied, due to their limited membrane fluidity and elasticity. As a result, their penetration into the deeper skin layers is inefficient, and they tend to accumulate in the outermost regions of the epidermis (Sala et al., 2018). This drawback has prompted modifications in liposome composition and architecture, giving rise to new categories of lipid-based carriers, it means, deformable liposomes, in particular niosomes, transfersomes, and ethosomes (Hua, 2015).

Niosomes are lipid-based vesicles that incorporate non-ionic surfactants and contain a lower cholesterol content compared to traditional liposomes. While they share many structural similarities with liposomes, niosomes are generally regarded as more stable, offering improved drug encapsulation and reduced production costs (Hua, 2015; Yu et al., 2021).

Transfersomes, on the other hand, consist of four key elements: (i) phospholipids (mainly phosphatidylcholine), (ii) an adjuvant to improve permeation called edge activator (EA) such as surfactants (e.g. sodium deoxycholate and Tween® 80), (iii) ethanol in a lower percentage and (iv) water as a vehicle. The edge activator plays a key role as it disturbs the organization of the lipid bilayer, enhancing the vesicles' flexibility by lowering interfacial tension (Fernández-García et al., 2020a).

Ethosomes represent another class of lipid vesicles, characterized by a high ethanol content (ranging from 20% to 45%) in combination with phospholipids. Ethanol imparts softness and flexibility to the vesicles, improving their ability to penetrate deeper skin layers. Additionally, ethanol acts as a known permeation enhancer, potentially disturbing SC lipids organization by increasing their fluidity and reducing the density of intercellular lipid domains, amplifying this system's transdermal delivery capabilities (Sala et al., 2018).

The increased deformability of these vesicles, compared to conventional liposomes, can help them to pass through the narrow intercellular spaces of the SC, thereby facilitating deeper skin drug delivery (Fernández-García et al., 2020a; Sala et al., 2018), as illustrated in Figure 22. In response to mechanical stress, such as moving through pores smaller than the liposome's diameter, the EA components shift toward areas with greater curvature or stress. In contrast, phospholipids tend to concentrate in bilayer regions with lower curvature. These structural rearrangements enable deformable liposomes to traverse narrow pores without disassembling (Perez et al., 2016).

Figure 22 – Illustrative representation of permeation mechanisms of lipid-based vesicles

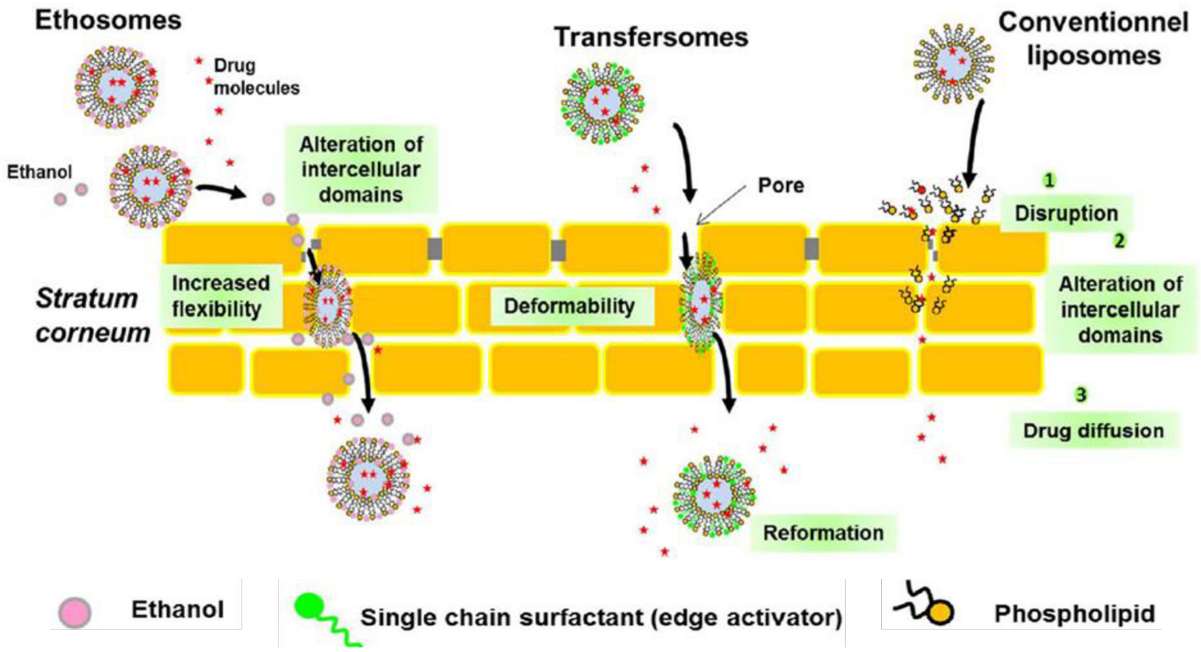

Source: Adapted from Sala et al. (2018).

The skin is the largest body organ, covering an area of 1.5−2 m^2 in adults, and acts as hydro and thermo-regulator in addition to be a protective barrier against external agents and UV radiation. It is organized into three primary layers: the epidermis, dermis, and hypodermis, each with distinct structural and functional roles (Cui et al., 2021; Fernández-García et al., 2020a; Yu et al., 2021).

Traditionally, the epidermis is segmented into distinct compartments, called (from deepest to most superficial): stratum basale, stratum spinosum, stratum granulosum, and SC. SC is the topmost layer with a thickness of 10−40 μm and is the main barrier to drug permeation, comprising layers of flattened and keratinized dead cells called corneocytes, embedded in a lipid matrix primarily made of ceramides, free fatty acids, and cholesterol, forming a “brick-and-mortar” structure (Cui et al., 2021; Sala et al., 2018). The remainder of the epidermis below the SC is the viable epidermis, containing different cell types, including keratinocytes (about 95%), as well as melanocytes, Langerhans cells, and Merkel cells. Beneath the epidermis lies the dermis (1–4 mm), a connective tissue rich in collagen and elastin, housing dermal dendritic cells, mast cells, blood vessels, nerve endings, hair follicles, sebaceous and sweat glands. This layer supports and nourishes the epidermis while providing strength and elasticity to the skin. The innermost layer, subcutaneous or hypodermis, consists largely of adipose tissue, providing thermal insulation and protection against external shocks (Cui et al., 2021; Sala et al., 2018).

In addition, it has been reported the existence of a skin metabolism, through enzymes such as peptidases and esterases that contribute to the biotransformation of endogenous compounds, including hormones and steroids, as well as the elimination of external molecules (Elmowafy, 2021).

Despite WHO efforts, no effective and safe topical treatment is available for CL (Dar et al., 2020). Neverthless, this route would be an interesting approach, as the topical drug delivery can reach affected tissues more efficiently with fewer adverse effects than parenteral or oral administration. In addition, topical formulations are usually more cost-effective option and provide greater patient compliance (Carneiro et al., 2012; Sala et al., 2018).

As previously stated, *Leishmania* parasites reside in the dermis in CL, so, an ideal topical formulation should be designed to reach dermis layer, while minimizing systemic passage (Jaafari et al., 2019). An important aspect of CL is that lesions usually evolve from a macule to ulcerate skin. This tissue damage and initial barrier impairment may enhance drug penetration, but the re-epithelialization during healing can pose additional challenges to maintain effective drug delivery through the skin. As such, an ideal formulation must be effective across all conditions: intact, partially, or completely damaged skin (Carneiro et al., 2012).

Some physicochemical properties of drugs are required for effective skin permeation. Optimal drug candidates typically have a molecular weight under 500 Da, a log *P* between 1–3, and a melting point below 200 °C (Yu et al., 2021). The ability to form hydrogen bonds and its degrees of ionization also must be considered (Elmowafy, 2021). These requirements explain why the development of topical formulations carrying AmB is very challenging. AmB has a high molecular weight (~ 924 Da), low aqueous solubility and a tendency to self-aggregation, leading to poor permeability across biological barriers, which cause retention in the SC with negligible amounts reaching the dermis layer (Perez et al., 2016). The 3% AmB cream (Anfoleish®) is a good exemple of AmB low permeation when topically applied. Only ~30% of patients fully healed after 28 days of treatment, despite its safety. Drug low transdermal permeation was confirmed by its absence in patient's plasma (López et al., 2018).

In this scenario, nanotechnology offers promising potential to enhance AmB delivery by modulating its physicochemical properties and improving skin penetration (Keservani & Santos, 2025). Some *in vivo* studies reported in the literature point to the successful use of liposomes, polymeric nanoparticles, cyclodextrin complex and nanostructured lipid carrier (NLC) carrying AmB and treating CL, as seen in Table 6. On the other hand, there are still no studies evaluating the topical administration of RA against CL.

Table 6 – Main studies of AmB-loaded nanocarriers to treat CL. (to be continued)

Composition	**Animal model (dose, regimen)**	***In vivo* outcomes**
AmB deoxycholate and Meglumine antimoniate (Glucantime®); Span 40; Tween 40; Cholesterol; Water; Carbopol® 934 and Triethanolamine.	BALB/c mice (uninformed, twice daily for 30 days).	Higher efficacy of the niosomes containing AmB-Meglumine antimoniate in experimental model of CL infected with *Leishmania major* (n = 6 per group), evidencing a significant reduction in lesion size compared to placebo (Carbopol® gel without drug) ($p < 0.001$) and compared to Glucantime® intramuscular ($p < 0.05$), although complete healing of the lesion was not observed. Additionally, the group treated with niosomes showed significant less ($p < 0.001$) parasite burden in spleen than placebo group.
AmB; Miltefosine; Phospholipon 90G; Tween-80; Phosphate buffered saline; Carbopol® 934 and Triethanolamine.	BALB/c mice (AmB 1.5 mg/kg/day, twice daily for 4 weeks).	The treatment with co-loaded AmB-Miltefosine ultra-deformable liposomes resulted in complete lesion resolution with no signs of scarring at the lesion site in BALB/c mice infected with *Leishmania mexicana* (n = 5 per group). Additionally, significant reduction ($p < 0.01$) in the parasite load on the skin was observed for this treated group, compared to all other groups: control group receiving Carbopol® gel, AmB gel or AmB in ultra-deformable liposomes alone.
AmB; Sodium deoxycholate; Soya phosphatidylcholine; Phosphate-buffered saline; Ethanol and Mannitol.	BALB/c mice (0.5 mg/mL, 20 mg of formulation/day, once a day for 10 consecutive days).	The experimental model of CL infected with *Leishmania amazonensis* (n = 4 per group) showed significant reduction ($p < 0.05$) in lesion size, compared to the control group (untreated) after treatment with transfersome-loaded AmB. The treated groups had an almost complete reduction in parasite load in lesion site.

Table 6 – Main studies of AmB-loaded nanocarriers to treat CL. (table completed)

Composition	**Animal model (dose, regimen)**	***In vivo* outcomes**
AmB; Glyceryl monostearate; Isopropyl myristate; Phospholipon 90G; Tween 80; Water; Carbopol® 934; Triethanolamine and Glycerol.	BALB/c mice (50 µL, 0.04% AmB, for 10 consecutive days).	Treatment with NLC delivering AmB led to a significant reduction ($p < 0.05$) of the parasite burden in lesion and lowest percentage increase in mean lesion size (mice infected with *Leishmania major*, n = 5 for treatment groups and n = 4 for control groups), even though a significant difference was not observed compared with the untreated control group.
AmB; γ-cyclodextrin; methyl cellulose and water.	Golden hamster (uninformed, twice daily for 21 consecutive days).	Higher reduction ($p < 0.05$) in lesion size with AmB-Cyclodextrin treatment, compared to the control group (untreated) in an experimental model of CL infected with *Leishmania amazonensis* (n = 6 per group).
AmB deoxycholate; Chitosan; Isobutyl cyanoacrylate and Pluronic F127.	BALB/c mice (uninformed, daily for 3 consecutive weeks).	The treatment with poly(isobutyl cyanoacrylate) nanoparticles coated with chitosan loading AmB showed partial healing of the lesion by histological analyzes after treatment of experimentally infected animals (*Leishmania major*, n = 6 per group). The treatment also led to the lowest parasitic load in skin, with significant reduction compared with the nontreated group.
AmB; Soya phosphatidylcholine; Cholesterol; Dimethyl sulfoxide; Propylene glycol; Oleic acid; Vitamin E; Methylparaben and Propylparaben.	BALB/c mice (50 mg liposomal AmB 0.4%, twice a day, for four weeks).	Higher efficacy of the liposomal formulation containing 0.4% AmB against *Leishmania major* in CL experimental model (n = 10 per group), showing significant reduction ($p < 0.001$) in lesion size, together with almost complete elimination of parasites in skin and spleens compared to mice treated with PBS or empty liposomes. No signs of kidney toxicity were observed in histopathological studies and no signs of irritancy was revealed in Draize test (skin and eyes).

Note: AmB – amphotericin B; NLC – nanostructured lipid carriers; CL – cutaneous leishmaniasis; PBS – phosphate-buffered saline. Source: Adapted from Keservani & Santos (2025).

The permeation of nanosystems through the skin depends on both the drug and formulation properties, such as lipid composition, particle size, and surface charge. Particle size is particularly important: particles with diameter ≥ 600 nm are not able to reach the deeper layers, those ≤ 300 nm can penetrate to some extent, and those ≤ 70 nm achieve the greatest passage (Hua, 2015). Factors related to the patient can also have an impact, such as age, skin condition and hydration level, application site and contact time (Sala et al., 2018).

The mechanisms by which lipid-based nanocarriers enhance drug deliver through the skin are not yet fully understood. Proposed explanations include: (i) penetration via skin appendages, such as hair follicles and sebaceous glands; (ii) desintegration on the skin surface, releasing this components to penetrate the SC with consequent fluidization and modification of SC lipids; (iii) occlusive effects that increase hydration and reduces corneocytes organization; (iv) and penetration in intact form using the intercellular route, throught the SC lipid matrix (Hua, 2015; Sala et al., 2018). These pathways can occur in a combined manner and are closely influenced by the nanosystem nature.

Drug combinations in topical CL treatment has been investigated, as seen in Table 6, but still under-explored. AmB was combined to meglumine antimoniate or miltefosine, searching for a synergistic effect (Table 6). In the present work, deformable liposomes, characterized as transfersomes were developed to deliver both AmB and RA.

3. OBJECTIVES

The present study aims to develop and characterize rigid and deformable liposomal formulations co-encapsulating AmB and RA as a novel therapeutic approach for CL.

To achieve this goal, the following specific objectives were established: to develop two distinct liposomal formulations—LAmB-RA, composed of rigid lipid bilayers, and DLAmB-RA, based on deformable liposomes; to characterize these formulations through comprehensive physicochemical analyses, including measurements of mean hydrodynamic diameter, polydispersity index (PdI), zeta potential (ZP), drug encapsulation efficiency (EE), and the aggregation state of AmB, given its impact on drug toxicity.

Another specific objective was to perform a preliminary stability study to monitor potential changes in colloidal properties over time, providing insight into the formulation's shelf-life. The next step was to assess the hemocompatibility of LAmB-RA by conducting an *in vitro* hemolysis assay using red blood cells (RBC), ensuring suitability for systemic administration. Subsequently, an *in vivo* pharmacokinetic study was carried out in healthy mice, employing a validated LC/MS method to quantify AmB in plasma and liver samples.

Finally, to evaluate the therapeutic efficacy of LAmB-RA, two CL murine models infected with *L. major* or *L. amazonensis* were used. Clinical outcomes were monitored by measuring lesion size growth and quantifying parasitic burden. Altogether, these evaluations aim to explore the potential of LAmB-RA and DLAmB-RA to treat CL effectively.

4. RESEARCH MOTIVATION

Leishmaniasis is endemic in more than 90 countries and territories, yet it is one of the most neglected diseases in the world, prolonging the cycle of poverty and social stigma. Given the drawbacks of existing therapies, which can lead to relapse, failure, and treatment abandonment, as well as disease high morbidity and wide geographical distribution, the need to develop new, more effective drugs is latent.

In addition, the lack of investment from private industry highlights the importance of academic research in this area. This work's main innovations lie in combining a potent chemotherapeutic agent, AmB, and a micronutrient obtained from retinol, RA, with potential immunomodulatory properties, into liposomes. Technological innovation is reinforced through the simplicity and high efficiency of the process developed by the Brazilian group for drug co-incorporation.

This proposal is also expected to overcome important limitations of existing treatments. Thus, the new topical formulations could be applied to treating pediatric patients. In contrast, the injectable formulations could treat severe patients, emphasizing immunocompromised ones. Therefore, this research could contribute to future technology transfer, an important goal in Brazil, where leishmaniasis is endemic, with the highest number of CL and VL cases in the Americas.

5. MATERIALS AND METHODS

5.1. Materials

Cholesterol (CHOL) was purchased from Sigma-Aldrich (St. Louis, MO, USA). Hydrogenated soybean phosphatidylcholine (HSPC), distearoylphosphatidylglycerol (DSPG), 1,2-distearoyl-sn-glycero-3-phosphoethanolamine-N-[methoxy (polyethylene glycol)-2000] (DSPE-PEG_{2000}), and Phospholipon® 90G (P90G) were obtained from Lipoid (Ludwigshafen, Germany). Sodium deoxycholate (DOC) was purchased from Sigma-Aldrich (St. Louis, MO, USA). AmBisome® was provided by Gilead Science Inc. (Foster City, CA, USA), and Anforicin B® by Laboratório Cristália (Itapira, São Paulo, Brazil). AmB solubilized was purchased from Sigma-Aldrich (A9528, USA). AmB (active pharmaceutical ingredient) was kindly provided by Laboratório Cristália (Itapira, São Paulo, Brazil). All-trans-retinoic acid (abbreviated as RA in this work) (SC200898) was purchased from Santa Cruz Biotechnology (Dallas, TX, USA). All other chemicals and reagents used in this study were of analytical grade.

5.2. Development of liposome formulation

5.2.1. *LAmB-RA*

LAmB-RA formulations were prepared through the incorporation of AmB and/or RA into pre-formed PEGylated liposomes made from HSPC:CHOL:DSPG:DSPE-PEG-2000 (5:2.5:2:0.5 molar ratio), using a modification of the method described by Ramos *et al*. (2022). A lipid film was first prepared and then hydrated in deionized water to form multilamellar liposomes at a final lipid concentration of 50 mM. These liposomes were transformed into unilamellar vesicles through repeated extrusions (5 times) across 200-nm and 100-nm pore-size polycarbonate membranes (Lipex® Extruder, Burnaby, BC, Canada). RA was first solubilized at 0.625 or 1.25 mg/mL with NaOH 0.1 M and protected from light for drug co-incorporation. Immediately after solubilization, 0.8 mL from RA-solution was added to 10 mg AmB under magnetic stirring. After that, 2 mL of pre-warmed (60 ºC) liposome suspension was added to the AmB-RA solution. The drug/liposome mixture was incubated at 60 ºC for 1 min 45 sec, followed by pH adjustment to 6.8 by adding 0.1 M acid HEPES solution. The final step was an incubation for 5 min at 60 ºC. Liposomes encapsulating AmB (LAmB) or RA (LRA) separately were prepared using the same protocol, except for adding one of the drugs. Empty liposomes (LEmpty) were also prepared using this protocol, but in the absence of any drug.

5.2.2. *DLAmB-RA*

DLAmB-RA formulations made from P90G:DOC:AmB:RA (7.68:1.92:0.27:0.13) were prepared using the ethanol injection method. For each 1 mL of formulation, the ethanolic phase (100 µL) was prepared containing 0.65 mg of RA and 95 mg of P90G. The aqueous phase (900 µL) comprised 8.88 mg of solubilized AmB (A9528, Sigma, USA), containing 45% AmB (4 mg) and 35% DOC (3,11 mg), the balance being sodium phosphate and sodium chloride. A further 9.89 mg of DOC was added to achieve 13 mg of surfactant. The organic phase was quickly injected into the aqueous phase using a syringe while stirring. The mixture was stirred for 10 min and then extruded (Mini-Extruder Kit, Avanti Polar Lipids, USA) 10 times through a 0.2 µm followed by 0.1 µm polycarbonate membranes. Deformable liposomes encapsulating only AmB (DLAmB) or RA (DLRA) were prepared using the same protocol. Empty deformable liposomes (DLEmpty) were also prepared using this protocol, in the absence of any drug. A micellar formulation containing only AmB (4 mg) and DOC (13 mg) was also prepared for comparison (AmB-DOC). A gelation test of the DLRA formulation was carried out with Natrosol, and the powder was added directly to the formulation under agitation for 10 min. The 0.5% (w/w) Natrosol concentration proved effective with a visual aspect suitable for topical application while maintaining size distribution (data not shown).

5.3. Physicochemical characterization of liposomal formulations

5.3.1. *Mean hydrodynamic diameter, polydispersity index, and zeta potential*

Nanocarriers' mean hydrodynamic diameter (size) and PdI were determined using the dynamic light scattering (DLS) method, with a fixed angle of 90° and a temperature of 25 °C. The ZP was determined by electrophoretic mobility analysis and DLS under the same conditions. All measurements were made using the Zetasizer Nano ZS90 (Malvern, UK). Formulations were previously diluted at a 1:100 ratio in deionized water for size measurement and 0.9% NaCl for ZP.

5.3.2. *Determination of AmB and RA encapsulation rates*

The analytical method used to quantify AmB and RA simultaneously followed the literature (Mansur-Alves et al., 2022; Marques Borges et al., 2020; Pharmacopeia, 2021). Method evaluations followed the guidelines outlined in the ANVISA RDC Nº 166, 2017 (ANVISA, 2017). AmB and RA quantification using high-performance liquid chromatography coupled to

a diode array detector (HPLC/DAD) was carried out in an Agilent 1260 series chromatograph (CA, USA) equipped with degasser, quaternary pump (G1311B), autoinjector (G1329B), thermostated column compartment (G1316A), diode array detector (DAD; G4212B) and EzChrom software. Analyses were conducted using a 1 mL/min flow rate, a Discovery® C18 column (250 × 4.6 mm; 5 µm), and a mobile phase consisting of acetonitrile: methanol: citric acid solution (4,2 g/L) pH 6 (48: 12: 40) with gradient. The injection volume was 20 µL. AmB and RA maximum absorption wavelengths chosen for detection were 405 and 340 nm, respectively. AmB and RA illustrative chromatograms are shown in Figure 23.

AmB and RA content (%) was determined by comparing unfiltered liposomes peak area (A_{unf}) with drug standard peak area ($A_{standard}$) at the same concentration, which means 10 µg/mL for AmB and 0.5 µg/mL for RA in rigid liposomes and 5 µg/mL for AmB and 0.8 µg/mL for RA in deformable ones, as seen in Equation 1. The encapsulation efficiency ($EE_{(\%)}$), in turn, was determined by comparing AmB and RA peak areas before liposome filtration (A_{unf}) and after filtration (A_f) using a polyvinylidene fluoride (PVDF) membrane filter (0.45 µm; Millipore, USA). This filtration eliminates the possible drug crystals formed (free drug). $EE_{(\%)}$ was calculated using Equation 2.

$$\text{Content}_{(\%)} = \frac{A_{unf}}{A_{standard}} \cdot 100 \quad (1)$$

$$EE_{(\%)} = \frac{A_f}{A_{unf}} \cdot 100 \quad (2)$$

Figure 23 – AmB and RA illustrative chromatogram

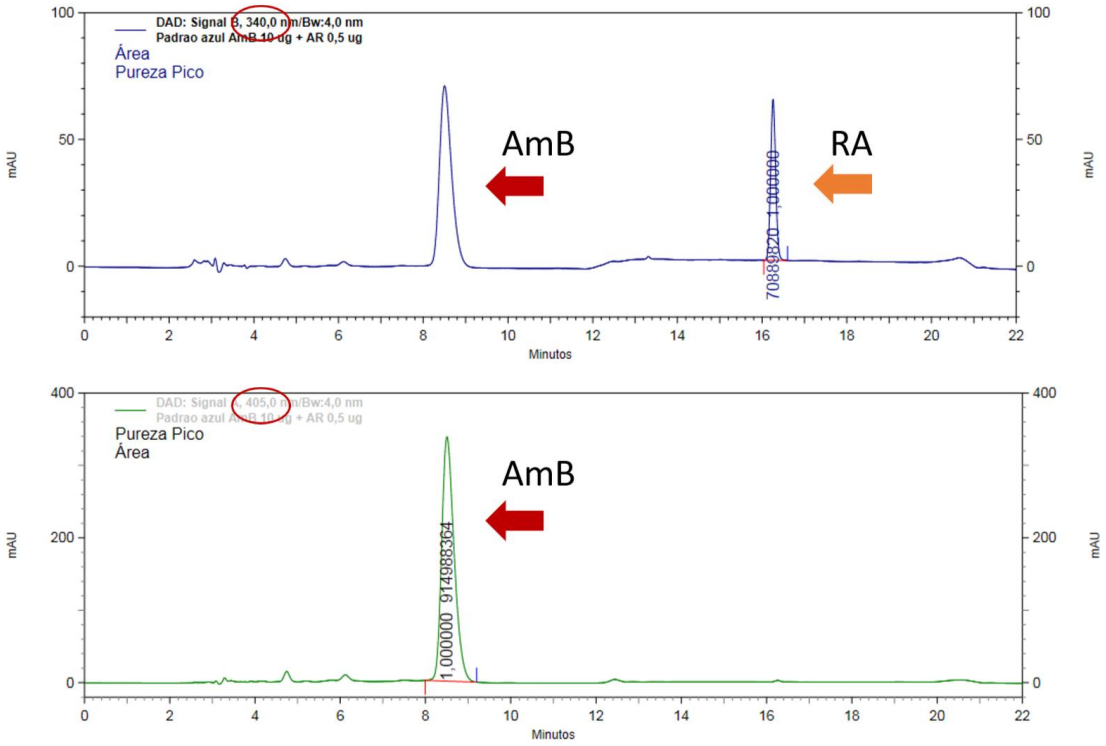

Note: Chromatogram of AmB standard at 10 µg/mL and RA at 0.5 µg/mL. AmB peak was observed at RT of 8.5 min, while RA was at 16.26 min.

5.3.3. *Preliminary study of the formulation stability*

5.3.3.1. *LAmB-RA*

This preliminary study of stability was conducted after in-house formulation preparation (LRA, LAmB, and LAmB-RA) and 30 days of storage in a refrigerator at 4 ºC. The formulations (n = 5 independent batches) were stored in glass containers under a nitrogen atmosphere. The size, PdI, ZP, and $EE_{(\%)}$ measurements were performed as described above (5.3.1 and 5.3.2). The AmB aggregation state was also evaluated. The evaluation was carried out by UV/Vis spectrophotometry and circular dichroism (CD), according to the literature (Ramos et al., 2022). In-house liposomal formulations were diluted 580-fold in PBS to obtain AmB 5 µg/mL. The commercial formulations AmBisome® and Anforicin B® (n = 1) were also evaluated for comparison purposes, being prepared according to the package leaflet, with reconstitution in ultrapure water, then diluted in 5% glucose to a concentration of 2 mg/mL AmB. Next, the AmBisome® and Anforicin B® preparations were diluted in PBS to obtain AmB 5 µg/mL. The absorption and CD spectra were obtained in triplicate and recorded in a 1.0-cm path-length quartz cuvette in the wavelength range from 300 to 450 nm. Spectra were recorded just after

dilution at 25 ºC under a nitrogen atmosphere on a computer-assisted Chirascan™spectropolarimeter (Applied Photophysics, Leatherhead, UK). The final spectra were obtained after PBS spectrum subtraction from sample spectra. The DC signal was smoothed using a factor of 4. No signal was observed for LEmpty. It should be noted that in-house formulations were not lyophilized like commercial AmB formulations.

5.3.3.2. *DLAmB-RA*

This preliminary study of stability was conducted after formulation preparation (DLRA, DLAmB, and DLAmB-RA) and 20 days of storage in a Biochemical Oxygen Demand (BOD) chamber at 25 ºC. The formulations (n = 3) were stored in glass containers under a nitrogen atmosphere. The size, PdI, ZP, and $EE_{(\%)}$ measurements were evaluated as previously described to assess the formulations' physicochemical characteristics. Due to the small volume of deformable formulations (1 mL) and since it was extruded through 0.1 µm polycarbonate membrane just before analysis, at time zero (T0), $EE_{(\%)}$ of AmB and RA were considered equal to the formulation content. The AmB aggregation state was evaluated at T7 as described in the 5.3.3.1 topic. The final spectra were obtained after PBS spectrum subtraction from sample spectra. No signal was observed for DLEmpty.

5.4. *In vitro* hemolytic activity of LAmB-RA

Hemolytic activity *in vivo* was carried out as previously described by Mansur-Alves et al. (2022). To separate RBC, rabbit blood in sodium citrate was centrifugated at 3,000 *g* for 5 min at 4 ◦C. The supernatant and the buffy coat were discarded, and RBC were washed with PBS pH 7.4 and centrifuged again; this procedure was performed twice. Two volumes of RBC were mixed with 11 parts of PBS pH 7.4 to obtain a stock suspension.

Subsequently, 1 mL of the RBC stock suspension was mixed with 1 mL of diluted formulations (LAmB, LRA, LAmB-RA, AmBisome® and Anforicin B®) in PBS pH 7.4 containing 20, 40, 75, 140, and 250 µg/mL of the AmB equivalent. Each concentration was tested in triplicate. RBC mixed with ultrapure water and PBS were used as positive and negative controls, respectively. Samples were incubated at 37 ºC for 3 h in a shaker bath and then centrifuged at 1,700 *g* for 10 min to separate the supernatant, which was allowed to stand at room temperature for 30 min to oxidize hemoglobin. Oxygenated hemoglobin absorbance was measured in a spectrophotometer (Evolution 201 UV-Visible Spectrophotometer, Thermo Fisher Scientific) at 540 nm. The hemolysis percentage ($H_{(\%)}$) was calculated using Equation 3.

$$H_{(\%)} = \frac{AB_s - AB_0}{AB_{100} - AB_0} \cdot 100 \quad (3)$$

Where AB_s is the sample absorbance, and AB_{100} and AB_0 are the absorbance of the positive and negative controls, in that order.

5.5. Pharmacokinetic study of LAmB-RA

5.5.1. *Treatment of animals and samples collection*

Female Swiss mice (4–6 weeks old) from Janvier Labs were randomly divided into three groups (n = 5 mice per group): LAmB, LAmB-RA, and AmBisome®. The animals received a single dose equivalent to 1 mg/kg of AmB by IV. Blood and liver were collected at 5 min, 0.5 h, 1 h, 4 h, and 24 h post-injection. The blood was collected by intracardiac puncture in microtubes containing 0.1 M EDTA. Blood was centrifuged at 1,400 *g* for 10 min, and the plasma samples (supernatant) and livers were frozen at -80 ºC until analysis. The experimental protocol was approved by the Ethical Committee for Animal Experimentation with the protocol number #30494-2021031617294635v1.

5.5.2. *Plasma sample preparation*

Plasma sample preparation was carried out by protein precipitation according to the protocol proposed by Pippa et al. (2021). Plasma aliquots of 25 µL were prepared by adding 25 µL of Internal Standard (IS) in methanol (piroxicam, 140 ng/mL), 25 µL of methanol, and 100 µL of 0.1% formic acid in methanol. Microtubes were shaken for 5 sec, then centrifuged at 4 °C for 15 min at 19,090 *g*. Next, 100 µL of the supernatant was transferred to the injection vial and mixed with 100 µL of 0.1% formic acid in water. 5 µL of the final mixture was subjected to chromatographic analysis. Standard calibration curves were prepared using plasma from untreated mice.

5.5.3. *Liver sample preparation*

Liver sample preparation was carried out using protein precipitation as described in the literature (Vogelsinger et al., 2006; Wang et al., 2021). The liver was manually macerated using a glass rod to obtain a homogenate. In a first step, a liver aliquot (200 ± 10 mg) was collected, then 50 µL of IS (piroxicam, 1,120 ng/mL) and 350 µL of methanol were added. This mixture was vortexed for 10 s and centrifuged at 4 °C for 15 min at 19,090 *g*. After that, 200 µL of the

supernatant was transferred to a microtube, and 25 µL was used for the second step. The second step was similar to the plasma preparation described above. Briefly, liver supernatant aliquots of 25 µL were prepared by adding 50 µL of methanol and 100 µL of 0.1% formic acid in methanol. Microtubes were shaken for 5 sec, then centrifuged at 4 °C for 15 min at 19,090 *g*. Next, 100 µL of the supernatant was transferred to the injection vial and mixed with 100 µL of the mobile phase. 5 µL of the final mixture was subjected to chromatographic analysis. Standard calibration curves were prepared using liver from untreated mice.

5.5.4. *Bioanalytical method validation*

A bioanalytical method was validated to determine AmB concentration in plasma and liver, employing high-performance liquid chromatography Vanquish Flex (Thermo Scientific, Boston USA) coupled to a mass spectrometer (LC-MS/MS). The analyses were conducted using a C8 column (150 × 2.1 mm; 4 µm), mobile phase composed of Methanol: Acetonitrile: Water: Formic acid (15: 40: 45: 0.1), and a 0.5 mL/min flow rate. The mass spectrophotometer Orbitrap Exploris 120 (Thermo Scientific, Boston, USA) from Drug and Metabolite Analysis Service (SAMM Platform) operating in heated electrospray ion source (HESI-II) mode was used. The quantification mode was targeted-tandem mass spectrometry (t-MS2). Each targeted compound is detected in its chromatographic segment using an inclusion mass list. The quadrupole selects the precursor ions with an isolation window of $m/z = 2$.

MS/MS analysis was performed using the positive ionization mode. The capillary voltage for electrospray ionization was set at 3.80 kV. The ion transfer tube and vaporizer temperatures were kept constant at 350 °C and 345 °C, respectively. The sheath and auxiliary gas flow rates were set at 45 and 15, respectively. Normalized High Collision Energy Dissociation (HCD) was used for collision purposes, 11% for AmB and 39% for piroxicam (IS). Even though piroxicam does not have much structural similarity to AmB, it was successfully used as IS in the literature for AmB quantification in plasma samples (Pippa et al., 2021).

The mass resolution was set at 120,000. MS^2 spectrum was registered between *m/z* 200 and 955 for AmB and between *m/z* 50 and 363 for the IS. The ion m/z 906.48, corresponding to the $[M + H - H_2O]^+$ adduct of AmB, was selected as the precursor ion for targeted MS^2 analysis. This ion is commonly formed during electrospray ionization due to the spontaneous dehydration of the protonated molecule, a well-known behavior of AmB (Dar et al., 2020). Due

to its stability and specificity, the resulting fragment ion at m/z 743.40 was selected for quantification. The signal of the daughter ion was extracted from the MS^2 spectrum (Table 7).

In the development of the analytical method for dosing AmB, the linearity of AmB in plasma was evaluated using five concentration levels, each analyzed in triplicate, ranging from 5 to 2160 ng/mL; in liver, concentrations ranged from 5 to 720 ng/mL, the matrix effect at a low concentration of AmB (20 ng/mL) and a high concentration (2160 ng/mL) was evaluated, as well as precision and accuracy. Sample stability was evaluated for 24 hours in an auto-injector (7 ºC) and after freezing at -80 ºC. Plasma samples were also evaluated during 2 cycles of freezing at -80 ºC and thawing at room temperature. In addition, selectivity and carry-over were evaluated. Validation was based on the Guideline on bioanalytical method validation (EMA, 2012) and in the literature (Pippa et al., 2021; Su et al., 2018). AmB and IS representative chromatograms and mass spectrums in plasma (Figure 24) and liver (Figure 25) samples are presented below.

The model that best fitted the plasma concentration-time data and the pharmacokinetic parameters was determined using the Rstrip 4.03 computer software. Fitted parameters included the early elimination phase half-life ($t_{1/2\alpha}$), the terminal phase half-life ($t_{1/2\beta}$), the area under the blood concentration-time curve, the mean residence time projected to infinity, and the elimination rate constant (Schettini et al., 2006).

Table 7 – MS/MS parameters used to quantify AmB in plasma and liver.

Analyte	Parent Ion	Extracted ion mass range	HCD (%)
AmB	906.4846	743.37 – 743.43	11
IS	332.07	95.058 – 95.062	39

Figure 24 – Representative chromatograms of AmB (a) and IS (c), and corresponding mass spectra (b, d) in plasma

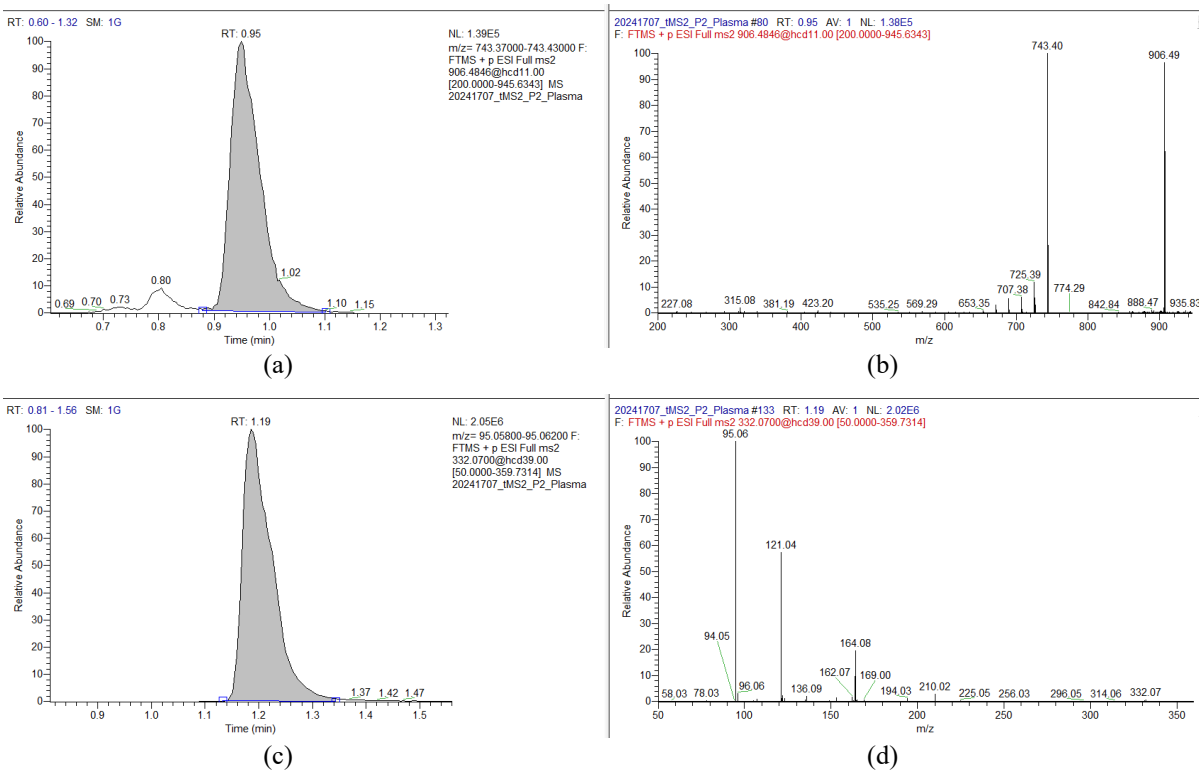

Note: Chromatogram and mass spectrum correspond to AmB and IS at 10 ng/mL concentration. The chromatographic peak for AmB corresponds to fragment ions detected at *m/z* 743.40 with a retention time (RT) of 0.95 min. For IS, fragment ions were detected at m/z 95.06 with RT 1.19 min.

Figure 25 – Representative chromatograms of AmB (a) and IS (c), and corresponding mass spectra (b, d) in liver

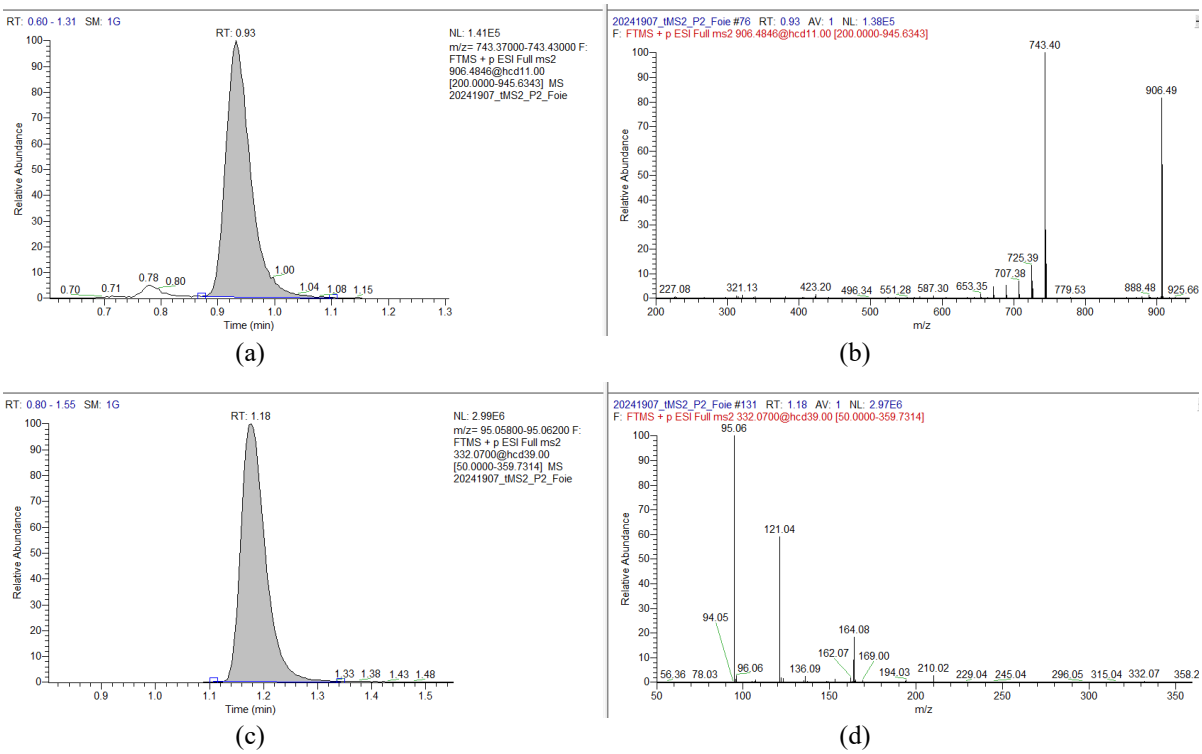

Note: Chromatogram and mass spectrum correspond to AmB and IS at 10 ng/mL concentration. The chromatographic peak for AmB corresponds to fragment ions detected at *m/z* 743.40 with a RT of 0.93 min. For IS, fragment ions were detected at m/z 95.06 with RT 1.18 min.

5.6. Assessment of LAmB-RA antileishmanial efficacy *in vivo*

5.6.1. *Infection of animals and treatment protocols*

Female BALB/c mice (4–6 weeks old) from Janvier Labs were infected subcutaneously at the tail's base with 100 µL of a suspension containing 1×10^7 *L. major* (MHOM/PT/92/CRE26) late-log promastigotes. After lesions development (27 days post-infection), animals were divided into six groups (n = 8 for each group, and n = 10 for Control), as follows: Group 1 - Control (untreated); Group 2 - LEmpty; Group 3 - LRA (0.25 mg/kg); Group 4 - LAmB (5 mg/kg); Group 5 - LAmB-RA (5 mg/kg - 0.25 mg/kg); and Group 6 - AmBisome® (5 mg/kg). Animals were treated IP (0.2 mL) every 2 days for 18 days. The experimental protocol was approved by the Ethical Committee for Animal Experimentation with protocol number #30494-2021031617294635v1.

In the CL murine model using *L. amazonensis* (IFLA/BR/1967/PH8), female BALB/c mice (4–6 weeks old) from Bioterism Center (Cebio, UFMG) were infected subcutaneously at the tail's base with amastigotes freshly recovered from infected hamster's paw, as previously described (Kawakami et al., 2021). Free access to a standard diet was allowed, and tap water was supplied *ad libitum*. After lesions development (44 days post-infection), animals were divided in five groups of 7 animals each: Group 1 - Control (untreated); Group 2 - LEmpty; Group 3 - LAmB at 5 mg AmB/kg; Group 4 - LAmB-RA at 5 mg AmB/kg and 0.25 mg RA/kg; and Group 5 - AmBisome® at 5 mg AmB/kg. Animals were treated by IP (0.2 mL) for 24 days, receiving administrations every 2 days. UFMG Ethical Committee for Animal Experimentation approved this study with protocol number 331/2022.

5.6.2. *Lesion size measurement*

Lesion size was determined with a caliper by obtaining the average diameter traced from one lesion border to another (Mansur-Alves et al., 2022). The lesion size growth was calculated for each animal based on the difference in the average lesion size during treatment and the 1st day of treatment. Lesions were photographed for qualitative comparison.

5.6.3. *Parasite load quantification*

In CL murine model using *L. major,* mice were euthanized three days after the end of treatment, and skin samples around the lesions were collected for each ainimal to evaluate the parasitic load by quantifying the *Leishmania* genomes using real-time PCR (qPCR), as previously

described (Malli et al., 2019). DNA was extracted from mouse skin using the QIAamp® DNA Mini Kit (Qiagen, Hilden, Germany), according to the manufacturer's instructions. Briefly, DNA extraction was done from skin samples (15 ± 5 mg) previously cut into tiny pieces, mixed with lysis buffer and Proteinase K, and incubated at 56 °C overnight. The concentration and purity of extracts were measured by UV spectrophotometry (absorbance at 280 and 260 nm) and DNA concentrations were adjusted to 5 ng/µL. For parasite load quantification, qPCR was performed in a CFX96 thermal cycler (Bio-Rad, USA) using the SSoADV Univer SYBR® Green Supermix (Bio-Rad, USA), from 4 µL of each sample in a 10-µL reaction volume. Each oligonucleotide, i.e. forward (5'-AAGTGCTTTCCCATCGCAACT-3') and reverse (5'-GACGCACTAAACCCCTCCAA-3') primers, designed for amplifying a short fragment of 18S rDNA gene in *Leishmania* (Malli et al., 2019), was used at 0.5-µM final concentration. The standard curve was obtained from serial dilutions of known copy numbers of *Leishmania* genomes, using DNA extracted from a culture of *L. major* (MHOM/PT/92/CRE26). Data are presented as numbers of *Leishmania* genomes per µg of total DNA.

Parasite load was similarly assessed for the *L. amazonensis* murine model. Mice were euthanized three days after the end of treatment. The spleen was immediately removed to evaluate the parasitic load as described previously (Carregal et al., 2019). DNA was extracted using the PureLink® Genomic DNA Mini Kit (Invitrogen, USA) according to the manufacturer's instructions. Briefly, DNA was extracted from an aliquot of spleen which was macerated before mixing with lysis buffer and Proteinase K, and incubated at 56 ºC overnight. The DNA concentrations were measured by spectrophotometry (absorbance at 280 and 260 nm) and adjusted to 5 ng/µL. The qPCR was performed in a Quantstudio 3 real-time PCR system (Applied Biosystems) using the PowerUp™ SYBR™ Green Master Mix (Invitrogen, USA), from 1 µL of each sample in a 10-µL reaction volume containing 10 pmol of each oligonucleotide, i.e. forward (5'-CGT GGGGGAGGGGCGTTCT-3') and reverse (5'-CCGAAGCAGCCGCCCCTATT-3') primers constructed for amplification of the mini-circle region present in the kinetoplast DNA (kDNA) (Carregal et al., 2019). The standard curve was obtained with serial dilutions of known DNA concentrations of *L. amazonensis* (IFLA/BR/1967/PH8) extracted from promastigote culture. Data are presented as nanogram (ng) amount of *Leishmania* DNA per µg of total DNA.

5.6.4. *Cytokine profile determination*

In *L. major* infected mice, a liver fraction (weighing approximately 200 mg) was collected after treatment and further macerated and homogenized using a glass rod in 1 mL of lysis buffer containing 50 mM Tris-base pH 7.4, 150 mM NaCl, and 5 mM EDTA. Buffer was supplemented with 1% Nonidet P-40, 1 mM PMSF, and a protease inhibitor cocktail (P8340, Sigma-Aldrich, USA). Liver homogenates were kept for 30 min on ice, then centrifuged for 10 min at 10,000 *g* and 4 ˚C. Supernatants were collected and stored at -20 ˚C until the next day for ELISA and bead-based cytokine quantification assay (Helou et al., 2021). Before analysis, samples were centrifuged for 2 min at 10,000 *g* at 4 ˚C to exclude potential debris. IFN-γ quantification was performed using the ELISA Max Standard set (BioLegend, USA). A panel of cytokines and chemokines: transforming growth factor-β (TGF-β1), CCL22, IL-10, IL-6, and granulocyte colony-stimulation factor (G-CSF) was assessed using the LEGENDplex bead-based immunoassay according to the manufacturer's instructions (BioLegend, USA).

In the CL murine model using *L. amazonensis* the spleen was used to assess the immune response. The spleen was macerated and homogenized, and the obtained cell suspension was adjusted at 5×10^6 cells/mL in RPMI supplemented with 10% of fetal bovine serum. Splenocytes were incubated in the absence or presence of different stimuli: Soluble *Leishmania* Antigen (SLA) - 50 µg/mL; Concanavalin A (ConA) - 10 µg/mL and Retinoic Acid (RA) - 0.5 nM for 48 h at 37 °C, 5% CO_2. The culture medium itself was used as a negative control. The concentrations of IFN-γ and IL-10 in the cell culture supernatants were performed by ELISA using the OptEIA™ Mouse Kit (BD Biosciences, USA) according to the manufacturer's instructions (Hernandez et al., 2021; Oliveira et al., 2022).

For SLA preparation, *L. amazonensis* parasites obtained from cultures at the beginning of the stationary growth phase were washed twice with PBS by centrifugation at 1,540 *g*, at 4 °C, for 10 min. They were then subjected to seven freeze cycles in liquid nitrogen and thawing at 37 °C. The efficiency of parasite lysis was monitored by optical microscopy (Afonso & Scott, 1993). Protein dosage of the extracts obtained was performed using the Bradford method (Bradford, 1976), using a commercial reagent (Sigma Aldrich, USA), according to the manufacturer's instructions. Cytokine assessment in the liver and spleen has been used in the literature to check the immunomodulatory effect of treatments and vaccines (Helou et al., 2021; Hernandez et al., 2021).

5.6.5. *Toxicity evaluation*

In *L. amazonensis*-infected mice, immediately after anesthesia with a mixture of ketamine (100 mg/kg) and xylazine (15 mg/kg), animal blood was collected by puncture of the brachial plexus in microtubes containing EDTA 0.1 M. After centrifugation at 1,700 *g* for 10 min, the plasma supernatant was collected for biochemical analyses using renal and hepatic markers. The enzymatic activity of alanine aminotransferase (ALT) and aspartate aminotransferase (AST) was evaluated for hepatic function. For renal function, urea and creatinine levels were determined. These analyses were performed in the Bioplus BIO-2000 semiautomatic analyzer (São Paulo, Brazil) using commercial kits and following the manufacturer's instructions. After blood collection, kidneys were also collected for histopathological examination. Phosphate buffered formalin (10%) was used to fix the samples, followed by dehydration in alcohol and embedding in paraffin blocks. After obtaining organ sections, they were stained with hematoxylin and eosin (H&E) (Coelho et al., 2023).

Images were made using a camera connected to an optical microscope (Olympus BX-40; Olympus, Tokyo, Japan). The kidney sections were evaluated for degenerative changes and inflammatory infiltration. A score of 0 to 8 was set to measure renal alterations, with 0 to 1: absent, 2 and 3: mild, 4 and 5: moderate, 6 and 7: intense, 8: severe. The total score was obtained by adding the degenerative changes and inflammatory infiltrate scores (Costa et al., 2023). The animals' weight was recorded on each day of treatment as a parameter for assessing toxicity in both *L. major* and *L. amazonensis* infected experimental murine models.

5.7. Statistical analysis

The statistical analyses were performed using GraphPad Prism (version 8). Data normality and variance homogeneity were assessed using the Shapiro–Wilk or Kolmogorov–Smirnov test, and the Brown–Forsythe or F test, respectively. One-way ANOVA with Tukey's, Dunnett's, or Holm–Šídák's post-test was used to analyze liposomes' physicochemical characteristics, *in vitro* hemolytic activity, parasite load and cytokine profiles in *L. major*-infected mice, and IFN-γ/IL-10 ratio. Non-parametric data were analyzed using the Kruskal–Wallis test with Dunn's post-test. The paired *t*-test was applied to compare formulation size, PdI, and ZP between time 0 and 30. Two-way ANOVA with appropriate post-tests was used for the stability study (AmB and RA content), pharmacokinetics, lesion size, cytokine levels after stimulation, and animal weight. A 95% confidence level was considered, with significance set at *p-value* (p) < 0.05.

6. RESULTS

This section is divided into two main parts: (I) the development and characterization of LAmB-RA and DLAmB-RA formulations, and (II) the evaluation of LAmB-RA antileishmanial efficacy in murine models. Results related to LAmB-RA have been submitted for patent application (EP25305594.1) and publication.

6.1. Liposomal drug formulation development and physicochemical characterization

6.1.1. *LAmB-RA*

The co-incorporation of RA and AmB in preformed PEGylated liposomes was achieved by exploiting the pH dependence of the solubility of both drugs. While RA and AmB are highly soluble in alkaline solutions, their solubility decreased at neutral pH, favoring their incorporation into the liposomal membrane. Two AmB/RA molar ratios were evaluated, as described in Table 8. The choice of the best molar ratio was based on the formulation's visual stability. Despite having suitable particle size distribution after preparation (diameter = 117.0 ± 3.3 nm; PdI = 0.15 ± 0.02), the liposome with the highest amount of RA showed precipitation 2 days after storage at 4 ºC. For this reason, the formulations containing 2.9 mg/mL of AmB and 0.145 mg/mL of RA were chosen for further evaluation.

Table 8 – AmB: RA ratio in liposomes.

Mass ratio AmB:RA	Molar ratio AmB:RA	RA solution in NaOH 0.1M
10:1	1:0.30	1.25 mg/mL
20:1	1:0.15	0.625 mg/mL

As depicted in Table 9, control PEGylated liposomes containing only AmB (LAmB), only RA (LRA), or no drug (LEmpty) were prepared for comparison with LAmB-RA (1:0.15 molar ratio). LAmB-RA exhibited a hydrodynamic diameter of 123.3 ± 6.5 nm, and a PdI of 0.11 ± 0.02, values comparable to those of LAmB (128.4 ± 4.1 and 0.10 ± 0.03). In contrast, LRA and LEmpty showed significantly smaller vesicle diameters ($p < 0.0001$). As no increase in size was observed between LRA and LEmpty, the vesicle enlargement was mainly attributed to AmB.

Table 9 – Liposomes' physicochemical characteristics.

Formulation	Size (nm)	PdI	ZP (mV)	AmB $EE_{(\%)}$	RA $EE_{(\%)}$
LEmpty	92.2 ± 9.7	0.09 ± 0.05	-4.9 ± 0.5	-	-
LRA	89.3 ± 9.2	0.13 ± 0.04	-5.5 ± 1.5	-	96.8 ± 5.0
LAmB	128.4 ± 4.1[a]	0.10 ± 0.03	-4.2 ± 1.1	96.8 ± 5.9	-
LAmB-RA	123.3 ± 6.5[a]	0.11 ± 0.02	-5.3 ± 1.2	97.1 ± 4.4	94.7 ± 5.2

Notes: Data are mean ± SD from at least 8 independent batches. [a]Significant difference compared to LEmpty and LRA ($p < 0.0001$) according to the one-way ANOVA followed by Tukey's multiple comparison post-test. $EE_{(\%)}$ – Encapsulation efficiency; PdI – Polydispersity index; ZP – Zeta potential.

PdI values close to 0.1 were observed for all liposomal formulations (Table 9), indicating a narrow and uniform particle size distribution. Such low PdI values are characteristic of monodispersed systems. The evaluation of the ZP, in turn, reflects particles' electrical potential, i.e., their surface charge (Ganta et al., 2014). Determination of the particle ZP showed similar slightly negative values around -5.0 mV for the different formulations (Table 9). Despite the low surface charge, liposome aggregation can be prevented by steric hindrance due to vesicles PEGylation. Table 9 also shows that encapsulation rate in LAmB-RA was 97.1 ± 4.4% for AmB and 94.7 ± 5.2% for RA. Interestingly, similar values of encapsulation rates were found in the formulations containing only AmB and RA.

6.2. Preliminary study of the formulation stability

6.2.1. *LAmB-RA*

The formulations' stability was evaluated for 30 days at 4 ºC. The physicochemical characteristics of LAmB, LRA and LAmB-RA remained stable over this period, with no significant changes in size, PdI, or ZP (Table 10) ($p > 0.05$). As shown in Table 11, the content of AmB and its $EE_{(\%)}$ remained stable in LAmB and LAmB-RA ($p > 0.05$). However, a significant reduction ($p < 0.05$) in the RA content was observed between time 0 (T0) and time 30 (T30) for the liposomes containing only RA (116 ± 6% vs. 102 ± 5%) and the liposomes having AmB-RA (111 ± 5% vs. 96 ± 10%). Nevertheless, the RA content in LRA and LAmB-RA remained high (> 95%).

Table 10 – Liposomes physicochemical stability 30 days at 4 ºC.

Formulation	Size (nm)		PdI		ZP (mV)	
	T0	**T30**	**T0**	**T30**	**T0**	**T30**
LRA	84.3 ± 1.1	84.9 ± 0.8	0.15 ± 0.03	0.16 ± 0.01	-4.3 ± 0.4	-4.2 ± 0.2
LAmB	128.4 ± 4.8	129.5 ± 4.5	0.10 ± 0.02	0.09 ± 0.02	-3.6 ± 0.6	-3.5 ± 0.2
LAmB-RA	120.6 ± 4.7	123.1 ± 5.6	0.13 ± 0.01	0.13 ± 0.0	-4.5 ± 0.4	-4.0 ± 0.8

Notes: Data are mean ± SD from 5 independent batches; PdI – Polydispersity index; ZP – Zeta potential.

Table 11 – AmB and RA content and liposomes encapsulation efficiency 30 days at 4 ºC.

Formulation	AmB content (%)		AmB $EE_{(\%)}$		RA content (%)		RA $EE_{(\%)}$	
	T0	T30	T0	T30	T0	T30	T0	T30
LRA	–	–	–	–	116.2 ± 5.7	102.0 ± 5.2[a]	94.9 ± 2.2	91.9 ± 4.3
LAmB	96.6 ± 4.9	94.8 ± 5.2	93.9 ± 5.8	94.7 ± 3.1	–	–	–	–
LAmB-RA	92.0 ± 5.7	85.7 ± 5.0	96.5 ± 5.4	96.4 ± 4.3	111.2 ± 4.9	96.2 ± 9.8[a]	95.2 ± 5.5	95.3 ± 5.0

Notes: Data are mean ± SD from 5 independent batches and analyzed through two-way ANOVA followed by Tukey's multiple comparison post-test. [a]Significant difference compared to T30 and T0 ($p < 0.05$). $EE_{(\%)}$ – Encapsulation efficiency.

UV-visible (UV-Vis) spectrophotometry has been described as a sensitive technique for evaluating the AmB aggregation state. Figure 26a and Figure 26b show that LAmB and LAmB-RA exhibited similar absorption profiles with four bands: an intense band centered at 329 nm and three bands of decreasing intensities at 364 nm, 388 nm, and 417 nm. The absorption spectrum of AmBisome® was close to in-house AmB formulations spectra, except for a blue shift of the most intense band (centered at 323 nm) attributed to a super-aggregated form of AmB in the liposome membrane (Rivnay et al., 2019). Anforicin B® also has an intense peak centered at 330 nm related to aggregated AmB species (Marques Borges et al., 2024; Ramos et al., 2022).

Figure 26 – Stability of AmB aggregation by UV-Vis spectrophotometry and circular dichroism (CD) in different formulations: (a) and (b) absorption spectra registered at time 0 and after 30 days, respectively, containing maximum absorption values; (c) and (d) CD spectra registered at time 0 and after 30 days, respectively, containing maximum mdeg values; (e) CD spectra registered at time 0 without Anforicin B® with inset showing a magnified view in spectrum without AmBisome®; (f) CD spectra registered after 30 days, without Anforicin B® (to be continued)

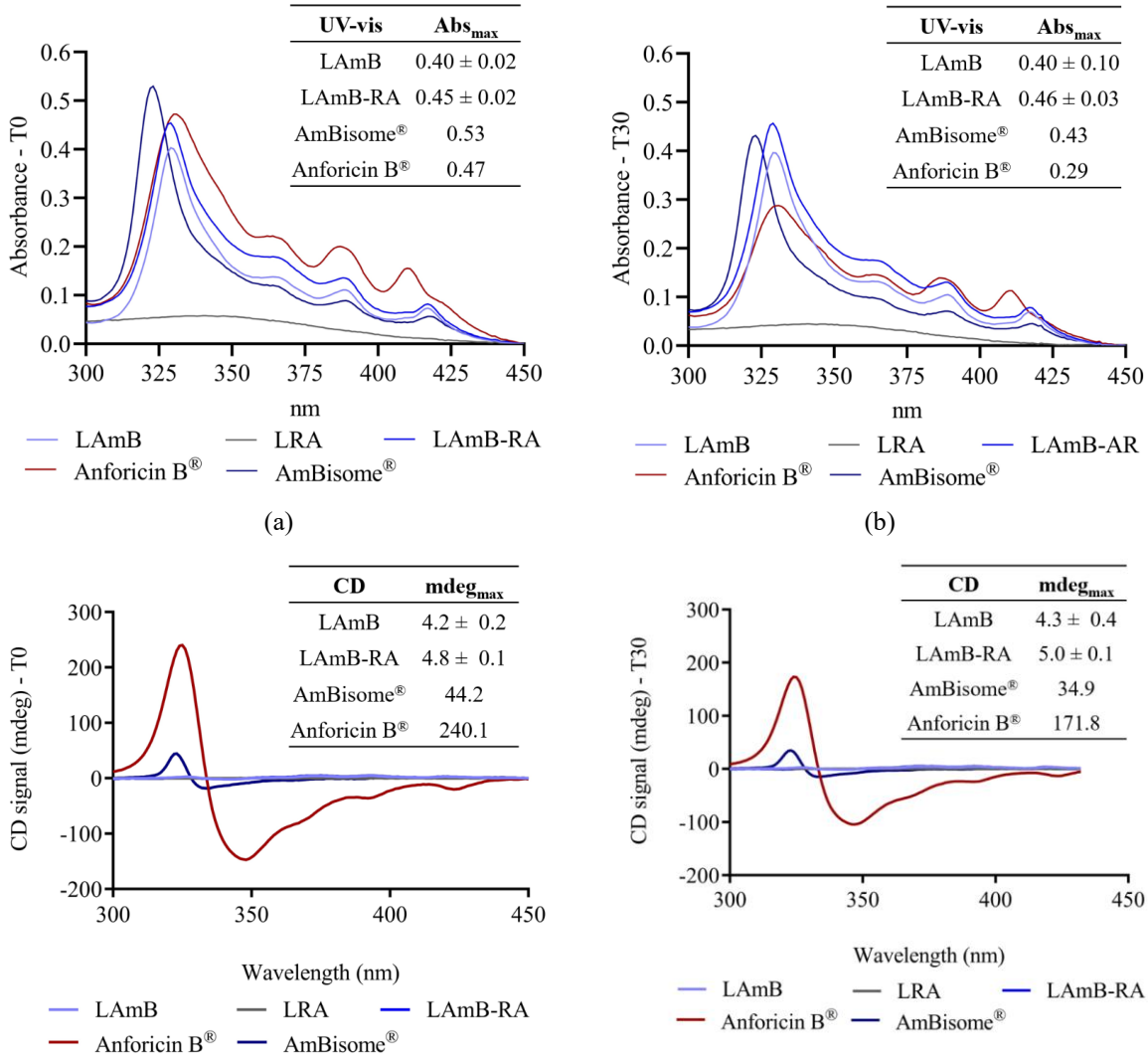

Figure 26 – Stability of AmB aggregation by UV-Vis spectrophotometry and circular dichroism (CD) in different formulations: (a) and (b) absorption spectra registered at time 0 and after 30 days, respectively, containing maximum absorption values; (c) and (d) CD spectra registered at time 0 and after 30 days, respectively, containing maximum mdeg values; (e) CD spectra registered at time 0 without Anforicin B® with inset showing a magnified view in spectrum without AmBisome®; (f) CD spectra registered after 30 days, without Anforicin B® (figure completed)

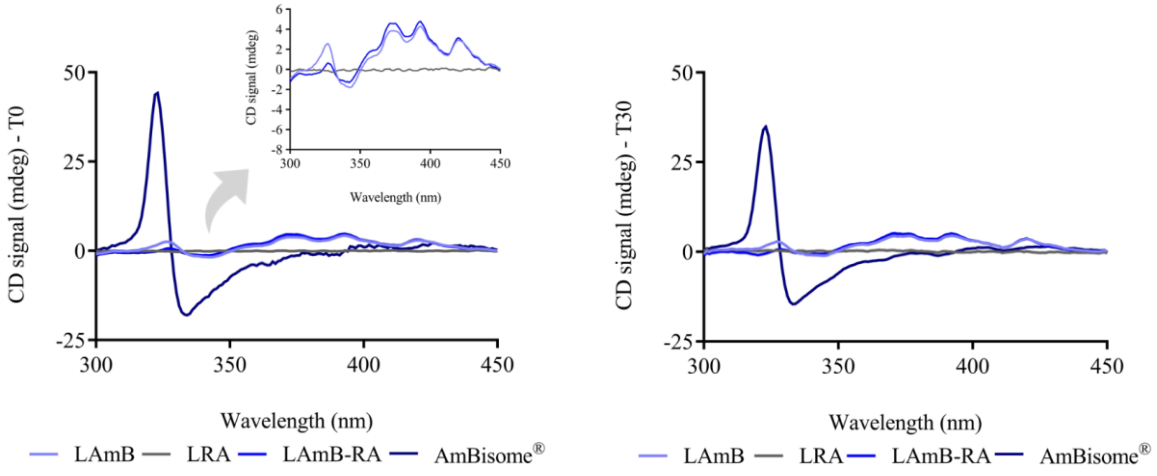

(e) (f)

Notes: The spectra were registered after 580-fold dilution in PBS (AmB 5 µg/mL). Maximum absorption wavelengths for UV-Vis and CD were: LAmB and LAmB-RA (329 and 393 nm); Anforicin B® (330 and 325 nm); and AmBisome® (323 nm for both methods). The formulations were stored at 4 ºC for 30 days.

Figure 26c and Figure 26d show that CD spectra of LAmB and LAmB-RA had similar profiles, with a positive band at 327 nm and a negative band at 342 nm. Of note, the signal intensity was higher for LAmB than LAmB-RA, which suggests that RA modulates the aggregation/organization state of AmB in the liposomes, as better visualized in Figure 26e inset. AmBisome® CD spectrum, in turn, is characteristic of an aggregated form of AmB, showing an intense couplet-type dichroic signal with a positive Cotton effect at 323 nm and a negative Cotton effect at 334 nm. Anforicin B® also has a doublet signal that is much more intense than that of liposomal AmB formulations. The difference in the CD spectral profile of LAmB and LAmB-RA compared to that of AmBisome® further supports that LAmB and LAmB-RA incorporate AmB in a less aggregated state.

Comparison of the AmB aggregation state between T0 and T30 by UV-Vis spectrophotometry and CD, indicated no significant difference for in-house liposomal formulations ($p > 0.05$). This outcome contrasts with the commercial formulations (AmBisome® and Anforicin B®) that showed a reduction in peak intensity at T30, indicating potential drug instability (Figure 26).

6.2.2. *DLAmB-RA*

The co-incorporation of RA and AmB in deformable liposomes was achieved through injection of an ethanolic solution of RA and soybean phosphatidylcholine (P90G) into an aqueous solution of AmB solubilized in DOC. In the present formulation, the molar ratio of AmB:DOC was 1:7, and the AmB:RA ratio was 1:0.5. Formulations with only RA or AmB, or with no drug, were used as controls. A formulation containing only AmB:DOC was also prepared. As shown in Table 12, after preparation, all formulations have a mean diameter around 100 nm, except AmB-DOC (206.3 ± 34.2 nm). This large size could mean a dispersion of the AmB rather than micellar formation. The particle size was found to be stable over 20 days for all formulations, except for DLRA and AmB-DOC which showed size increase over time. Additionally, the AmB-DOC was the only formulation with a visible AmB precipitation after 20 days of storage Figure 27.

Figure 27 – Photos of AmB-DOC formulation (a) just after preparation and (b) after 20 days of storage at 25 ºC

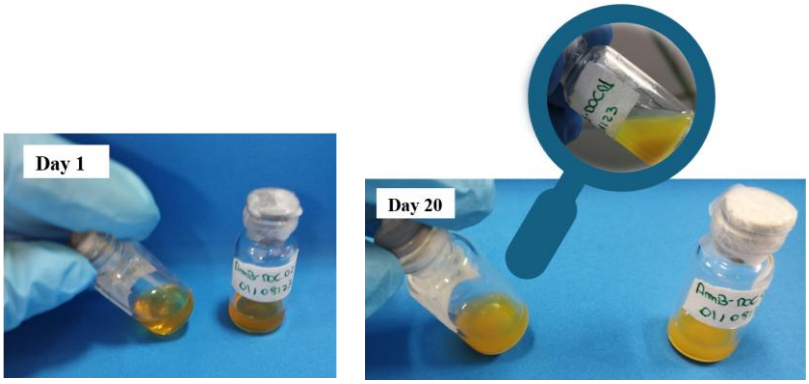

(a) (b)

The PdI, in turn, was less than 0.3 for all liposomes, remaining stable for 20 days. It is interesting to note that the formulations containing AmB tended to have higher PdI than those without the drug. The AmB-DOC formulation had the greatest size dispersion, with a PdI value of 0.29 at the beginning, with no significant change during storage (Table 12). As seen in Table 12, the liposome formulations showed ZP values in the range of -9 and -10 mV, while the ZP of AmB-DOC formulation was around -13 mV. Only the DLRA showed a significant reduction of ZP during storage (-9.9 ± 0.9 vs -7.5 ± 1.1 mV).

Table 12 – Liposomes physicochemical stability 20 days at 25 ºC.

Formulation	Size (nm)		PdI		ZP (mV)	
	T0	T20	T0	T20	T0	T20
AmB-DOC	206.3 ± 34.2	716.0 ± 19.3	0.29 ± 0.00	0.20 ± 0.08	-12.7 ± 0.8	-15.0 ± 1.6
DLEmpty	110.2 ± 1.5	110.4 ± 1.7	0.10 ± 0.01	0.06 ± 0.00	-9.5 ± 1.0	-9.1 ± 1.0
DLRA	105.6 ± 7.2	108.7 ± 7.2[a]	0.06 ± 0.04	0.09 ± 0.01	-9.9 ± 0.9	-7.5 ± 1.1[a]
DLAmB	105.5 ± 9.9	107.3 ± 7.7	0.16 ± 0.03	0.13 ± 0.01	-9.1 ± 0.3	-8.6 ± 0.2
DLAmB-RA	101.4 ± 1.3	106.1 ± 4.3	0.20 ± 0.01	0.18 ± 0.01	-9.0 ± 1.0	-9.4 ± 0.7

Notes: Data are mean ± SD from 3 independent batches and 2 batches for AmB-DOC. Data was analyzed through paired t-test. [a]Significant difference comparing T20 to T0 ($p < 0.05$). PdI – Polydispersity index; ZP – Zeta potential.

Concerning AmB loading (Figure 28), an increase in AmB content was observed in both formulations, DLAmB (99.8 ± 3.0% vs 120.4 ± 3.9%) and DLAmB-RA (103.7 ± 2.7% vs 117.3 ± 5.5%). This is probably due to the increase in viscosity of these formulations over time, leading to a pipetting error. On the other hand, the $EE_{(\%)}$ of AmB remained above 90%. The RA content (Figure 29), in turn, was significantly reduced in DLRA (88.1 ± 9.2% vs 29.5 ± 10.3%), which may be attributed to drug degradation. In contrast, the RA content remained stable in DLAmB-RA, indicating that the association of RA and AmB in the same formulation resulted in the stabilization of RA. In addition, the $EE_{(\%)}$ was higher than 90% in both RA formulations over the 20 days.

Figure 28 – (a) AmB content and (b) encapsulation efficiency in liposomes after 20 days at 25 ºC.

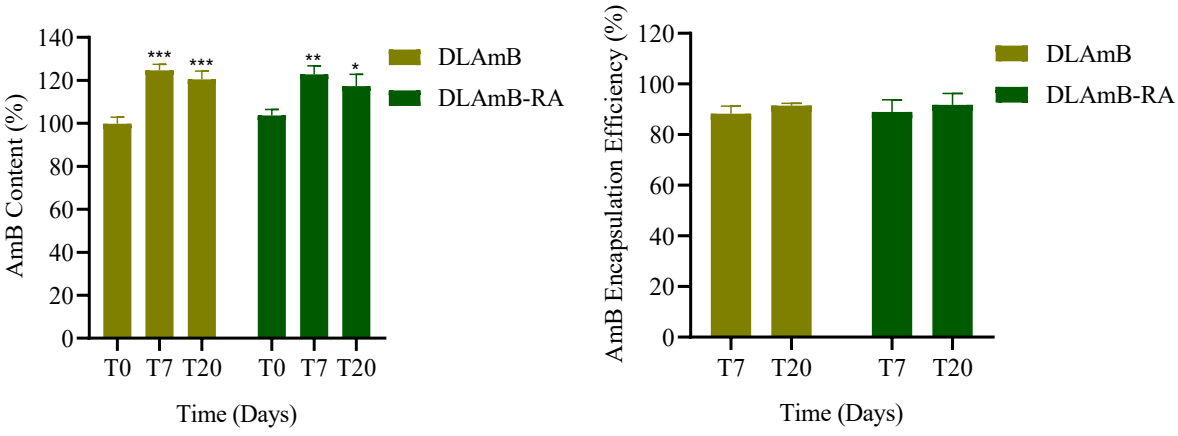

Notes: Data are mean ± SD from 3 independent batches. Data was analyzed through one-way ANOVA followed by Dunnett's multiple comparison post-test for AmB content (%) or paired t-test for AmB $EE_{(\%)}$. [a]Significant difference comparing AmB content (%) in different times to T0 ($p < 0.05$). Since the formulation was extruded at 0.1 µm, at T0, the $EE_{(\%)}$ was considered equal to the formulation content at T0. $EE_{(\%)}$ – Encapsulation efficiency.

Figure 29 – (a) RA content and (b) encapsulation efficiency in liposomes after 20 days at 25 ºC

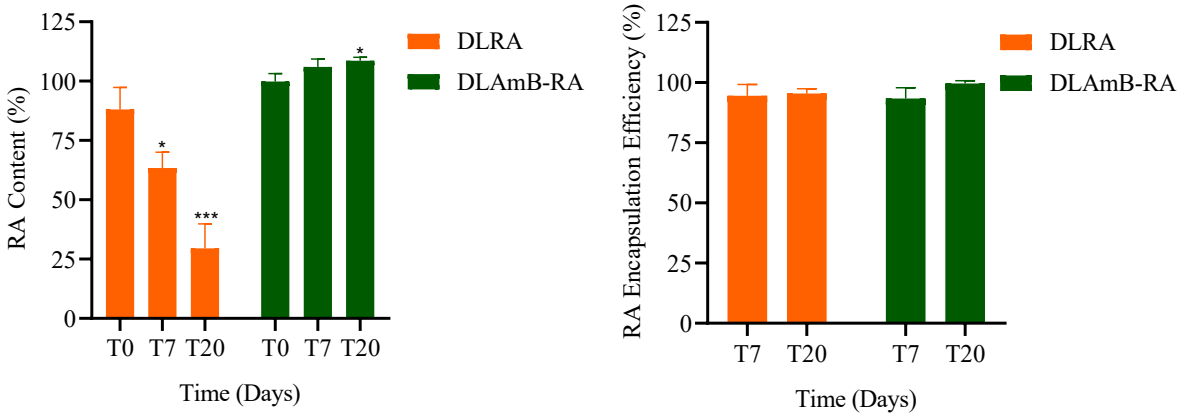

(a) (b)

Notes: Data are mean ± SD from 3 independent batches. Data was analyzed through one-way ANOVA followed by Dunnett's multiple comparison post-test for RA content (%) or paired t-test for RA $EE_{(\%)}$. [a]Significant difference comparing RA content(%) in different times to T0 ($p < 0.05$). Since the formulation was extruded at 0.1 µm, at T0, the $EE_{(\%)}$ was considered equal to the formulation content at T0. $EE_{(\%)}$ – Encapsulation efficiency.

The UV-Vis spectra of DLAmB and DLAmB-RA (Figure 30a) showed similar absorption profiles with four bands and max absorption at 323 nm. AmB-DOC, on the other hand, exhibited an intense band centered at 337 nm. The absorption bands detected in the 328–340 nm range are characteristic of AmB aggregation in the form of oligomers (Frézard et al., 2023). The CD spectra of DLAmB and DLAmB-RA (Figure 30b) were superposable, showing an intense couplet-type dichroic signal with a positive Cotton effect at 318 nm and a negative Cotton effect at 331 nm. AmB-DOC also had a doublet signal with a maximum of 328 nm and a minimum of 352 nm. Its signal was less intense and defined than that of liposomal formulations.

Figure 30 – AmB aggregation state by (a) UV-Vis spectrophotometry and (b) circular dichroism (CD) in different formulations after 7 days at 25 ºC

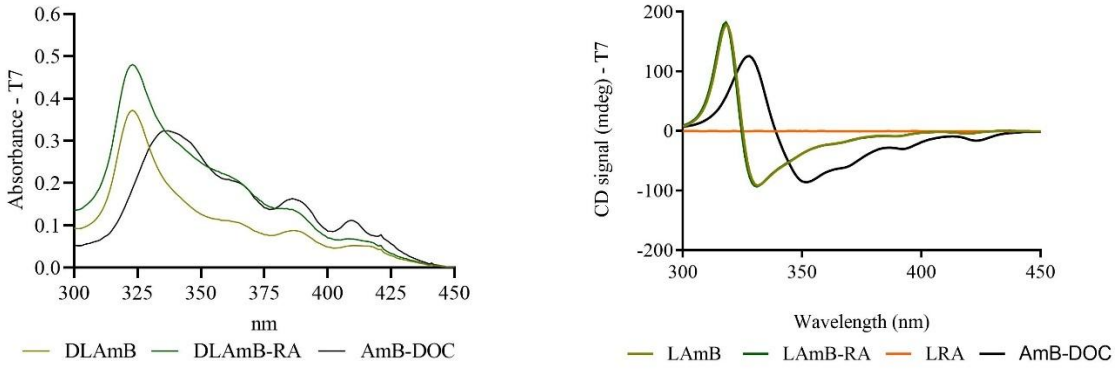

(a) (b)

6.3. *In vitro* hemolytic activity of LAmB-RA

The liposome formulations of AmB with and without RA were further characterized regarding *in vitro* hemolytic activity. Figure 31a illustrates the hemolytic activity across various AmB concentrations. For each liposomal AmB formulation, the hemolytic activity increased with AmB concentration. At the highest AmB concentration (250 µg/mL) (Figure 31b), lower toxicity is observed for AmBisome® (14.9 ± 0.8%), followed by LAmB-RA (21.6 ± 0.2%) and LAmB (28.0 ± 0.2%). It is worth noting that adding RA reduced significantly ($p < 0.0001$) the hemolysis percentage (LAmB vs. LAmB-RA). In contrast, Anforicin B® caused 99.7± 0.2% hemolysis even at the lowest AmB content (20 µg/mL).

Figure 31 – *In vitro* hemolytic activity caused by different formulations of AmB: (a) AmB formulations in different concentrations; (b) comparison between AmB formulations without Anforicin B® at the highest AmB concentration (250 µg/mL) for better visualization

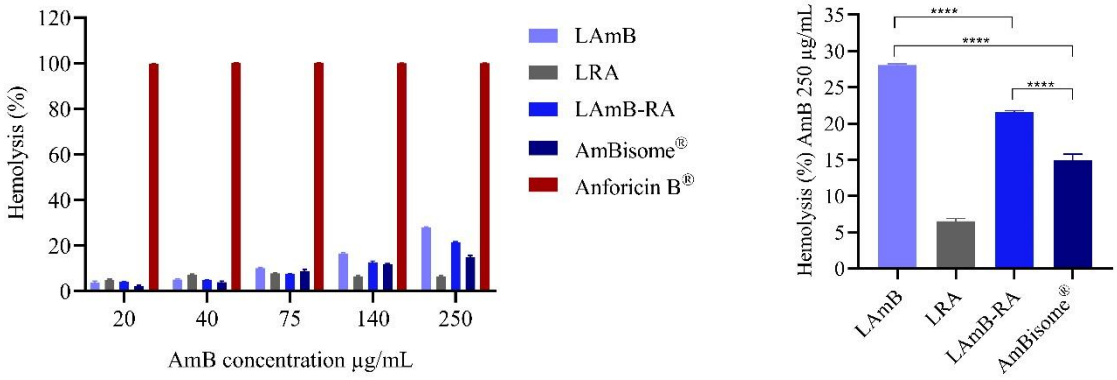

(a) (b)

Notes: Data are mean ± SD (n = 3) and analyzed through one-way ANOVA followed by Tukey's multiple comparison post-test. ****Significant differences observed between the AmB-containing formulations ($p < 0.0001$).

6.4. Pharmacokinetic study of AmB from LAmB-RA

LAmB-RA was further compared to LAmB and AmBisome® regarding the pharmacokinetic of AmB in plasma and liver of mice after IV bolus administration at 1 mg AmB/kg. Figure 32 displays the concentration of AmB in mouse plasma as a function of time for each formulation. A two-compartment open model with IV bolus input best fitted experimental plasma concentration-time data. Table 13 shows the calculated pharmacokinetic parameters. LAmB and LAmB-RA showed early elimination half-life ($t_{1/2\alpha}$) values (0.38 h and 0.44 h, respectively) comparable to that of the commercial formulation (0.60 h). On the other hand, both formulations exhibited a higher terminal phase half-life ($t_{1/2\beta}$), greater areas under the

concentration-time curve (AUC), and mean residence times of AmB, compared to AmBisome®. Notably, the LAmB group had the highest $AUC_{0\text{-inf}}$, (54,541 ng/mL*h) around 2 times higher than AmBisome® (23,733 ng/mL*h).

Figure 32 – Plasma pharmacokinetics of AmB in Swiss mice after intravenous administration of LAmB, LAmB-RA, or AmBisome® at a dose of 1 mg/kg: logarithmic plasma concentration-time curves

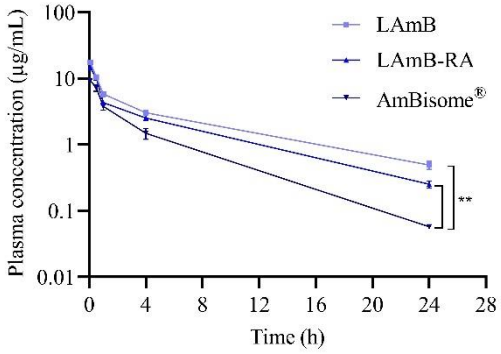

Notes: Data are mean ± SEM (n = 5). Time 24h was analyzed through two-way ANOVA followed by Dunnett's multiple comparison post-test. **Significant differences observed at 24h compared to AmBisome® group ($p < 0.01$).

Table 13 – Pharmacokinetic parameters of LAmB, LAmB-RA, and AmBisome® formulations.

Parameters	**Groups**		
	LAmB	**LAmB-RA**	**AmBisome®**
C_{max} (ng/mL)	18,656	15,648	9,658
$t_{1/2\alpha}$ (h)	0.38	0.44	0.60
$t_{1/2\beta}$ (h)	8.80	9.13	6.54
AUC0-t (ng/mL*h)	47,562	37,237	22,402
AUC0-inf (ng/mL*h)	54,541	42,830	23,733
MRT0-inf (h)	10.85	10.76	6.98
k_{el} [1] (h^{-1})	0.079 ± 0.036	0.076 ± 0.063	0.106 ± 0.162
k_{el} [2] (h^{-1})	1.810 ± 0.220	1.579 ± 0.283	1.157 ± 0.341

Notes: C_{max} – maximum concentration in plasma; $t_{1/2\ \alpha}$ – early elimination phase half-life; $t_{1/2\ \alpha}$ – terminal phase half-life; AUC – area under the concentration-time curve; MRT – mean residence time; k_{el} – elimination rate constant expressed as mean ± SD (n = 5).

Figure 33 shows the concentration of AmB in mouse liver at different time intervals after administration. Interestingly, the AmBisome® group showed the highest AmB level in the liver compared to the other two formulations. It is also noteworthy that AmB levels in the liver increased over time in the AmBisome® group, which has not been observed in the LAmB and LAmB-RA groups.

Figure 33 – AmB concentration in the liver of Swiss mice at different times after intravenous administration of LAmB, LAmB-RA, or AmBisome® (1 mg/kg)

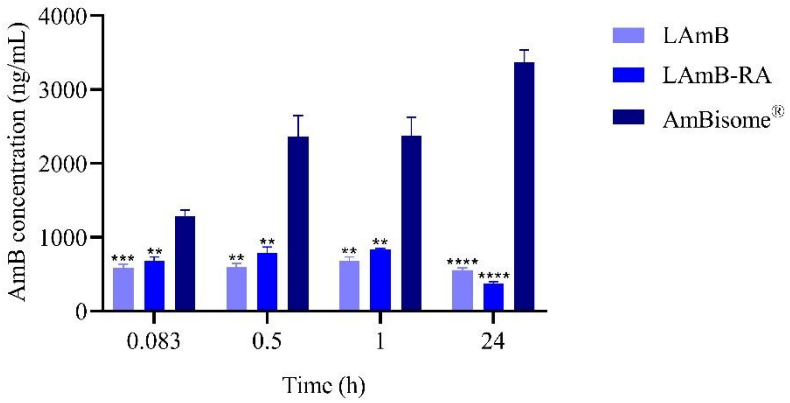

Notes: Data are represented as mean ± SEM (n = 5) and analyzed through two-way ANOVA followed by Dunnett's multiple comparison post-test. Significant differences were observed compared to the AmBisome® group at each time point (**$p < 0.01$, ***$p < 0.001$, ****$p < 0.0001$).

6.5. Assessment of LAmB-RA antileishmanial efficacy *in vivo*

6.5.1. *CL caused by L. major*

LAmB-RA, LAmB and LRA were evaluated for their therapeutic efficacies in a mouse model of CL caused by *L. major*. The impact of treatments was assessed on the lesion size growth and the parasite load in the lesion and cytokine production in the liver, in comparison to non-treated Control and groups receiving empty liposomes and AmBisome®.

A significant reduction in lesion size growth ($p < 0.05$) compared to the Control (Figure 34) was observed in the groups treated with liposomal AmB formulations. In particular, *L. major*-infected mice receiving PEGylated liposomal AmB, with or without RA, led to smaller lesions at the end of treatment compared to the first day. This result was not observed in the group treated with AmBisome® where only the progression of the lesion size was slowed down compared to the Control. Lesion photographs for qualitative comparison were taken on the last day of treatment, as shown in Figure 35. Interestingly, LRA did not reduce lesion growth compared to the Control: no beneficial or harmful effects were observed. Possibly, at this dose, RA alone has no potent antileishmanial effect, and a combination with AmB is necessary. The benefit of RA in combination with AmB was supported by the reduction of the parasite load in the lesion (Figure 36). LAmB-RA was the group with the most significant decrease in parasite load compared to the Control (99%), followed by LAmB (94%). It should be noted that there was no substantial reduction in the parasite load when animals were treated with AmBisome® (51%).

Figure 34 – Impact of treatment with different liposomal AmB formulations by IP route on lesion size (LS) growth in *L. major*-infected mice: (a) during treatment and (b) at the end of treatment

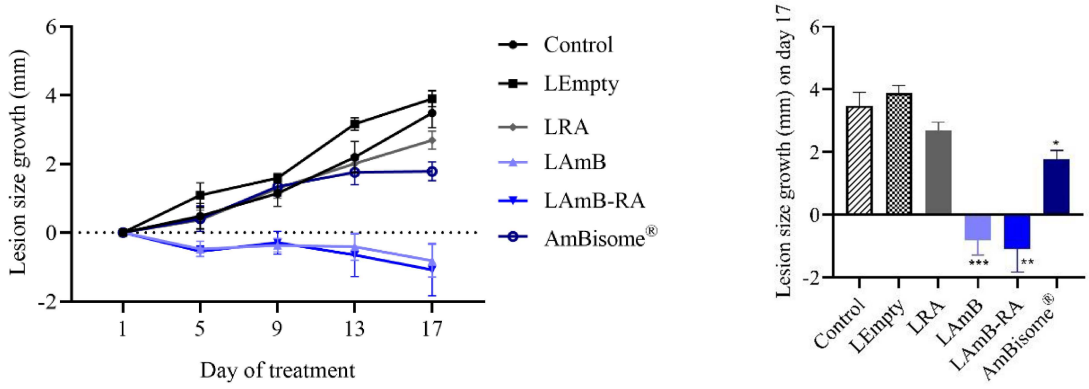

(a) (b)

Notes: LS growth was calculated for each animal based on the difference in the average LS during treatment and the 1st day of treatment. *L. major*-infected BALB/c mice were treated for 18 days every 2 days. Data are mean ± SEM (n = 8 for each group, and n = 10 for the Control) and analyzed through repeated measures two-way ANOVA followed by Tukey's multiple comparison post-test. Significant differences were observed compared to the Control group (*$p < 0.05$, **$p < 0.01$, ***$p < 0.001$).

Figure 35 – Impact of treatment with different liposomal AmB formulations by IP route on the macroscopic aspect of lesions in *L. major*-infected mice on the 17th day of treatment. LS is the lesion size mean ± SD on day 17 in each group

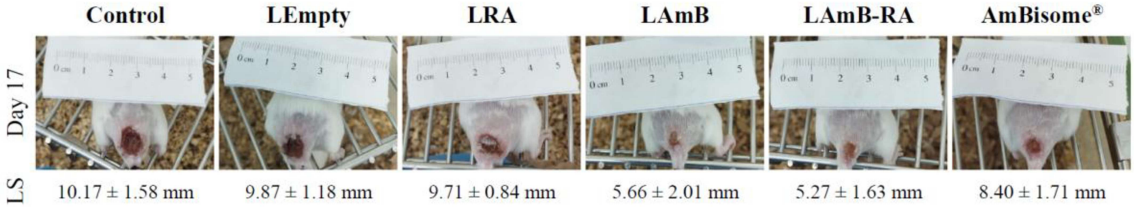

Figure 36 – Impact of treatment with different liposomal AmB formulations by IP route on parasite load in the lesion of *L. major*-infected mice

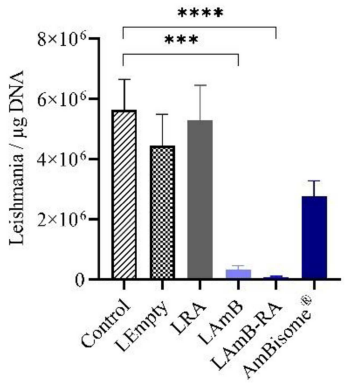

Notes: Parasite load was measured by qPCR. Data are mean ± SEM (n = 8 for each treatment group, and n = 10 for the Control group) and analyzed through one-way ANOVA followed by Tukey's multiple comparison post-test. Significant differences were observed compared to the Control group (***$p < 0.001$, ****$p < 0.0001$).

Cytokines and chemokines were assessed directly in the supernatant obtained from liver homogenates, after animals treatment. A significant increase in IFN-γ levels was observed only for the LRA (474.63 ± 56.29 pg/mL) and AmBisome® (612.45 ± 47.65 pg/mL) groups (Figure 37a), in comparision to the Control. When looking at IL-10 levels, on the other hand, there were higher levels in the group treated with LAmB, but none of the treatments led to a significant increase compared to the Control (Figure 37b). Thus, evaluating the IFN-γ/IL-10 ratio indicated a significantly lower ratio in LAmB compared to AmBisome® and an intermediate ratio in the case of LAmB-RA (Figure 37c).

A panel of cytokines and chemokines involved in anti-inflammatory and tissue-repairing activities was also evaluated. M2 macrophages decrease immune reactions and promote tissue repair by releasing different factors, such as Free Active TGF-β1, CCL22 (MDC), IL-6, and G-CSF. These cytokines and chemokines counteract the immunopathology caused by pro-inflammatory cytokines and, depending on the disease course, are also responsible for maintaining parasites in the infection site and chronicity. A significant increase in TGF-β1 was observed for LEmpty compared to LAmB, but differences compared to the Control group were not observed (Figure 37d). A reduction in CCL22 level in LAmB-RA group was observed in comparison to AmBisome® (Figure 37e). The chemokine CCL22 is known to recruit regulatory T cells (Tregs) to the site of infection, suppressing inflammatory immune responses (Tomiotto-Pellissier et al., 2018). However, no significant difference was observed for this chemokine compared to the Control group. Similarly, there were no significant differences between the groups for IL-6 or G-CSF levels (Figure 37f and Figure 37g).

Figure 37 – Impact of treatment with different liposomal AmB formulations by IP route on the cytokine and chemokine profile in liver lysates of *L. major*-infected mice: (a) IFN -γ, (b) IL-10, (c) IFN -γ / IL-10 Ratio, (d) TGF – β1 (e) CCL22, (f) IL-6, and (g) G-CSF

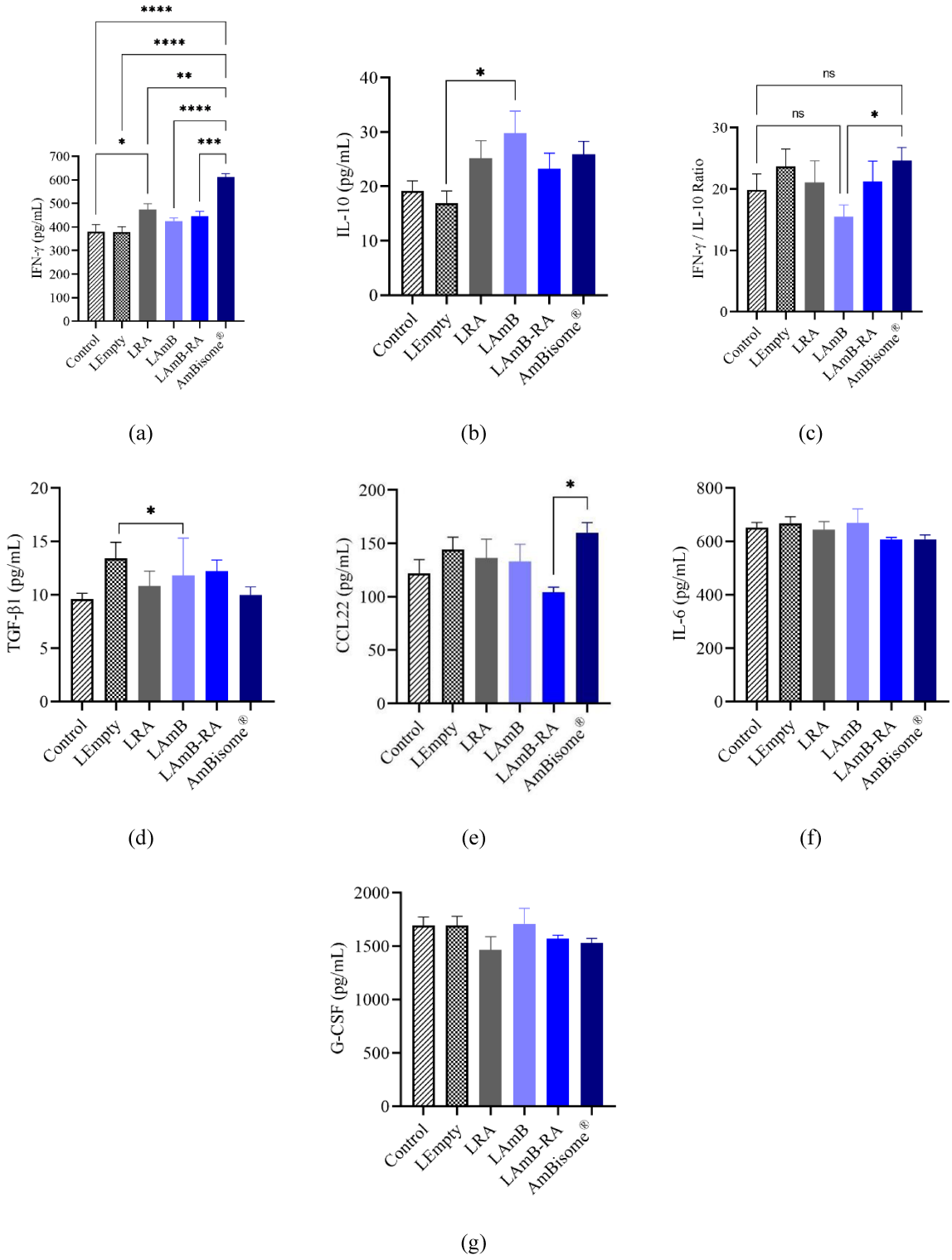

Notes: Data are mean ± SEM (n = 6) and analyzed through one-way ANOVA followed by Tukey's multiple comparison post-test. IFN-γ/L-10 ratio was analyzed through one-way ANOVA followed by Holm-Sidak's multiple comparison post-test. Significant differences were observed (*$p < 0.05$, **$p < 0.01$, ***$p < 0.001$, ****$p < 0.0001$).

Mice weight was monitored as an indirect parameter of treatment toxicity. Even though the animals receiving AmB fluctuated in weight during the treatment, no significant weight loss was observed for any treatments comparing the animals' weight at the beginning and the end of treatment (Figure 38).

Figure 38 – Impact of treatment with different liposomal AmB formulations on body weight of *L. major*-infected mice as a function of time

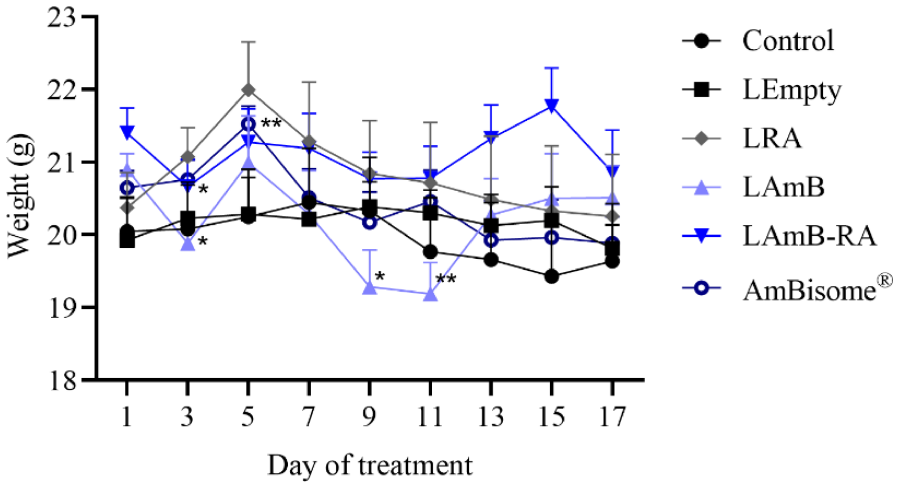

Notes: Data are mean + SEM (n = 8 for each group, and n = 10 for the Control) and analyzed through repeated measures two-way ANOVA followed by Dunnett's multiple comparison post-test. Significant differences were observed compared to Day 1 (*$p < 0.05$, **$p < 0.01$).

6.5.2. *CL caused by L. amazonensis*

The therapeutic efficacy of liposomal AmB formulations was further evaluated in a murine model of CL caused by the New World *Leishmania* species, *L. amazonensis*. The impact of treatments was assessed on the lesion size growth, immune response, and parasite load in the spleen, compared to non-treated Control and groups receiving empty liposomes and AmBisome®.

Evaluation of lesion size growth at the end of treatment (Figure 39) showed a marked reduction ($p < 0.05$) in mice treated with LAmB-RA (1.1 ± 0.7 mm) and LAmB (1.3 ± 1.6 mm) compared to the untreated Control (3.3 ± 1.4 mm). Notably, only LAmB-RA significantly reduced the animal's lesion size growth compared to AmBisome® (2.5 ± 0.8 mm; $p < 0.05$). All treated groups (LAmB, LAmB-RA, and AmBisome®) also exhibited significantly less pronounced lesion size growth, when compared to LEmpty group (4.0 ± 0.5 mm; $p < 0.05$).

Lesions photographs for qualitative comparison were taken on the 1st and 23rd days of treatment, as seen in Figure 40.

Figure 39 – Impact of treatment with different liposomal AmB formulations by IP route on lesion size (LS) growth in *L. amazonensis*-infected mice: (a) during treatment and (b) at the end of treatment

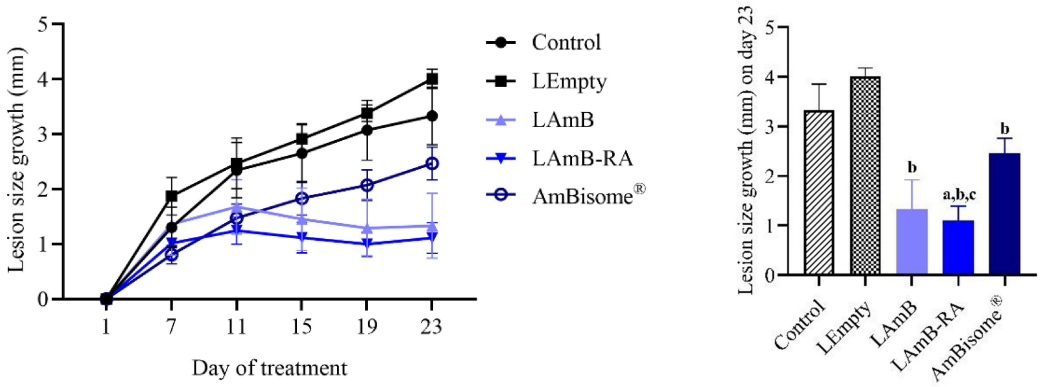

(a) (b)

Notes: LS growth was calculated for each animal based on the difference in the average LS during treatment and the 1st day of treatment. *L. amazonensis*-infected BALB/c mice were treated for 24 days every 2 days. Data are mean ± SEM (n = 7) and analyzed through repeated measures of two-way ANOVA followed by Tukey's multiple comparison post-test. [a]Significant differences observed compared to Control ($p < 0.05$); [b]Significant differences observed compared to LEmpty; [c]Significant differences observed compared to AmBisome®.

Figure 40 – Impact of treatment with different liposomal AmB formulations by IP route on the macroscopic aspect of lesions in *L. amazonensis*-infected mice on the 1st and 23rd days of treatment. LS is the lesion size mean ± SD on each day in each group

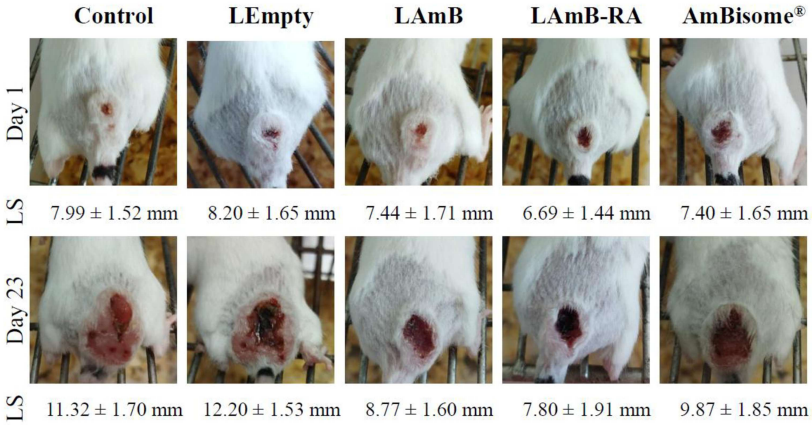

As shown in Figure 41a, for the splenocytes stimulated with culture medium, there was greater IFN-γ production for cells recovered from animals treated with LAmB-RA compared to the Control group (untreated). Stimulation with RA, in turn, significantly increased ($p < 0.05$) IFN-γ production in all groups (Control, LEmpty, LAmB, and AmBisome®) compared to the culture medium. This increase was not significant in the LAmB-RA group. Similarly,

stimulation with SLA led to a significant increase in IFN-γ levels in all groups compared to culture medium exposition. The cellular response to stimulation with the pathological agent can explain this phenomenon. Notably, LAmB-RA was the only group with significantly higher production of IFN-γ in response to *Leishmania* antigen stimulation, compared to the Control group ($p < 0.001$). This effect of LAmB-RA supports the induction of an antigen-specific Th1 immune response. Splenocytes were also stimulated with ConA, a positive control of activation. Regarding IL-10 production (Figure 41b), the group treated with LAmB showed the highest IL-10 levels compared to the other groups for the different stimuli (RA, SLA, and ConA). Interestingly, incorporation of RA into LAmB significantly reduced IL-10 production to levels comparable to those of AmBisome®.

Notably, the incorporation of RA into AmB-containing liposomes significantly increased the IFN-γ/IL-10 ratio after stimulation with SLA, showing a clear shift towards a Th1-type antigen-specific immune response (Figure 41c). It should be noted that BALB/c mice are highly susceptible to CL, with this susceptibility being linked to a genetic inability to produce IL-12, an essential cytokine for Th1 cell differentiation. This immune impairment causes progressive skin lesions and visceral invasion (Maspi et al., 2016). Thus, it is expected from the literature that the induction of a Th1-type immune response can result in better treatment efficacy, as reported in our study. The group receiving RA alone was not included in this study, as in the *L. major* model no beneficial or harmful effects were observed with LRA (Figure 34 and Figure 36), so we decided to evaluate only its additional effect with AmB in *L. amazonensis*-infected mice. Since the parasite can visceralize in BALB/c mice infected with *L. amazonensis*, the parasite load was assessed in the spleen in this model. In line with the control of lesion size growth and the Th1-type immune response, a significant reduction ($p < 0.05$) in parasite load was observed only for the group treated with LAmB-RA (60%) when compared to the Control group (Figure 42).

Figure 41 – Impact of treatment with different liposomal AmB formulations by IP route on the cytokine profile in splenocytes culture from *L. amazonensis*-infected mice, after stimulation: (a) IFN-gamma, (b) IL-10, and (c) IFN-γ/IL-10 ratio

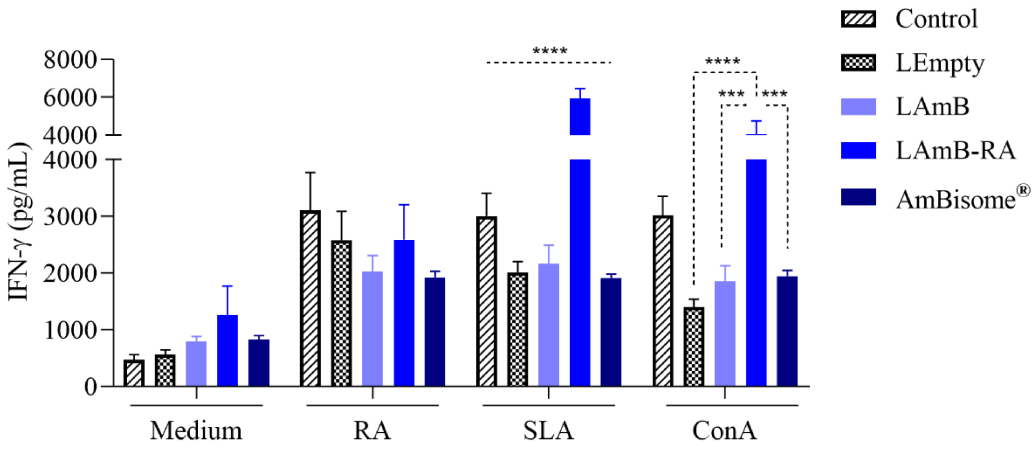

(a)

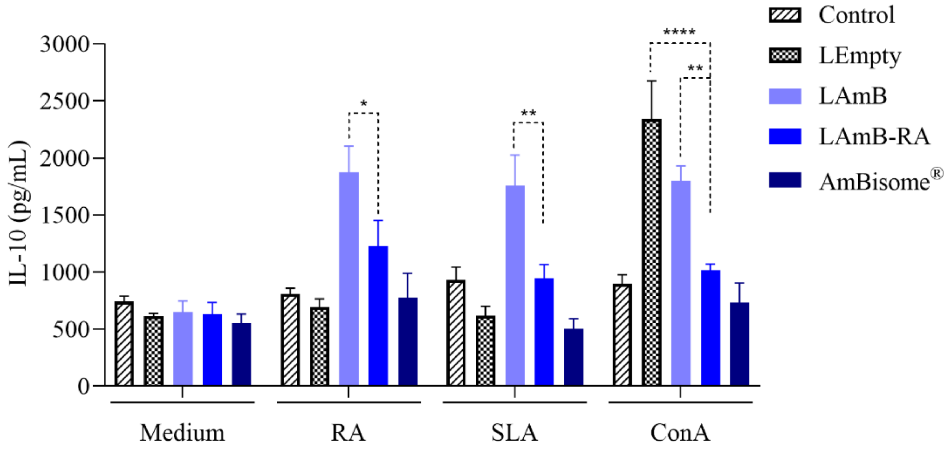

(b)

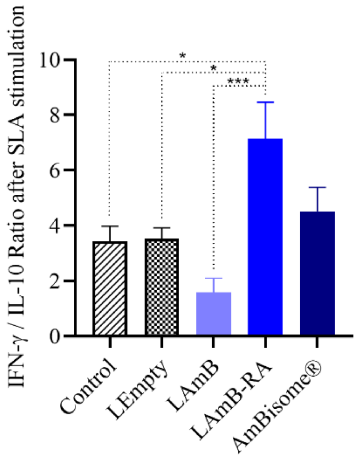

(c)

Notes: Animals were euthanized 3 days after the last dose, the spleens were collected, and splenocytes were submitted to different stimulations: medium, retinoic acid (RA), Soluble *Leishmania* Antigen (SLA), and

Concanavalin A (ConA) before cytokines evaluation by ELISA. Data are mean ± SEM (n = 7) and analyzed through two-way ANOVA followed by Tukey's multiple comparison post-test. IFN-γ/IL-10 ratio was analyzed through one-way ANOVA followed by Tukey's multiple comparison post-test. Significant differences were observed compared to the LAmB-RA group (*$p < 0.05$, **$p < 0.01$, ***$p < 0.001$, ****$p < 0.0001$).

Figure 42 – Impact of treatment with different liposomal AmB formulations by IP route on parasite load in the spleen of *L. amazonensis*-infected BALB/c mice

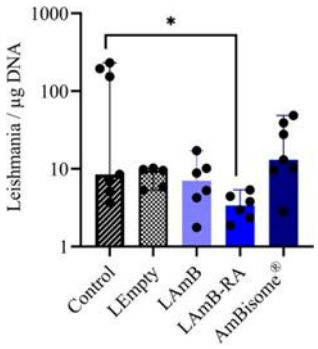

Notes: Parasite load was measured by qPCR. Data are medians + 95% confidence intervals (n = 7) and analyzed through Kruskal-Wallis followed by Dunn's multiple comparison post-test. Significant differences were observed compared to the Control group (*$p < 0.05$).

Assessments of biochemical markers of renal and hepatic functions were performed after treatment in *L. amazonensis*-infected mice (Table 14). This analysis showed an increase in creatinine in animals treated with AmB: LAmB-RA (0.33 ± 0.06 mg/dL), AmBisome® (0.33 ± 0.03 mg/dL), and LAmB (0.38 ± 0.07 mg/dL), the last one leading to a more significant increase compared to the Control (0.25 ± 0.04 mg/dL), suggesting some renal toxicity (Table 14). All other markers (ALT, ASAT, urea) did not show significant differences between experimental groups.

Table 14 – Biochemical markers of renal and hepatic functions in *L. amazonensis*-infected BALB/c mice after treatment with different liposome formulations of AmB.

Parameters	**Groups**				
	Control	**LEmpty**	**LAmB**	**LAmB-RA**	**AmBisome®**
Creatinine (mg/dL)	0.25 ± 0.04	0.27 ± 0.04	0.38 ± 0.07***	0.33 ± 0.06*	0.33 ± 0.03*
Urea (mg/dL)	54.6 ± 7.8	51.6 ± 8.9	57.6 ± 16.3	59.6 ± 9.6	64.6 ± 8.8
ALT (U/L)	30.5 ± 11.4	32.2 ± 4.7	27.9 ± 8.2	28.7 ± 5.3	29.9 ± 3.8
AST (U/L)	104.5 ± 23.1	110.1 ± 31.9	87.5 ± 29.4	87.0 ± 18.0	113.0 ± 25.8

Notes: Data are mean ± SD (n = 7). Significant differences were observed compared to the Control group ($^{*}p < 0.05$, $^{***}p < 0.001$). ALT – alanine aminotransferase; AST – aspartate aminotransferase.

Histopathological examination of *L. amazonensis*-infected mice kidneys showed low to mild renal alterations in all the groups that received AmB. As shown in Figure 43, the main

alterations observed were hyaline cylinders, indicating protein accumulation, pyknotic nuclei typical of cell death, and the presence of mononuclear leukocytes and neutrophils as inflammatory infiltrates. Notably, none of the groups had severe toxicity.

Figure 43 – Impact of treatment with different liposomal AmB formulations by IP route on kidney toxicity in *L. amazonensis*-infected mice. (a) A score of 0 to 8 was set to measure renal alterations, with 0 to 1: absent, 2 and 3: mild, 4 and 5: moderate, 6 and 7: intense, 8: severe. G1 = untreated; G2 = LEmpty; G3 = LAmB; G4 = LAmB-RA; G5 = AmBisome® (graph Group × Total score). The total score was obtained by adding the degenerative changes and inflammatory infiltrate scores. Data are the median with range (n = 7). (b-f) Kidney histological sections of mice are either (b) untreated or (c) treated with LEmpty, (d) LAmB, (e) LAmB-RA, or (f) AmBisome®

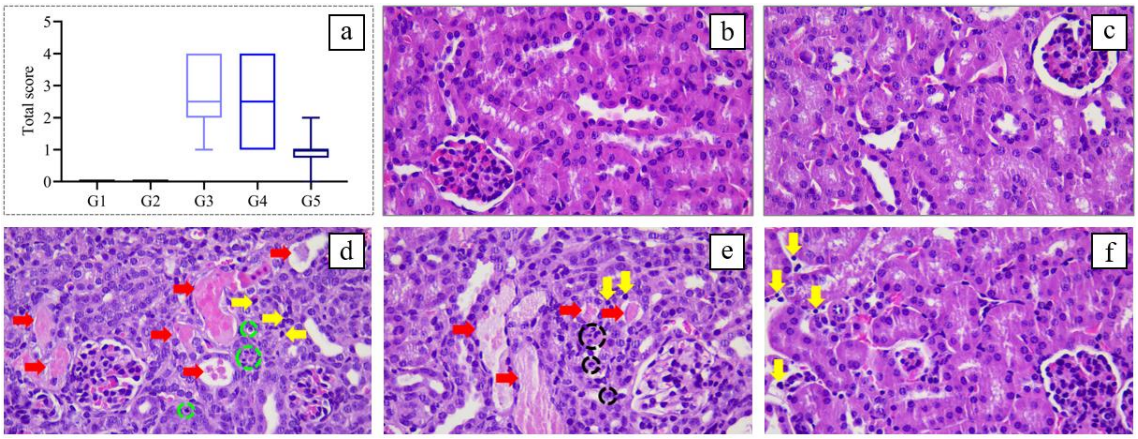

Notes: Yellow arrows indicate mononuclear leukocytes, red arrows represent hyaline cylinders, green circles indicate pyknotic nuclei (cell death), and black circles show neutrophils.

Despite the significant weight fluctuations of animals during treatment, no significant weight loss was observed (Figure 44) when comparing the weight at the beginning and the end of treatment administrations (Day 1 *vs*. Day 23).

Figure 44 – Impact of treatment with different liposomal AmB formulations on body weight of *L. amazonensis*-infected mice as a function of time

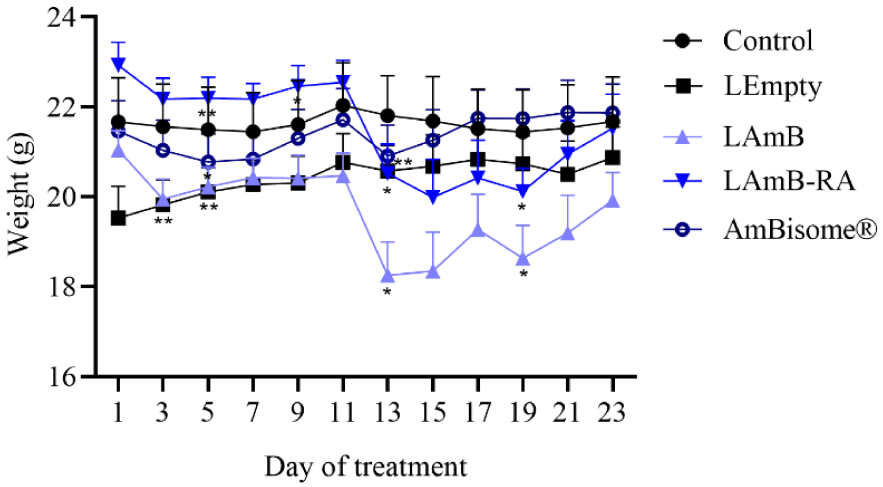

Notes: Data are mean + SEM (n = 7) and analyzed through repeated measures two-way ANOVA followed by Dunnett's multiple comparison post-test. Significant differences were observed compared to Day 1 (*$p < 0.05$, **$p < 0.01$).

7. DISCUSSION

In this thesis, two novel liposomal formulations were developed to combine the antileishmanial drug AmB with the immunomodulatory agent RA, looking for an enhanced therapeutic effect. The first formulation consisted of rigid PEGylated liposomes made from high transition temperature phospholipids and cholesterol, intended for parenteral administration. This formulation was designed to treat more serious cases, such as disseminated forms of leishmaniasis (DCL, MCL, PKDL, HIV co-infection). The second formulation was made from deformable vesicles containing DOC and low transition temperature lecithin, intended for topical application. This formulation was intended for topical treatment of uncomplicated CL cases (with one or a few lesions), especially for pediatric patients.

7.1. LAmB-RA formulation made from rigid liposomes

CL treatment is challenging as the increase in resistance, relapses, and toxicity of current drugs impact patient compliance and disease control. The therapeutic arsenal has evolved little in recent years. AmB is recognized for its high antileishmanial effect, being commercialized as micellar (Anforicin B®) and liposomal (AmBisome®) forms. Liposomal AmB is the least toxic and has consolidated use in VL treatment but not CL. This study hypothesized that combining AmB with an immunomodulator could increase its efficacy, potentially reducing the treatment dose/duration and toxicity. In this context, RA seemed to be a good alternative as it is a physiological molecule and is already used in the clinic to treat skin disorders and cancer (APL). Considering all the regulatory requirements for the development of a new drug, repositioning is a great strategy.

In contrast to the commercial AmB-liposome, the new liposome developed in this work was PEGylated, seeking long-circulating properties. This new liposomal formulation was first characterized by particle size and zeta potential, drug content, encapsulation efficiency, and aggregation state. The comparison was made with liposomes containing one of the two drugs, empty liposomes and commercial formulations, Anforicin B® and AmBisome®.

The LAmB-RA formulation exhibited vesicles with hydrodynamic diameter of 123.3 ± 6.5 nm, which is within the range recommended by the United States Pharmacopeia for injectable lipid emulsions using light-scattering techniques, a range also adopted for liposomes administered by parenteral route (≤ 500 nm) (Pharmacopeia, 2023a, 2023b). This fact is due to the risk of microvascularization occlusion and embolism, mainly in the lungs where capillaries with diameters of up to 5 μm are found (Hörmann & Zimmer, 2016). On the other hand, vesicles

smaller than 10 nm may undergo rapid renal clearance (Ganta et al., 2014). It has also been proposed that nanoparticles' size should be less than 200 nm to guarantee lower uptake by MPS cells and longer circulation time (Kaur et al., 2008). Regarding leishmaniasis treatment, nanoparticle uptake by MPS cells contributes to passive drug targeting, as macrophages are the target cells. However, in CL, the excessive uptake of nanoparticles can lead to early elimination from the bloodstream so that they do not reach the lesion in adequate concentrations (Wijnant et al., 2018c).

The hydrodynamic diameter of vesicles in LAmB-RA was comparable to that in LAmB, but was significantly ($p < 0.0001$) greater than those in LRA and LEmpty. This means that incorporation of AmB in liposomes contributes to their increased size, which aligns with previous reports that high AmB-to-lipid ratios enlarge liposomes (van Haute et al., 2019) and decrease membrane deformability (Perez et al., 2016). All formulations showed low polydispersity index values, close to 0.1, evidencing monodisperse vesicles. PdI values of up to 0.25 are acceptable for injectable nanoparticles. In contrast, dispersions with higher values are characteristic of non-uniform distributions, being a limiting factor for some administration routes, such as IV (Müller et al., 2004).

The evaluation of the ZP, in turn, reflects particles' electrical potential, i.e., their surface charge (Ganta et al., 2014). Determination of the particle ZP showed similar slightly negative values (around -5 mV) for the different formulations. As expected from the literature, coating the liposome surface with hydrated hydrophilic PEG polymer chains led to a charge-shielding effect (Sadzuka et al., 2002). Despite the low surface charge, colloidal stability through steric hindrance was observed in the stability study. Furthermore, AmB content and its $EE_{(\%)}$ remained stable over at least 30 days. On the other hand, RA content was found to decrease over time. This effect may be due to RA oxidation. Nevertheless, the RA content and its $EE_{(\%)}$ remained high (> 90%), especially considering that it is a liquid formulation (non-lyophilized). The inclusion of an antioxidant in the formulation may further improve its stability, as commercial products containing RA have this component (FDA, [n.d.]).

The UV-Vis and CD spectra of LAmB and LAmB-RA are also consistent with a less aggregated state of AmB, in comparison to commercial formulations (Anforicin B® and AmBisome®). Interestingly, comparison of CD spectra between LAmB-RA and LAmB indicated slightly different aggregated states of AmB. Importantly, the spectral characteristics of in-house liposomal formulations did not change over the 30-day period. This contrasts with AmBisome® and Anforicin B®, that showed a reduction in peak intensity at T30, indicating drug instability.

In a second set of experiments, the new liposomal formulation was characterized regarding potential hemolytic activity, pharmacokinetics after IV administration in mice and therapeutic efficacy in murine models of CL.

The *in vitro* hemolysis assay revealed that liposomal AmB formulations had lower hemolytic activity than the micellar formulation. Indeed, Anforicin B® hemolitic activity is well-documented and attributed to the fast release of AmB and the presence of sodium deoxycholate (Lemke et al., 2005). Thus, the greater the AmB availability for interaction with red blood cells, the higher the hemolytic activity. These findings are consistent with clinical studies showing improved tolerance to AmB with continuous 24-hour infusion compared to shorter infusions, further supporting the role of sustained drug release in reducing toxic effects (Eriksson et al., 2001; Peleg & Woods, 2004).

The higher hemolytic activity of LAmB-RA and LAmB in comparison to AmBisome® may be attributed to the lower aggregation state of AmB and its more rapid release from liposomal membrane (Frézard et al. 2023). It is generally assumed that AmB tends to self-assemble, forming monomers, oligomers, and super-aggregates. Monomers show a safer profile by selectively binding ergosterol, while oligomers cause cell lysis by forming channels in cholesterol- or ergosterol-containing membranes. Super-aggregates, in turn, can act as AmB reservoirs with sustained AmB release, reducing cytotoxicity (da Costa et al., 2024).

Interestingly, adding RA to LAmB formulation reduced significantly ($p < 0.0001$) the hemolysis percentage. This protective effect of RA incorporation may be related to the difference in AmB aggregation state between LAmB-RA and LAmB, as evidenced by CD. From this perspective, future studies should investigate how the presence of RA affects AmB release kinetics. Since the 1990s, efforts have focused on developing systems to immobilize AmB within their structures, addressing the toxicity of micellar formulations, by reducing free drug levels in the bloodstream and minimizing harm to mammalian cells (Lemke et al., 2005).

As the next step, pharmacokinetic analysis of AmB was assessed in mice comparing in-house liposomes and AmBisome®. A major difference between LAmB and LAmB-RA compared to AmBisome® is that in-house formulations are PEGylated. Accordingly, pharmacokinetic data showed increased C_{max}, prolonged mean residence time, and reduced hepatic AmB accumulation from PEGylated liposomes, compared to AmBisome®. These findings align with the already-known effect of PEGylation on the stealthiness of nanoparticles, reducing their uptake by MPS cells and, consequently, their passive targeting to organs such as the liver, in addition to prolonging their blood circulation time. There are few studies in the literature evaluating the pharmacokinetics of PEGylated liposomes carrying AmB.

Van Etten et al. (1995a, 1995b) showed that including DSPE-PEG_{1900} into AmB-liposomes resulted in a prolonged blood residence time compared to non-PEGylated liposomes after a single IV injection in mice. These authors observed a relatively high hepatosplenic uptake (34%–43%) of these liposomes at 24 h after administration (van Etten et al., 1995b). Jung et al. (2009) also reported a positive impact of lipid nanoparticle PEGylation on the following pharmacokinetic parameters: AUC, C_{max}, and $t_{1/2}$. Interestingly, both works correlated their results with a greater efficacy on fungal infections. Moreover, Kohno et al. (1997) showed higher plasma concentrations of AmB after mice treatment with AmB-containing PEGylated liposomes, compared to AmBisome®, and lower AmB concentration in the liver. This result was further confirmed by Otsubo et al. (1998).

Regarding AmBisome®, our results align with published data showing a peak of AmB plasma concentration followed by a rapid decay close to zero, 24 h after administration. In addition, an increase in liver concentration was also observed over time with this commercial formulation of AmB (Voak et al., 2017). Iman and colleagues (2017) also found a maximum concentration of AmB in mice livers at 24 h following AmBisome® administration. The liver was also the organ with the highest AmB levels after autopsy in humans treated with AmBisome® (Vogelsinger et al., 2006).

It is known that AmB pharmacokinetics parameters are influenced by different factors, such as animal strain (Abdollahizad et al., 2023), gender (Wang et al., 2021), formulation (Vyas & Gupta, 2006; Wijnant et al., 2018c), and dose (Voak et al., 2017). After administration, AmB may coexist in free, protein-bound, and liposome-associated forms, each with distinct pharmacokinetic profile. A complete characterization of AmB concentration in each pool could be considered in future works.

The therapeutic efficacy of LAmB-RA was further studied in two different murine models of CL using an Old-World *Leishmania* species, *L. major*, or a New-World, *L. amazonensis*. In the first model, lesion size and parasite load in the lesion were assessed, in addition to cytokine levels in the liver. In the second model, in order to investigate systemic efficacy and toxicity, in addition to lesion size, parasite load and cytokines in the spleen, and renal toxicity were evaluated.

Here, we investigated for the first time the effect of parenteral administration of nanoencapsulated RA on leishmaniasis. Since a stable liposomal formulation co-incorporating RA and AmB was only obtained at a low RA:AmB mass ratio (1:20), the dose of RA investigated was limited to 0.25 mg/kg. At this dose, the liposomal formulation containing only RA (LRA) showed no therapeutic improvement in the mouse model infected with *L. major*,

despite the induction of a slight increase in IFN-γ level in the liver. Campione and colleagues, for example, showed a dose-dependent antifungal effect for RA *in vitro* (Campione et al., 2021). The AmB dose of 5 mg/kg was defined by a previous study using LAmB treatment for CL (Ramos et al., 2022).

In the *L. major* model, treatment with LAmB-RA significantly reduced lesion size growth and parasite burden compared to the Control. LAmB-RA was the group with the most significant decrease in parasite load compared to the Control, followed by LAmB. It should be noted that AmBisome® was less effective than LAmB-RA and LAmB in controlling the lesion size growth and did not promote a substantial reduction in the parasite load despite a marked increase in IFN-γ level in the liver. These effects are consistent with the pharmacokinetic data of AmBisome®, which support the high liver targeting of conventional liposomes, the short mean residence time of AmB in plasma, and, potentially, lower drug accumulation in the skin lesion.

Regarding IL-10 levels in the liver, there was a higher level in the group treated with LAmB, but none of the treatments led to a significant increase compared to the Control. Thus, evaluating the IFN-γ/IL-10 ratio indicated a significantly lower ratio in LAmB compared to AmBisome® and an intermediate ratio for LAmB-RA. Therefore, our data suggests that incorporating RA into LAmB modulates the Th1/Th2 balance, leading to a profile close to that observed after AmBisome® treatment.

A panel of cytokines involved in anti-inflammatory and tissue-repairing activities was also evaluated from the liver of treated animals: Free Active TGF-β1, CCL22 (MDC), IL-6, and G-CSF. These cytokines counteract the immunopathology caused by pro-inflammatory cytokines and, depending on the disease course, are also responsible for maintaining parasites in the infection site and chronicity. A reduction in CCL22 was observed when comparing LAmB-RA to AmBisome®. The chemokine CCL22 is known to recruit regulatory T cells (Tregs) to the site of infection, suppressing inflammatory immune responses (Tomiotto-Pellissier et al., 2018**).** However, no significant difference was observed for these cytokines compared to the Control group.

One should keep in mind that the cytokine profile obtained from the liver may be different from the profile found in the lesion, as shown by Carvalho et al. (2024). Furthermore, evaluating the amount of cytokine in the organ strongly depends on the disease's progression and the animal's immune profile at euthanasia. Also, Gogulamudi and colleagues (2019) showed that the change in the cytokine production profile is dependent on treatment time; they observed a greater reduction in parasite load, a significant increase in serum Th1 cytokines after

28 days of treatment with vitamin D_3/RA and chenodeoxycholic acid/RA combinations than after 7, 14 or 21 days (Gogulamudi et al., 2019). Thus, our cytokine data should be interpreted with caution as they may not provide a complete picture of the immune response during the disease.

In the second infection model, LAmB-RA, LAmB, and AmBisome® showed a similar efficacy profile as that observed in *L. major*, with a greater ability of LAmB-RA to reduce the lesion size growth compared to Controls and AmBisome®. These results are consistent with a previous report about the *L. amazonensis* murine model, showing that LAmB reduced the lesion size growth and parasite load more effectively than AmBisome® (Ramos et al., 2022). Interestingly, in this infection model, the treatments promoted a slowdown of the lesion growth but not a reduction in the lesion size as observed in the *L. major* model. The discrepancy between the models may be attributed to treatment initiated later in the *L. amazonensis* model (27 *vs.* 44 days post-infection) or to the difference in virulence or drug sensitivity between the *Leishmania* species.

It is well known that the *L. amazonensis* infection in humans leads to high resistance to treatment and frequent relapses, as it is related to the anergic pole without a specific cellular response to *Leishmania* antigens, leading to DCL. In this manifestation, marked parasite proliferation and infection dissemination are observed (Brasil, 2017; Scorza et al., 2017).

In the *L. amazonensis* mice model, the immune response was evaluated specifically in the spleen after stimulation with *Leishmania* antigen. Notably, LAmB-RA is the only group with significantly higher IFN-γ production than the Control group ($p < 0.001$). The differences observed in the cytokine profile between the two CL models could be due to the organ since the spleen, a well-established lymphoid organ, may better reflect systemic immune modulation than the liver. Also, different types of immune responses can be observed during different *Leishmania spp*. infections (Rossi & Fasel, 2018; Scorza et al., 2017).

As *Leishmania* is an intracellular parasite, one of the physiological mechanisms for its elimination by the body is cell activation, which is done through the induction of a Th1-type immune response and secretion of pro-inflammatory cytokines. Activated macrophages can eliminate the parasite by producing reactive oxygen species (Brasil, 2017; Rossi & Fasel, 2018). The increased IFN-γ production in LAmB-RA group compared to all other groups supports the role of RA in enhancing specific Th1-type immune responses. LAmB-RA also showed significantly lower level of IL-10 in comparison with LAmB, resulting in significantly higher IFN-γ/IL-10 ratio and confirming that introduction of RA into AmB-liposomes led to a shift towards a Th1-type response.

These data agree with recent reports of RA immunomodulatory effects *in vitro* and *in vivo*. *In vitro* studies showed that *L. donovani*-infected macrophages exhibited lower expression of enzymes responsible for converting retinol into RA. Evaluating the inhibition of these enzymes and, consequently, RA production, they observed a shift in the Th2 immune response and permissive environment to the parasite (Verma et al., 2019). Other authors pointed to a context-dependent role of RA. *In vitro*, RA induced IL-10 production in T cells and monocytes from healthy children but prevented its increase in cells from VL children when combined with SLA (Maciel et al., 2014). The combination of vitamin D_3/RA and CDCA/RA was evaluated *in vitro* and *in vivo* against *L. donovani* infection. It was observed that the treatment of macrophages with these combinations prevented parasite entry and promoted early phagosome maturation. Animals treatment with vitamin D_3/RA (384 ng/30 ng/mice) and CDCA/RA (78 ng/30 ng/mice) was carried out by VO for up to 28 days, resulting in suppressing Th2 immune responses (IL-4, IL-5) while enhancing Th1 immunity (IL-2, IFN-γ, TNF-α) (Gogulamudi et al., 2015; Gogulamudi et al., 2019).

Conversely, results pointing to an anti-inflammatory effect (Th2) have also been reported in the literature, with RA (Pereira et al., 2011; Vellozo et al., 2017), but also with vitamin A (Frankenburg et al., 1998; Garg et al., 2004) treatment. Thus, because of the conflicting reports on the immunomodulary action of RA, the results obtained in our study could not have been anticipated.

It should be noted that BALB/c mice are highly susceptible to CL, with this susceptibility linked to a genetic inability to produce IL-12, an essential cytokine for Th1 cells differentiation. This immune impairment causes progressive skin lesions and visceral invasion (Maspi et al., 2016). Thus, this fact reinforces that the production of Th1-type cytokines is directly related to animal treatment. In line with the production of pro-inflammatory cytokines, a significant reduction in parasite load was observed in the spleen for the LAmB-RA group (60%) in *L. amazonensis*-infected mice, demonstrating the efficacy of the therapy systemically. On the other hand, only a 17% reduction was achieved by LAmB, and no reduction was observed for AmBisome®.

Regarding the potencial toxicity of the treatment, creatinine and ureia were investigated as serum markers of the renal function and hispathological evaluations were carried out. The slight increase in serum creatinine and changes in histopathological score, in the groups receiving liposomal AmB formulations are indicative of mild renal toxicity. Nephrotoxicity is a known adverse effect of AmB (Lemke et al., 2005), attributed mainly to LDL receptor-mediated uptake in renal cells, causing vasoconstriction and reduced glomerular filtration

(Carolus et al., 2020). This adverse effect remains the most common, affecting more than 40% of patients receiving liposomal AmB (Chivinski et al., 2023). No significant weight loss was observed for any treatments comparing the animal's weight at the beginning and at the end of treatment in both models.

7.2. DLAmB-RA made from deformable vesicles

A deformable formulation was developed to deliver AmB (0.4%) and RA (0.065%) by topical route. The amount of AmB and RA chosen for this formulation took into account a study evaluating liposomes containing 0.1%, 0.2%, or 0.4% AmB, showing safety and better anti-leishmanial efficacy in *L. major* murine model for the formulation containing AmB 0.4% (Jaafari et al., 2019). In addition, RA is commonly used in commercial formulations between 0.01 and 0.1% ranges to treat skin-related diseases (FDA, [n.d.]). In addition to the active ingredients, P90G was used as a bilayer-forming phospholipid and DOC as a surfactant, being an edge activator. Although DOC may lead to skin irritation, it was shown to be safe, without dermatological toxicity, in a study evaluating transfersomes delivery by topical route (Fernández-García et al., 2020b).

DLAmB-RA had a size of around 100 nm, as a result of extrusion through 100-nm polycarbonate membranes. Interestingly, no significant difference was observed when comparing the particle size of DLAmB-RA, DLAmB and DLRA formulations. Unlike rigid liposomes (LAmB-RA), AmB incorporation did not increase the particle size. The concentration of AmB in the deformable liposome compared to the rigid one is close, but slightly higher (4 mg/mL *vs.* 2.9 mg/mL), so the presence of DOC and low transition temperature phospholipid and the absence of cholesterol in the lipid membrane, conferring greater flexibility, could contribute to a better ability of the membrane to adapt/reorganize itself with AmB insertion.The use of a different preparation method involving a final extrusion step after drug incorporation may also contribute to the differential characteristics of the formulation.

Deformable liposomes PdI was < 0.25, showing a uniform particle size distribution. Although the topical route is less restrictive than the IV regarding particle size and its distribution, transfersome's size below 300 nm may ensure better skin penetration when applied under non-occlusive conditions (Fernández-García et al., 2020a). The skin is an organ that acts as a barrier against external agents, protecting humans from dangerous substances and potential pathogens. On the other hand, it also hinders the passage of drugs in treating skin diseases,

especially when reaching the lower layers, such as the dermis in leishmaniasis (Perez et al., 2016; Sala et al., 2018).

The surface charge was approximately -9.4 mV for all liposomes, being more negative than rigid liposomes (around -5.0 mV). This is likely due to the absence of PEGylation and also to the presence of DOC, an anionic surfactant. However, the observed surface charge is still slightly negative. This could be due to the high ionic strength of the solvent used for the ZP measurement: NaCl 0.9%, considered a physiological solution. At higher ionic strengths, particles exhibited a pronounced shift toward less negative ZP values. Elevated ionic strength compresses the electrical double layer, thereby reducing the measured ZP (Nobbmann, 2018).

The nanocarrier's charge is one of the parameters impacting permeation through the skin. However, the type of charge that produces better skin absorption is controversial. Positively charged particles can interact with the negatively charged SC, while negatively charged particles face penetration difficulties due to electrostatic repulsion. On the other hand, it is also proposed that this repulsion may create temporary channels in the skin, facilitating particle permeation. Additionally, improved permeation has also been observed with neutral particles (Elmowafy, 2021). It is therefore difficult to predict the impact of nanocarrier's charge on skin permeation.

Compared to the liposomes, the formulation composed only of AmB and DOC had a significantly higher PdI and PZ. Surprisingly, larger size than the liposomes (about 2x larger) was also observed, being much larger than the expected size of micelles (10–80 nm) (Torchilin, 2007). This may be explained by the complexation of AmB with DOC, self-association of AmB and formation of large aggregates. It was demonstrated elsewhere that increasing the solution ionic strength (e.g., through the presence of electrolytes such as NaCl) promotes micellar growth due to the electrolyte screening effect. This effect reduces the electrostatic repulsion between the polar heads of DOC molecules, favoring aggregation (Serafim et al., 2016). Indeed, these aggregates showed instability, with an increase in size and AmB precipitation over time. In this context, P90G (soybean lecithin) consisting mainly of phosphatidylcholine (> 90%), emerged as a critical component, playing an important role in confering stability of the nanosystem.

The change in the aggregation state of AmB upon addition of P90G to the AmB-DOC suspension was clearly demonstrated by the blue shift of the UV-Vis absorption band and the couplet-type dichroic signal. On the other hand, the CD spectrum of DLAmB and DLAmB-RA differed greatly from those of the rigid liposome formulations, supporting higher aggregation state of AmB in the deformable membrane.

Concerning drug loading, AmB content(%) and $EE_{(\%)}$ remained high (> 90%) during 20 days at 25ºC. The combined effect of soya phosphatidylcholine and DOC may promote apolar interactions within their hydrophobic domains and AmB, along with electrostatic interactions between the carboxyl group of DOC and the primary amine group of AmB, contributing to the high $EE_{(\%)}$ (Fernández-García et al., 2020b).

For DLAmB and DLAmB-RA, an increase in AmB content was observed, which may have been due to the formulations' increased viscosity, which led to a pipetting error. An increase in viscosity over time was observed in the formulations containing AmB, P90G, and DOC (DLAmB or DLAmB-RA), whereas no such change was detected in the formulations without AmB (DLEmpty or DLRA) or in the formulation lacking the phospholipid (AmB-DOC). This suggests that an interaction between these components occurs, likely mediated by the formation of interconnected networks through hydrogen bonding and hydrophobic interactions. It has been reported that DOC solutions can form shear-thinning gels at physiological pH and concentrations around 0.010 mol/L or higher, a phenomenon attributed to the formation of wormlike micelles that entangle into network structures (Serafim et al., 2016). Furthermore, when the phosphatidylcholine content is high, gelation can occur upon the addition of water to a lecithin-organic solvent solution, as water molecules bind to the polar head groups of lecithin, promoting the formation of linear networks. In addition, the polar groups of bile salts, such as DOC, can interact with the phosphate groups of lecithin via hydrogen bonding (Waghule et al., 2022), further contributing to the development of a structured network.

Regarding RA content, on the other hand, a significant reduction was observed for DLRA over time. As previously mentioned, RA is a photosensitive molecule that can oxidize easily, even though the formulation was protected from light and stored under a nitrogen atmosphere. Commercial formulations containing RA, such as Altreno®(lotion), Renova® (cream), and Retin-A® (cream), have the antioxidant butylated hydroxytoluene (BHT) or butylated hydroxyanisole (BHA) in Vesanoid® which proves to be important for shelf-life (FDA, [n.d.]). Interestingly, the RA content from the DLAmB-RA remained stable. How AmB prevented RA degradation is still unclear.

The presence of AmB in a solution containing polyunsaturated fatty acid, *cis*-parinaric acid (PnA), and peroxyl radicals led to a significant decrease in PnA oxidation. Authors showed that PnA and AmB mutually inhibit the oxidation of each other, most likely by competing for the peroxyl radicals. In fact, AmB has seven conjugated double bonds, being susceptible to autoxidation, but in this study, authors point to AmB's ability to scavenge peroxyl radicals

(Osaka et al., 1997). In this sense, AmB's antioxidant effectiveness is superior to that of retinoids, as they have only five conjugated double bonds. The $EE_{(\%)}$ was higher than 90% in both RA formulations (DLRA and DLAmB-RA) over the 20 days. This could indicate that the remaining RA in DLRA (29.5 ± 10.3%) is almost totally incorporated in the liposome.

It is interesting to note that the rigid liposomes promoted greater RA stability, which may be due to the storage condition (30 days at 4 ºC). However, this could also indicate a lower retention capacity of the RA in the deformable vesicle. Once free, it may degrade, explaining why the $EE_{(\%)}$ remains high, as only the encapsulated RA has been preserved. This observation points to another possibility for the protective AmB effect: interaction of RA with AmB-DOC complexes and its retention in the lipid bilayer. However, the occurrence of such interaction was not evidenced by UV-Vis spectroscopic analyses. This hypothesis has to be confirmed in future studies, such as those on RA release *in vitro*.

Although preliminary, this stability study provides interesting results, as another study evaluating a transfersome encapsulating AmB achieved stability of only 1 week for the liquid formulation (not freeze-dried) at 25ºC. In addition, in that study, AmB was at a lower concentration (0.086% w/v) than in the present study (0.4% w/v) (Fernández-García et al., 2020). Even though AmB preparations are recommended to be refrigerated, other authors showed stability at room temperature (25ºC) without lyophilization for up to 20 months (Jaafari et al., 2019).

8. OVERVIEW AND FINAL REMARKS

In this research, two new formulations co-incorporating AmB and RA in either rigid (LAmB-RA) and deformable liposomes (DLAmB-RA) were developed and characterized physicochemically. LAmB-RA was further characterized regarding potential hemolytic activity, pharmacokinetics after IV administration in mice and therapeutic efficacy in murine models of CL. Based on these analyses, the following conclusions can be drawn:

i. The LAmB-RA formulation was successfully developed, showing size, PdI, and ZP values suitable for parenteral administration. High encapsulation efficiencies for both AmB and RA were achieved, demonstrating effective drug loading. UV-Vis and CD spectrocopic analyses revealed that the aggregation state of AmB in the LAmB-RA formulation differs from that of commercial products (AmBisome® and Anforicin B®), suggesting a lower AmB aggregation state.

ii. The LAmB-RA formulation demonstrated stability for at least 30 days at 4 ºC without requiring lyophilization, surpassing the stability of commercial formulations such as Anforicin B®, which is stable for one week, and AmBisome®, which must be used within 24 hours after reconstitution. This prolonged stability in solution offers a significant advantage, particularly for treatments requiring multiple administrations.

iii. The LAmB-RA formulation was much less hemolytic *in vitro* than Anforicin B® and significantly less hemolytic than LAmB. The reduced hemolytic activity may be attributed to slower and more sustained release of AmB.

iv. For the first time, the pharmacokinetics of AmB from LAmB and LAmB-RA formulations were reported and compared to AmBisome®. The PEGylated liposomes showed higher C_{max} and prolonged mean residence time, along with reduced AmB concentrations in the liver, indicating lower uptake by MPS cells. This pharmacokinetic profile resulted in higher and more prolonged plasma AmB levels, suggesting greater drug concentrations at the lesion site, aided by the unique characteristics of CL, such as local inflammation and increased vascular permeability. These findings support the enhanced therapeutic effect of LAmB-RA, due to higher intralesional drug concentrations.

v. The LAmB-RA formulation significantly reduced lesion size growth and parasite load in murine models infected with *L. major* and *L. amazonensis* to higher levels compared to AmBisome®. The incorporation of RA into LAmB was found to induce a Th1-type

pro-inflammatory response, with a notable increase in IFN-γ levels in splenocytes cultures from *L. amazonensis* infected-mice. At the same time, different cytokine profiles were observed in the liver of the *L. major* model, reflecting the pleiotropic nature of cytokines in infection.

vi. Treatment with LAmB-RA showed mild renal toxicity, as indicated by altered creatinine levels and histopathological evaluation, although body weight remained stable, suggesting good overall tolerability. Given the high susceptibility of the animal model used (BALB/c) to *Leishmania* infections, PEGylated liposome efficacy is encouraging, reducing the likelihood of spontaneous remission.

vii. The deformable liposomal formulation (DLAmB-RA) was successfully developed, showing favorable characteristics for topical delivery. The unique composition, with phospholipid and surfactant, contributed to the vesicle's stability and may lead to higher deformability, contributing to skin drug penetration. Drug content and EE remained high (> 90%) over 20 days for both AmB and RA at 25 ºC, which is highly appreciated for a topical formulation to be used in endemic tropical and subtropical areas.

It is worth noting that these findings are limited to the analyses conducted in this study. Future research could evaluate cytokine levels at the lesion site and lymph nodes to better understand the immune response triggered by the LAmB-RA formulations. Studying RA signaling-related pathways to understand its action mechanism would also be interesting. Additionally, exploring higher doses of RA in a dose-response study may show enhanced therapeutic effect. Long-term stability studies, particularly with antioxidants, are also necessary to ensure the formulation's viability for commercial use. A repeated dose pharmacokinetic study evaluating both drugs' plasma concentration and biodistribution would significantly contribute. Further studies to elucidate the mechanisms by which AmB protects RA from degradation in DLAmB-RA—whether through radical scavenging, bilayer retention, or molecular interaction—could provide help optimizing these formulations. Finally, exploring the skin permeation of these deformable liposomes and *in vivo* efficacy studies are necessary to validate their therapeutic potential.

The results presented in this thesis suggest that co-loading AmB and RA into PEGylated rigid or deformable liposomes is a promising strategy against CL, a neglected and endemic disease in more than 90 countries and territories.

REFERENCES

Abdeladhim, M., Kamhawi, S., & Valenzuela, J. G. (2014). What's behind a sand fly bite? The profound effect of sand fly saliva on host hemostasis, inflammation and immunity. *Infection, Genetics and Evolution*, *28*, 691–703. https://doi.org/10.1016/j.meegid.2014.07.028

Abdollahizad, E., Dadashzadeh, S., Bahri, S., Abbasian, Z., & Rezaee, E. (2023). Amphotericin B Pharmacokinetics: Inter-strain differences in rats following intravenous administration of the most commonly marketed formulations of the drug. *Iranian Journal of Pharmaceutical Research*, *22*(1), 1–8. https://doi.org/10.5812/ijpr-134772

Abu Ammar, A., Nasereddin, A., Ereqat, S., Dan-Goor, M., Jaffe, C. L., Zussman, E., & Abdeen, Z. (2019). Amphotericin B-loaded nanoparticles for local treatment of cutaneous leishmaniasis. *Drug Delivery and Translational Research*, *9*(1), 76–84. https://doi.org/10.1007/s13346-018-00603-0

Afonso, L. C. C., & Scott, P. (1993). Immune responses associated with susceptibility of C57BL/10 mice to *Leishmania amazonensis*. *Infection and Immunity*, *61*(7), 2952–2959. https://doi.org/10.1128/iai.61.7.2952-2959.1993

Agência Nacional de Vigilância Sanitária (ANVISA). (2017). *Resolução RDC no 166, de 24 de julho de 2017*. Brasília: *Ministério da Saúde*.

Agência Nacional de Vigilância Sanitária (ANVISA). (2025). *Resolução - RE nº 11, de 02/01/2025*. Brasília: *Ministério da Saúde*. https://anvisalegis.datalegis.net/action/ActionDatalegis.php?acao=abrirTextoAto&link=S&tipo=RES&numeroAto=00000011&seqAto=000&valorAno=2025&orgao=RE/GGMED/ANVISA/MS&codTipo=&desItem=&desItemFim=&cod_modulo=293&cod_menu=8499

Akhoundi, M., Kuhls, K., Cannet, A., Votýpka, J., Marty, P., Delaunay, P., & Sereno, D. (2016). A historical overview of the classification, evolution, and dispersion of *Leishmania* parasites and sandflies. *PLoS neglected tropical diseases*, *10*(3), e0004349. https://doi.org/10.1371/journal.pntd.0004349

Ali, D. A., El Hamdi, A., Boumeshouli, N., Hakem, A., El Khiat, A., El Koutbi, M., ... & Khabbache, H. (2025). Assessing the health-related quality of life of cutaneous Leishmaniasis patients in Draa-Tafilalet, southeastern Morocco. *Parasitology International*, *104*, 102963. https://doi.org/10.1016/j.parint.2024.102963

Alvar, J., Yactayo, S., & Bern, C. (2006). Leishmaniasis and poverty. *Trends in Parasitology*, *22*(12), 552–557. https://doi.org/10.1016/j.pt.2006.09.004

Alves, M. M. D. M., Arcanjo, D. D. R., Figueiredo, K. A., Oliveira, J. S. D. S. M., Viana, F. J. C., Coelho, E. D. S., ... & Carvalho, F. A. D. A. (2020). Gallic and ellagic acids are promising adjuvants to conventional amphotericin B for the treatment of cutaneous leishmaniasis. *Antimicrobial Agents and Chemotherapy*, *64*(12), 10–1128. https://doi.org/10.1128/aac.00807-20

Arantes, V. T., Faraco, A. A., Ferreira, F. B., Oliveira, C. A., Martins-Santos, E., Cassini-Vieira, P., ... & Goulart, G. A. (2020). Retinoic acid-loaded solid lipid nanoparticles surrounded by chitosan film support diabetic wound healing in *in vivo* study. *Colloids and Surfaces B: Biointerfaces*, *188*, 110749. https://doi.org/10.1016/j.colsurfb.2019.110749

Arruda, G. J. B., Rossanezi, G., Scarpa, M. V., do Egito, E. S. T., & de Oliveira, A. G. (2016). Estratégias tecnológicas para formulações de anfotericina B em sistemas lipídicos disponíveis no mercado farmacêutico e outros promissores sistemas de administração. *Infarma-Ciências Farmacêuticas*, *28*(2), 59-67. https://doi.org/10.14450/2318-9312.v28.e2.a2016.pp59-67

Asilian, A., Sadeghinia, A., Faghihi, G., & Momeni, A. (2004). Comparative study of the efficacy of combined cryotherapy and intralesional meglumine antimoniate (Glucantime®) *vs*. cryotherapy and intralesional meglumine antimoniate (Glucantime®) alone for the treatment of cutaneous leishmaniasis. *International Journal of Dermatology*, *43*(4), 281–283. https://doi.org/10.1111/j.1365-4632.2004.02002.x

Atia, A. M., Mumina, A., Tayler-Smith, K., Boulle, P., Alcoba, G., Elhag, M. S., ... & Zachariah, R. (2015). Sodium stibogluconate and paromomycin for treating visceral leishmaniasis under routine conditions in eastern Sudan. *Tropical Medicine & International Health*, *20*(12), 1674–1684. https://doi.org/10.1111/tmi.12603

Bangham, A. D., Standish, M. M., & Watkins, J. C. (1965). Diffusion of univalent ions across the lamellae of swollen phospholipids. *Journal of Molecular Biology*, *13*(1), 238–252. https://doi.org/10.1016/S0022-2836(65)80093-6

Barratt, G., & Bretagne, S. (2007). Optimizing efficacy of Amphotericin B through nanomodification. *International journal of nanomedicine*, *2*(3), 301-313.

Ben Salah, A., Louzir, H., Chlif, S., Mokni, M., Zaâtour, A., Raouene, M., ... & Dellagi, K. (2005). The predictive validity of naturally acquired delayed-type hypersensitivity to leishmanin in resistance to *Leishmania major*-associated cutaneous leishmaniasis. *The Journal of infectious diseases*, *192*(11), 1981–1987. https://doi.org/10.1086/498042

Bernardo, L., Solana, J. C., Sanchez, C., Torres, A., Reyes-Cruz, E. Y., Carrillo, E., & Moreno, J. (2023). Immunosuppressants alter the immune response associated with Glucantime® treatment for *Leishmania* infantum infection in a mouse model. *Frontiers in Immunology*, *14*, 1285943. https://doi.org/10.3389/fimmu.2023.1285943

Borges, G. S. M., Lima, F. A., Carneiro, G., Goulart, G. A. C., & Ferreira, L. A. M. (2021). All-trans retinoic acid in anticancer therapy: how nanotechnology can enhance its efficacy and resolve its drawbacks. *Expert Opinion on Drug Delivery*, *18*(10), 1335–1354. https://doi.org/10.1080/17425247.2021.1919619

Bradford, M. M. (1976). A rapid and sensitive method for the quantitation of microgram quantities of protein utilizing the principle of protein-dye binding. *Analytical biochemistry*, *72*(1–2), 248–254.

Brasil. Ministério da Saúde. (2020). *Nota Informativa Nº 13/2020-CGZV/DEIDT/SVS/MS*. Brasília: *Ministério da Saúde*. https://www.gov.br/saude/pt-br/centrais-de-conteudo/publicacoes/estudos-e-notas-informativas/2020/nota-informativa-miltefosina.pdf/view

Brasil. Ministério da Saúde. (2021). *Nota Técnica Nº 66/2021-CGZV/DEIDT/SVS/MS*. Brasília: *Ministério da Saúde.* https://www.gov.br/saude/pt-br/assuntos/saude-de-a-a-z/l/leishmaniose-visceral/notas-tecnicas-e-informativas/6-nota-tecnica-n-66-2021-cgvz-deidt-svs-ms/view

Brasil. Ministério da Saúde. Secretaria de Vigilância em Saúde e Ambiente. Departamento de Ações Estratégicas de Epidemiologia e Vigilância em Saúde e Ambiente. (2024). *Guia de vigilância em saúde* (6th ed. revised). Brasília: *Ministério da Saúde*.

Brasil. Ministério da Saúde. Secretaria de Vigilância em Saúde. Departamento de Vigilância Epidemiológica. (2014). *Manual de vigilância e controle da leishmaniose visceral* (1st ed., 5th reprint). Brasília: *Ministério da Saúde*.

Brasil. Ministério da Saúde. Secretaria de Vigilância em Saúde. Departamento de Vigilância Epidemiológica. (2011). *Leishmaniose visceral: recomendações clínicas para redução da letalidade* (1st ed.). Brasília: *Ministério da Saúde*.

Brasil. Ministério da Saúde. Secretaria de Vigilância em Saúde. Departamento de Vigilância das Doenças Transmissíveis. (2017). *Manual de vigilância da leishmaniose tegumentar* (1st ed.). Brasília: *Ministério da Saúde*.

Bruni, N., Stella, B., Giraudo, L., Della Pepa, C., Gastaldi, D., & Dosio, F. (2017). Nanostructured delivery systems with improved leishmanicidal activity: a critical

review. *International Journal of Nanomedicine*, 5289–5311. https://doi.org/10.2147/IJN.S140363

Campione, E., Gaziano, R., Doldo, E., Marino, D., Falconi, M., Iacovelli, F., ... & Orlandi, A. (2021). Antifungal effect of all-trans retinoic acid against *Aspergillus fumigatus in vitro* and in a pulmonary aspergillosis *in vivo* model. *Antimicrobial Agents and Chemotherapy*, *65*(3), 10–1128. https://doi.org/10.1128/AAC.01874-20

Campione, E., Gaziano, R., Marino, D., & Orlandi, A. (2016). Fungistatic activity of all-trans retinoic acid against *Aspergillus fumigatus* and *Candida albicans*. *Drug Design, Development and Therapy*, 1551-1555. https://doi.org/10.2147/DDDT.S93985

Carneiro, G., Aguiar, M. G., Fernandes, A. P., & Ferreira, L. A. M. (2012). Drug delivery systems for the topical treatment of cutaneous leishmaniasis. *Expert Opinion on Drug Delivery*, *9*(9), 1083-1097. https://doi.org/10.1517/17425247.2012.701204

Carolus, H., Pierson, S., Lagrou, K., & Van Dijck, P. (2020). Amphotericin B and other polyenes—Discovery, clinical use, mode of action and drug resistance. *Journal of Fungi*, *6*(4), 321. https://doi.org/10.3390/jof6040321

Carregal, V. M., Lanza, J. S., Souza, D. M., Islam, A., Demicheli, C., Fujiwara, R. T., ... & Frézard, F. (2019). Combination oral therapy against *Leishmania amazonensis* infection in BALB/c mice using nanoassemblies made from amphiphilic antimony (V) complex incorporating miltefosine. *Parasitology research, 118*, 3077–3084. https://doi.org/10.1007/s00436-019-06419-2

Carvalho, A. M., Costa, R. S., Lago, A., Bacellar, O., Beiting, D. P., Scott, P., ... & Carvalho, E. M. (2024). *In situ* versus systemic immune response in the pathogenesis of cutaneous leishmaniasis. *Pathogens*, 13(3), 199. https://doi.org/10.3390/pathogens13030199

Carvalho, A. M., Guimarães, L. H., Costa, R., Saldanha, M. G., Prates, I., Carvalho, L. P., ... & Carvalho, E. M. (2021). Impaired Th1 response is associated with therapeutic failure in patients with cutaneous Leishmaniasis caused by *Leishmania braziliensis*. *The Journal of Infectious Diseases*, *223*(3), 527–535. https://doi.org/10.1093/infdis/jiaa374

Cavassin, F. B., Baú-Carneiro, J. L., Vilas-Boas, R. R., & Queiroz-Telles, F. (2021). Sixty years of amphotericin B: an overview of the main antifungal agent used to treat invasive fungal infections. *Infectious diseases and therapy*, *10*(1), 115-147. https://doi.org/10.1007/s40121-020-00382-7

Chivinski, J., Nathan, K., Naeem, F., Ekmekjian, T., Libman, M. D., & Barkati, S. (2023). Intravenous liposomal Amphotericin B efficacy and safety for cutaneous and mucosal

leishmaniasis: A systematic review and meta-analysis. *Open Forum Infectious Diseases*, *10*(7), 1–9. https://doi.org/10.1093/ofid/ofad348

Coelho, L. D., Souza, M. M., Cassali, G. D., Silva, R. A., Paiva, M. J., Barros, A. L., ... & Oliveira, M. C. (2023). Emetic tartar-loaded liposomes as a new strategy for leishmaniasis treatment. *Pharmaceutics*, *15*(3), 904. https://doi.org/10.3390/pharmaceutics15030904

Costa, W. C., Beltrami, V. A., Campolina-Silva, G. H., Queiroz-Junior, C. M., Florentino, R. M., Machado, J. R., ... & Pinho, V. (2023). Therapeutic treatment with phosphodiesterase-4 inhibitors alleviates kidney injury and renal fibrosis by increasing MMP-9 in a doxorubicin-induced nephrotoxicity mouse model. *International Immunopharmacology*, *115*, 109583. https://doi.org/10.1016/j.intimp.2022.109583

Cota, G. F., de Sousa, M. R., Fereguetti, T. O., Saleme, P. S., Alvarisa, T. K., & Rabello, A. (2016). The cure rate after placebo or no therapy in American cutaneous leishmaniasis: a systematic review and meta-analysis. *PLoS One*, *11*(2), e0149697. https://doi.org/10.1371/journal.pone.0149697

Cui, M., Wiraja, C., Chew, S. W. T., & Xu, C. (2020). Nanodelivery systems for topical management of skin disorders. *Molecular Pharmaceutics*, *18*(2), 491-505. https://doi.org/10.1021/acs.molpharmaceut.0c00154

Custodio E, López-Alcade, J, Herrero, M, Bouza, C, Jimenez, C, Bonsmann, S. S. g., ... & Alvar, J. (2018). Nutritional supplements for patients being treated for active visceral leishmaniasis. *Cochrane Database of Systematic Reviews*, 3. https://doi.org/10.1002/14651858.CD012261.pub2

da Costa, V. M., Santos, T. T., Pinto, N. V., Carneiro, G., Frézard, F., & Marques Borges, G. S. (2024). To heat or not to heat: the impact of temperature on the aggregation state of amphotericin B in drug delivery systems. *Nanomedicine*, *19*(24), 1953-1956. https://doi.org/10.1080/17435889.2024.2382669

Dar, M. J., Khalid, S., McElroy, C. A., Satoskar, A. R., & Khan, G. M. (2020). Topical treatment of cutaneous leishmaniasis with novel amphotericin B-miltefosine co-incorporated second generation ultra-deformable liposomes. *International journal of pharmaceutics*, *573*, 118900. https://doi.org/10.1016/j.ijpharm.2019.118900

Deray, G. (2002). Amphotericin B nephrotoxicity. *Journal of antimicrobial chemotherapy*, *49*(suppl_1), 37-41. https://doi.org/10.1093/jac/49.suppl_1.37

Doni, S., Yeneneh, K., Hailemichael, Y., Gebremichael, M., Skarbek, S., Ayele, S., ... & Gadisa, E. (2023). Health-related quality of life of adults with cutaneous leishmaniasis at

ALERT Hospital, Addis Ababa, Ethiopia. *PLoS Neglected Tropical Diseases*, *17*(10), e0011196. https://doi.org/10.1371/journal.pntd.0011196

Dorlo, T. P., Balasegaram, M., Beijnen, J. H., & de Vries, P. J. (2012). Miltefosine: a review of its pharmacology and therapeutic efficacy in the treatment of leishmaniasis. *Journal of Antimicrobial Chemotherapy*, *67*(11), 2576–2597. https://doi.org/10.1093/jac/dks275

Drugs for Neglected Diseases Initiative (DNDi). (2021). *Cheaper, shorter, more effective combination therapy for visceral leishmaniasis in Africa*. Geneva: *DNDi*. https://dndi.org/research-development/portfolio/ssg-pm/

Drugs for Neglected Diseases Initiative (DNDi). (2025a). *Adoption of new visceral leishmaniasis treatments in South Asia*. Geneva: *DNDi*. https://dndi.org/research-development/portfolio/new-vl-treatments-south-asia/

Drugs for Neglected Diseases Initiative (DNDi). (2025b). *Miltefosine + Paromomycin combination (Africa)*. Geneva: *DNDi*. https://dndi.org/research-development/portfolio/miltefosine-paromomycin-combo/

Drugs for Neglected Diseases Initiative (DNDi). (2025c). *Safe and effective treatment for people living with both visceral leishmaniasis and HIV*. https://dndi.org/research-development/portfolio/new-treatments-vl-hiv/

Drugs for Neglected Diseases Initiative (DNDi). (2025d). *New treatments for PKDL (Eastern Africa)*. Geneva: *DNDi*. https://dndi.org/research-development/portfolio/new-treatments-pkdl-eastern-africa/

Drugs for Neglected Diseases Initiative (DNDi). (2025e). *New treatments for PKDL (South Asia)*. Geneva: *DNDi*. https://dndi.org/research-development/portfolio/new-treatments-pkdl-south-asia/

Drugs for Neglected Diseases Initiative (DNDi). (2025f). *Miltefosine + thermotherapy for cutaneous leishmaniasis*. Geneva: *DNDi*. https://dndi.org/research-development/portfolio/miltefosine-thermotherapy-cutaneous-leishmaniasis/

Drugs for Neglected Diseases Initiative (DNDi). (2025g). *CpG-D35 (DNDI-2319)*. Geneva: *DNDi*. https://dndi.org/research-development/portfolio/dndi-2319/

Elmowafy, M. (2021). Skin penetration/permeation success determinants of nanocarriers: Pursuit of a perfect formulation. *Colloids and Surfaces B: Biointerfaces*, *203*, 111748. https://doi.org/10.1016/j.colsurfb.2021.111748

Eskandari, S. E., Firooz, A., Nassiri-Kashani, M., Jaafari, M. R., Javadi, A., Mohammadi, A. M., & Khamesipour, A. (2019). Safety evaluation of topical application of nano-

liposomal form of amphotericin B (SinaAmpholeish) on healthy volunteers: phase I clinical trial. *Iranian journal of parasitology*, *14*(2), 197.

European Medicine Agency (EMA). (2012). Guideline on bioanalytical method validation. *EMA Guidance Document 192217/2009 Rev. 1 Corr. 2*, 1–23.

European Medicine Agency (EMA). (2013). Reflection paper on the data requirements for intravenous liposomal products developed with reference to an innovator liposomal product. *EMA/Committee for Human Medicinal Products 806058/2009/Rev. 02*, *44*(February), 1–13.

Fernández-García, R., de Pablo, E., Ballesteros, M. P., & Serrano, D. R. (2017). Unmet clinical needs in the treatment of systemic fungal infections: The role of amphotericin B and drug targeting. *International journal of pharmaceutics*, *525*(1), 139-148. https://doi.org/10.1016/j.ijpharm.2017.04.013

Fernández-García, R., Lalatsa, A., Statts, L., Bolás-Fernández, F., Ballesteros, M. P., & Serrano, D. R. (2020a). Transferosomes as nanocarriers for drugs across the skin: Quality by design from lab to industrial scale. *International journal of pharmaceutics*, *573*, 118817. https://doi.org/10.1016/j.ijpharm.2019.118817

Fernández-García, R., Statts, L., De Jesus, J. A., Dea-Ayuela, M. A., Bautista, L., Simão, R., ... & Serrano, D. R. (2020b). Ultradeformable lipid vesicles localize amphotericin B in the dermis for the treatment of infectious skin diseases. *ACS infectious diseases*, *6*(10), 2647-2660. https://doi.org/10.1021/acsinfecdis.0c00293

Ferreira, B. A., Coser, E. M., de la Roca, S., Aoki, J. I., Branco, N., Soares, G. H., ... & Coelho, A. C. (2024). Amphotericin B resistance in *Leishmania amazonensis*: *In vitro* and *in vivo* characterization of a Brazilian clinical isolate. *PLOS Neglected Tropical Diseases*, *18*(5), e0012175. https://doi.org/10.1371/journal.pntd.0012175

Ferreira, R., Napoli, J., Enver, T., Bernardino, L., & Ferreira, L. (2020). Advances and challenges in retinoid delivery systems in regenerative and therapeutic medicine. *Nature Communications*, *11*(1), 4265. https://doi.org/10.1038/s41467-020-18042-2

Food and Drug Administration (FDA). ([n.d.]). *Drugs@FDA: FDA-Approved Drugs*. https://www.accessdata.fda.gov/scripts/cder/daf/index.cfm?event=BasicSearch.process

Food and Drug Administration (FDA). (2018). *Liposome Drug Chemistry, Manufacturing, and Controls; Human Products Pharmacokinetics and Bioavailability; and Labeling Documentation*. *27*(16), 1835–1840.

Frankenburg, S., Wang, X., & Milner, Y. (1998). Vitamin A inhibits cytokines produced by type 1 lymphocytes *in vitro*. *Cellular Immunology*, *185*(1), 75–81. https://doi.org/10.1006/cimm.1998.1268

Frézard, F., Aguiar, M. M., Ferreira, L. A., Ramos, G. S., Santos, T. T., Borges, G. S., ... & De Morais, H. L. (2022). Liposomal amphotericin B for treatment of leishmaniasis: from the identification of critical physicochemical attributes to the design of effective topical and oral formulations. *Pharmaceutics*, *15*(1), 99. https://doi.org/10.3390/pharmaceutics15010099

Ganta, S., Talekar, M., Singh, A., Coleman, T. P., & Amiji, M. M. (2014). Nanoemulsions in translational research - Opportunities and challenges in targeted cancer therapy. *AAPS PharmSciTech*, *15*(3), 694–708. https://doi.org/10.1208/s12249-014-0088-9

Garg, R., Singh, N., & Dube, A. (2004). Intake of nutrient supplements affects multiplication of *Leishmania donovani* in hamsters. *Parasitology*, *129*(6), 685–691. https://doi.org/10.1017/S0031182004006055

Gatto, M. S., Johnson, M. P., & Najahi-Missaoui, W. (2024). Targeted Liposomal Drug Delivery: Overview of the Current Applications and Challenges. *Life*, *14*(6). https://doi.org/10.3390/life14060672

Gautam, S., Kumar, R., Maurya, R., Nylén, S., Ansari, N., Rai, M., ... & Sacks, D. (2011). IL-10 neutralization promotes parasite clearance in splenic aspirate cells from patients with visceral leishmaniasis. *Journal of Infectious Diseases*, *204*(7), 1134–1137. https://doi.org/10.1093/infdis/jir461

Giordani, S., Marassi, V., Zattoni, A., Roda, B., & Reschiglian, P. (2023). Liposomes characterization for market approval as pharmaceutical products: Analytical methods, guidelines and standardized protocols. *Journal of Pharmaceutical and Biomedical Analysis*, *236*(July), 115751. https://doi.org/10.1016/j.jpba.2023.115751

Gogulamudi, V. R., Dubey, M. L., Kaul, D., Atluri, V. S. R., & Sehgal, R. (2015). Downregulation of host tryptophan–aspartate containing coat (TACO) gene restricts the entry and survival of *Leishmania donovani* in human macrophage model. *Frontiers in Microbiology*, *6*, 946. https://doi.org/10.3389/fmicb.2015.00946

Gogulamudi, V. R., Dubey, M. L., Kaul, D., Hubert, D. J., Kandimalla, R., & Sehgal, R. (2019). Vitamins (A&D) and Isoprenoid (Chenodeoxycholic acid) molecules are accompanied by Th1 immunostimulatory response and therapeutic cure *in vivo*: possible antileishmanial drugs. *Scientific Reports*, *9*(1). https://doi.org/10.1038/s41598-019-44630-4

Golenser, J., & Domb, A. (2006). New formulations and derivatives of amphotericin B for treatment of leishmaniasis. *Mini reviews in medicinal chemistry*, *6*(2), 153-162. https://doi.org/10.2174/138955706775476037

Guery, R., Henry, B., Martin-Blondel, G., Rouzaud, C., Cordoliani, F., Harms, G., ... & French Cutaneous Leishmaniasis Study group & the LeishMan network. (2017). Liposomal Amphotericin B in travelers with cutaneous and muco-cutaneous leishmaniasis: Not a panacea. *PLoS Neglected Tropical Diseases*, *11*(11), e0006094. https://doi.org/10.1371/journal.pntd.0006094

Guimarães, D., Cavaco-Paulo, A., & Nogueira, E. (2021). Design of liposomes as drug delivery system for therapeutic applications. *International Journal of Pharmaceutics*, *601*(April). https://doi.org/10.1016/j.ijpharm.2021.120571

Haas, N., Hauptmann, S., Paralikoudi, D., Muche, M., & Kolde, G. (2002). Interferon-γ treatment induces granulomatous tissue reaction in a case of localized cutaneous leishmaniasis. *The American Journal of Dermatopathology*, *24*(4), 319–323.

Hamad, I., Hunter, A. C., Szebeni, J., & Moghimi, S. M. (2008). Poly(ethylene glycol)s generate complement activation products in human serum through increased alternative pathway turnover and a MASP-2-dependent process. *Molecular Immunology*, *46*(2), 225–232. https://doi.org/10.1016/j.molimm.2008.08.276

Hamill, R. J. (2013). Amphotericin B formulations: a comparative review of efficacy and toxicity. *Drugs*, *73*, 919–934. https://doi.org/10.1007/s40265-013-0069-4

Helou, D. G., Mauras, A., Fasquelle, F., Lanza, J. S., Loiseau, P. M., Betbeder, D., & Cojean, S. (2021). Intranasal vaccine from whole *Leishmania donovani* antigens provides protection and induces specific immune response against visceral leishmaniasis. *PLoS Neglected Tropical Diseases*, *15*(8), e0009627. https://doi.org/10.1371/journal.pntd.0009627

Heras-Mosteiro, J., Monge-Maillo, B., Pinart, M., Pereira, P. L., Garcia-Carrasco, E., Cuadrado, P. C., ... & López-Vélez, R. (2017). Interventions for Old World cutaneous leishmaniasis. *Cochrane database of systematic reviews*, (11). https://doi.org/10.1002/14651858.CD005067.pub4

Hernandez, F. M. D. O., Santos, M. O., Venturin, G. L., Bragato, J. P., Rebech, G. T., Melo, L. M., ... & de Lima, V. M. (2021). Vitamins A and D and zinc affect the leshmanicidal activity of canine spleen leukocytes. *Animals*, *11*(9), 2556. https://doi.org/10.3390/ani11092556

Herve, M., Debouzy, J. C., Borowski, E., Cybulska, B., & Gary-Bobo, C. M. (1989). The role of the carboxyl and amino groups of polyene macrolides in their interactions with sterols and their selective toxicity. A 31P-NMR study. *Biochimica et Biophysica Acta (BBA)-Biomembranes*, *980*(3), 261-272. https://doi.org/10.1016/0005-2736(89)90312-X

Hofheinz, R. D., Gnad-Vogt, S. U., Beyer, U., & Hochhaus, A. (2005). Liposomal encapsulated anti-cancer drugs. *Anti-Cancer Drugs*, *16*(7), 691–707. https://doi.org/10.1097/01.cad.0000167902.53039.5a

Hörmann, K., & Zimmer, A. (2016). Drug delivery and drug targeting with parenteral lipid nanoemulsions—A review. *Journal of Controlled Release*, *223*, 85–98. https://doi.org/10.1016/j.jconrel.2015.12.016

Hua, S. (2015). Lipid-based nano-delivery systems for skin delivery of drugs and bioactives. *Frontiers in pharmacology*, *6*, 219. https://doi.org/10.3389/fphar.2015.00219

Iman, M., Huang, Z., Alavizadeh, S. H., Szoka Jr, F. C., & Jaafari, M. R. (2017). Biodistribution and *in vivo* antileishmanial activity of 1, 2-distigmasterylhemisuccinoyl-sn-glycero-3-phosphocholine liposome-intercalated Amphotericin B. *Antimicrobial Agents and Chemotherapy*, *61*(9), 10–1128. https://doi.org/10.1128/aac.02525-16

Isakov, N. (1988). Regulation of T-cell-derived protein kinase C activity by vitamin A derivatives. *Cellular Immunology*, *115*(2), 288–298. https://doi.org/10.1016/0008-8749(88)90182-7

Jaafari, M. R., Hatamipour, M., Alavizadeh, S. H., Abbasi, A., Saberi, Z., Rafati, S., ... & Khamesipour, A. (2019). Development of a topical liposomal formulation of Amphotericin B for the treatment of cutaneous leishmaniasis. *International journal for parasitology: drugs and drug resistance*, *11*, 156-165. https://doi.org/10.1016/j.ijpddr.2019.09.004

Jung, S. H., Lim, D. H., Jung, S. H., Lee, J. E., Jeong, K. S., Seong, H., & Shin, B. C. (2009). Amphotericin B-entrapping lipid nanoparticles and their *in vitro* and *in vivo* characteristics. *European Journal of Pharmaceutical Sciences*, *37*(3–4), 313–320. https://doi.org/10.1016/j.ejps.2009.02.021

Jurj, A., Braicu, C., Pop, L. A., Tomuleasa, C., Gherman, C. D., & Berindan-Neagoe, I. (2017). The new era of nanotechnology, an alternative to change cancer treatment. *Drug Design, Development and Therapy*, *11*, 2871–2890. https://doi.org/10.2147/DDDT.S142337

Kaur, I. P., Bhandari, R., Bhandari, S., & Kakkar, V. (2008). Potential of solid lipid nanoparticles in brain targeting. *Journal of Controlled Release*, *127*(2), 97–109. https://doi.org/10.1016/j.jconrel.2007.12.018

Keservani, R.K., & Santos, J.S. (Eds.). (2025). *Novel Nanocarriers for Skin Diseases: Advances and Applications* (1st ed.). Apple Academic Press. https://doi.org/10.1201/9781032725956

Kohno, S., Otsubo, T., Tanaka, E., Maruyama, K., & Hara, K. (1997). Amphotericin B encapsulated in polyethylene glycol-immunoliposomes for infectious diseases. *Advanced Drug Delivery Reviews*, *24*(2–3), 325–329. https://doi.org/10.1016/S0169-409X(96)00474-7

Kopeckova, K., Eckschlager, T., Sirc, J., Hobzova, R., Plch, J., Hrabeta, J., & Michalek, J. (2019). Nanodrugs used in cancer therapy. *Biomedical Papers*, *163*(2), 122–131. https://doi.org/10.5507/bp.2019.010

Lafleur, A., Daffis, S., Mowbray, C., & Arana, B. (2024). Immunotherapeutic strategies as potential treatment options for cutaneous leishmaniasis. *Vaccines*, *12*(10), 1179. https://doi.org/10.3390/vaccines12101179

Lanza, J. S., Pomel, S., Loiseau, P. M., & Frézard, F. (2019). Recent advances in Amphotericin B delivery strategies for the treatment of leishmaniases. *Expert opinion on drug delivery*, *16*(10), 1063–1079. https://doi.org/10.1080/17425247.2019.1659243

Lavudi, K., Nuguri, S. M., Olverson, Z., Dhanabalan, A. K., Patnaik, S., & Kokkanti, R. R. (2023). Targeting the retinoic acid signaling pathway as a modern precision therapy against cancers. *Frontiers in Cell and Developmental Biology*, *11*, 1254612. https://doi.org/10.3389/fcell.2023.1254612

Lei, G. S., Zhang, C., Shao, S., Jung, H. W., Durant, P. J., & Lee, C. H. (2013). All-trans retinoic acid in combination with primaquine clears pneumocystis infection. *PLoS One*, *8*(1), e53479. https://doi.org/10.1371/journal.pone.0053479

Lemke, A., Kiderlen, A. F., & Kayser, O. (2005). Amphotericin B. *Applied Microbiology and Biotechnology*, *68*(2), 151–162. https://doi.org/10.1007/s00253-005-1955-9

Lipoldová, M., & Demant, P. (2006). Genetic susceptibility to infectious disease: lessons from mouse models of leishmaniasis. *Nature Reviews Genetics*, *7*(4), 294–305. https://doi.org/10.1038/nrg1832

Liu, P., Chen, G., & Zhang, J. (2022). A review of liposomes as a drug delivery system: current status of approved products, regulatory environments, and future perspectives. *Molecules*, *27*(4), 1372. https://doi.org/10.3390/molecules27041372

López, L., Valencia, B., Alvarez, F., Ramos, A. P., Llanos-Cuentas, A., Echevarria, J., ... & Arana, B. (2022). A phase II multicenter randomized study to evaluate the safety and efficacy of combining thermotherapy and a short course of miltefosine for the treatment of uncomplicated cutaneous leishmaniasis in the New World. *PLoS Neglected Tropical Diseases*, *16*(3), e0010238. https://doi.org/10.1371/journal.pntd.0010238

López, L., Vélez, I., Asela, C., Cruz, C., Alves, F., Robledo, S., & Arana, B. (2018). A phase II study to evaluate the safety and efficacy of topical 3% amphotericin B cream (Anfoleish) for the treatment of uncomplicated cutaneous leishmaniasis in Colombia. *PLoS Neglected Tropical Diseases*, *12*(7), e0006653. https://doi.org/10.1371/journal.pntd.0006653

López-Carvajal, L., Cardona-Arias, J. A., Zapata-Cardona, M. I., Sánchez-Giraldo, V., & Vélez, I. D. (2016). Efficacy of cryotherapy for the treatment of cutaneous leishmaniasis: Meta-analyses of clinical trials. *BMC Infectious Diseases*, *16*(1), 1–11. https://doi.org/10.1186/s12879-016-1663-3

Luz, K. G., Succi, R. C. D. M., & Torres, E. (2001). Nível sérico da vitamina A em crianças portadoras de leishmaniose visceral. *Revista da Sociedade Brasileira de Medicina Tropical*, *34*, 381–384. https://doi.org/10.1590/s0037-86822001000400013

Machado, P. R., Ribeiro, C. S., França-Costa, J., Dourado, M. E., Trinconi, C. T., Yokoyama-Yasunaka, J. K., ... & Uliana, S. R. (2018). Tamoxifen and meglumine antimoniate combined therapy in cutaneous leishmaniasis patients: a randomised trial. *Tropical Medicine & International Health*, *23*(9), 936–942. https://doi.org/10.1111/tmi.13119

Maciel, B. L. L., Lacerda, H. G., Queiroz, J. W., Galvão, J., Pontes, N. N., Dimenstein, R., ... & Jerônimo, S. M. (2008). Association of nutritional status with the response to infection with *Leishmania chagasi*. *The American Journal of Tropical Medicine and Hygiene*, *79*(4), 591–598. https://doi.org/10.4269/ajtmh.2008.79.591

Maciel, B. L. L., Valverde, J. G., Rodrigues-Neto, J. F., Freire-Neto, F., Keesen, T. S. L., & Jeronimo, S. M. B. (2014). Dual Immune modulatory effect of vitamin a in human visceral leishmaniasis. *PLoS One*, *9*(9). https://doi.org/10.1371/journal.pone.0107564

Madusanka, R. K., Silva, H., & Karunaweera, N. D. (2022). Treatment of cutaneous leishmaniasis and insights into species-specific responses: A narrative review. *Infectious Diseases and Therapy*, *11*(2), 695–711. https://doi.org/10.1007/s40121-022-00602-2

Mahor, H., Mukherjee, A., Sarkar, A., & Saha, B. (2023). Anti-leishmanial therapy: Caught between drugs and immune targets. *Experimental Parasitology*, *245*(December 2022). https://doi.org/10.1016/j.exppara.2022.108441

Malli, S., Pomel, S., Ayadi, Y., Deloménie, C., Da Costa, A., Loiseau, P. M., & Bouchemal, K. (2019). Topically applied chitosan-coated Poly(isobutylcyanoacrylate) nanoparticles are active against cutaneous leishmaniasis by accelerating lesion healing and reducing the parasitic load. *ACS Applied Bio Materials*, *2*(6), 2573–2586. https://doi.org/10.1021/acsabm.9b00263

Mansur-Alves, I., Lima, B. L. F., Santos, T. T., Araújo, N. F., Frézard, F., Islam, A., ... & Aguiar, M. M. (2022). Cholesterol improves stability of Amphotericin B nanoemulsion: Promising use in the treatment of cutaneous leishmaniasis. *Nanomedicine*, *17*(18), 1237–1251. https://doi.org/10.2217/nnm-2021-0489

Marques Borges, G. S., Oliveira Ferencs, M. D., Mello Gomide Loures, C. D., Abdel-Salam, M. A., Gontijo Evangelista, F. C., Sales, C. C., ... & Miranda Ferreira, L. A. (2020). Novel self-nanoemulsifying drug-delivery system enhances antileukemic properties of all-trans retinoic acid. *Nanomedicine*, *15*(15), 1471–1486. https://doi.org/10.2217/nnm-2020-0061

Marques Borges, G. S., Santos, T. T., Pinto, C. M., Frézard, F., Blanco, V. F., Ondei, R., ... & Castro Goulart, G. A. (2024). Distearoyl phosphatidylglycerol and dioleoyl phosphatidylglycerol increase the retention and reduce the toxicity of Amphotericin B-loaded in nanoemulsions. *Nanomedicine*, *19*(5), 383–396. https://doi.org/10.2217/nnm-2023-0256

Maspi, N., Abdoli, A., & Ghaffarifar, F. (2016). Pro- and anti-inflammatory cytokines in cutaneous leishmaniasis: a review. *Pathogens and Global Health*, *110*(6), 247–260. https://doi.org/10.1080/20477724.2016.1232042

Mastroianni, A. (2004). Liposomal amphotericin B and rHuGM-CSF for treatment of visceral leishmaniasis in AIDS. *Infez med*, *12*(3), 197–204.

Milton Harris, J., Martin, N. E., & Modi, M. (2001). Pegylation: A novel process for modifying pharmacokinetics. *Clinical Pharmacokinetics*, *40*(7), 539–551. https://doi.org/10.2165/00003088-200140070-00005

Monteiro, M. J. D. S. D., Silva, M. N. P. D., Paiva, A. D. A., Marreiro, D. D. N., Luzia, L. A., Henriques, G. S., ... & Costa, D. L. (2021). Nutritional status and vitamin A and zinc levels in patients with kala-azar in Piauí, Brazil. *Revista da Sociedade Brasileira de Medicina Tropical*, *54*, e0800-2020. https://doi.org/10.1590/0037-8682-0800-2020

Mueller, M., Ritmeijer, K., Balasegaram, M., Koummuki, Y., Santana, M. R., & Davidson, R. (2007). Unresponsiveness to AmBisome in some Sudanese patients with

kala-azar. *Transactions of the Royal Society of Tropical Medicine and Hygiene*, *101*(1), 19–24. https://doi.org/10.1016/j.trstmh.2006.02.005

Mukhopadhyay, R., & Madhubala, R. (1994). Effect of antioxidants on the growth and polyamine levels of *Leishmania donovani*. *Biochemical Pharmacology*, *47*(4), 611–615. https://doi.org/10.1016/0006-2952(94)90122-8

Müller, R. H., Schmidt, S., Buttle, I., Akkar, A., Schmitt, J., & Brömer, S. (2004). SolEmuls® - Novel technology for the formulation of i.v. emulsions with poorly soluble drugs. *International Journal of Pharmaceutics*, *269*(2), 293–302. https://doi.org/10.1016/j.ijpharm.2003.09.019

Murray, H. W., Montelibano, C., Peterson, R., & Sypek, J. P. (2000). Interleukin-12 regulates the response to chemotherapy in experimental visceral leishmaniasis. *The Journal of Infectious Diseases*, *182*(5), 1497–1502. https://doi.org/10.1086/315890

Musa, A. M., Mbui, J., Mohammed, R., Olobo, J., Ritmeijer, K., Alcoba, G., ... & Alves, F. (2023). Paromomycin and miltefosine combination as an alternative to treat patients with visceral leishmaniasis in eastern Africa: A randomized, controlled, multicountry trial. *Clinical Infectious Diseases*, *76*(3), e1177–e1185. https://doi.org/10.1093/cid/ciac643

Musa, A., Khalil, E., Hailu, A., Olobo, J., Balasegaram, M., Omollo, R., ... & Wasunna, M. (2012). Sodium stibogluconate (SSG) & paromomycin combination compared to SSG for visceral leishmaniasis in East Africa: a randomised controlled trial. *PLoS Neglected Tropical Diseases*, *6*(6), e1674. https://doi.org/10.1371/journal.pntd.0001674

National Institutes of Health (NIH). (2025). *Vitamin A and Carotenoids*. https://ods.od.nih.gov/factsheets/VitaminA-HealthProfessional/

National Nanotechnology Initiative (NNI). ([n.d.]). *About Nanotechnology*. https://www.nano.gov/about-nanotechnology

Nazarnezhad, S., Salehi, M., Samadian, H., Ehtermi, A., Kasaiyan, N., Khastar, H., ... & Ziaei, H. (2022). *In vitro* and *in vivo* evaluation of porous alginate hydrogel containing retinoic acid for skin wound healing applications. *Journal of Bioactive and Compatible Polymers*, *37*(4), 332–342. https://doi.org/10.1177/08839115221104071

Nobbmann, U. (2018). *Zeta potential in salt solution (or any other ions)*. https://www.malvernpanalytical.com/en/learn/knowledge-center/insights/zeta-potential-in-salt-solution-or-any-other-ions

Norwegian Institute of Public Health/WHO Collaborating Centre for Drug Statistics Methodology (NIPH/WHO). ([n.d.]). Antiinfectives for systemic use – Antibiotics. Oslo, *NIPH/WHO*. https://atcddd.fhi.no/atc_ddd_index/?code=J02AA01&showdescription=yes

Oliveira, L. G., Souza-Testasicca, M. C., Ricotta, T. N. Q., Vago, J. P., Dos Santos, L. M., Crepaldi, F., ... & Fernandes, A. P. (2022). Temporary shutdown of ERK1/2 phosphorylation is associated with activation of adaptive immune cell responses and disease progression during *Leishmania amazonensis* infection in BALB/c mice. *Frontiers in Immunology*, *13*, 762080. https://doi.org/10.3389/fimmu.2022.762080

Osaka, K., Ritov, V. B., Bernardo, J. F., Branch, R. A., & Kagan, V. E. (1997). Amphotericin B protects cis-parinaric acid against peroxyl radical-induced oxidation: amphotericin B as an antioxidant. Antimicrobial agents and chemotherapy, 41(4), 743-747. https://doi.org/10.1128/aac.41.4.743

Otsubo, T., Maruyama, K., Maesaki, S., Miyazaki, Y., Tanaka, E., Takizawa, T., ... & Kohno, S. (1998). Long-circulating immunoliposomal Amphotericin B against invasive pulmonary aspergillosis in mice. *Antimicrobial Agents and Chemotherapy*, *42*(1), 40–44. https://doi.org/10.1128/aac.42.1.40

Ozpolat, B., Lopez-Berestein, G., Adamson, P., Fu, C. J., & Williams, A. H. (2003). Pharmacokinetics of intravenously administered liposomal all-trans-retinoic acid (ATRA) and orally administered ATRA in healthy volunteers. *J Pharm Pharm Sci*, *6*(2), 292-301.

Pan American Health Organization (PAHO). (2020). Interactive atlas of leishmaniasis in the Americas: Clinical aspects and differential diagnosis. Washington, D.C.: *PAHO*. https://doi.org/10.37774/9789275121900

Pan American Health Organization (PAHO). (2022). Guideline for the treatment of leishmaniasis in the Americas (2nd ed.). Washington, D.C.: *PAHO*. https://doi.org/10.37774/9789275125038

Pan American Health Organization (PAHO). (2024). Manual of procedures for leishmaniasis surveillance and control in the region of the Americas (2nd ed.). Washington, D.C.: *PAHO*. https://doi.org/10.37774/9789275127346

Pan American Health Organization/World Health Organization (PAHO/WHO). (2017). Plan of action to strengthen the surveillance and control of leishmaniasis in the Americas 2017–2022. Washington, D.C.: *PAHO/WHO*. https://iris.paho.org/bitstream/handle/10665.2/34147/PlanactionLeish20172022-eng.pdf?sequence=5

Pan American Health Organization/World Health Organization (PAHO/WHO). (2020). *Leishmaniasis*. Washington, D.C.: *PAHO/WHO*. https://www.paho.org/en/topics/leishmaniasis

Panagiotopoulos, A., Stavropoulos, P. G., Hasapi, V., Papakonstantinou, A. M., Petridis, A., & Katsambas, A. (2005). Treatment of cutaneous leishmaniasis with cryosurgery. *International Journal of Dermatology*, *44*(9), 749–752. https://doi.org/10.1111/j.1365-4632.2005.02628.x

Paz, S. (2024). The potential of climatic suitability indicator for *Leishmania* transmission modelling in Europe: insights and suggested directions. *The Lancet Regional Health - Europe*, *43*(July), 100995. https://doi.org/10.1016/j.lanepe.2024.100995

Pereira, W. F., Ribeiro-Gomes, F. L., Guillermo, L. V. C., Vellozo, N. S., Montalvão, F., DosReis, G. A., & Lopes, M. F. (2011). Myeloid-derived suppressor cells help protective immunity to *Leishmania major* infection despite suppressed T cell responses. *Journal of Leukocyte Biology*, *90*(6), 1191–1197. https://doi.org/10.1189/jlb.1110608

Perez, A. P., Altube, M. J., Schilrreff, P., Apezteguia, G., Celes, F. S., Zacchino, S., ... & Morilla, M. J. (2016). Topical Amphotericin B in ultradeformable liposomes: Formulation, skin penetration study, antifungal and antileishmanial activity *in vitro*. *Colloids and Surfaces B: Biointerfaces, 139*, 190–198. https://doi.org/10.1016/j.colsurfb.2015.12.003

Pharmacopeia, B. (2021). *Amphotericin*. Rockville: *Pharmacopeia* https://www.pharmacopoeia.com/bp-2021/monographs/amphotericin.html?date=2021-07-01&text=amphotericin

Pharmacopeia, U. S. (2023a). *General Chapter, ⟨1⟩ Injections and Implanted Drug Products (Parenterals)—Product Quality Tests*. Rockville: *Pharmacopeia*. https://doi.org/10.31003/USPNF_M98730_03_01

Pharmacopeia, U. S. (2023b). *General Chapter, ⟨729⟩ Globule Size Distribution in Lipid Injectable Emulsions*. Rockville: *Pharmacopeia*. https://doi.org/10.31003/USPNF_M99505_02_01

Pinart, M., Rueda, J. R., Romero, G. A., Pinzón-Flórez, C. E., Osorio-Arango, K., Maia-Elkhoury, A. N. S., ... & Tweed, J. A. (2020). Interventions for American cutaneous and mucocutaneous leishmaniasis. *Cochrane Database of Systematic Reviews*, (8). https://doi.org/10.1002/14651858.CD004834.pub3

Pippa, L. F., Marques, M. P., Silva, A. C. T. D., Vilar, F. C., de Haes, T. M., Fonseca, B. A. L. D., ... & Lanchote, V. L. (2021). Sensitive LC-MS/MS methods for Amphotericin

B analysis in cerebrospinal fluid, plasma, plasma ultrafiltrate, and urine: application to clinical pharmacokinetics. *Frontiers in Chemistry*, *9*, 782131. https://doi.org/10.3389/fchem.2021.782131

Pistoia, E. S., Cosio, T., Campione, E., Pica, F., Volpe, A., Marino, D., ... & Gaziano, R. (2022). All-trans retinoic acid effect on Candida albicans growth and biofilm formation. *Journal of Fungi*, *8*(10), 1049. https://doi.org/10.3390/jof8101049

Polcz, M. E., & Barbul, A. (2019). The role of vitamin A in wound healing. *Nutrition in Clinical Practice*, *34*(5), 695–700. https://doi.org/10.1002/ncp.10376

Prakash, S., & Kumar Rai, A. (2022). Retinoic acid increases the cellular cholesterol predominantly in a mTOR-independent manner. *Immunologic Research*, *70*(4), 530–536. https://doi.org/10.1007/s12026-022-09292-x

Prakash, S., & Rai, A. K. (2022). Retinoic acid increases cellular cholesterol in *Leishmania donovani*-infected macrophages in an mTOR-independent manner. *Microbiology Spectrum*, *10*(6). https://doi.org/10.1128/spectrum.02699-22

Prakash, S., & Rai, A. K. (2023). Retinoic acid shows direct parasiticidal activity by targeting ergosterol pathway in *Leishmania donovani*: a potential therapeutic advancement. *Journal of Biomolecular Structure and Dynamics*, *41*(23), 14473–14483. https://doi.org/10.1080/07391102.2023.2193983

Prakash, S., Saini, S., Kumari, S., Singh, B., Kureel, A. K., & Rai, A. K. (2022). Retinoic acid restores the levels of cellular cholesterol in *Leishmania donovani* infected macrophages by increasing npc1 and npc2 expressions. *Biochimie*, *198*, 23–32. https://doi.org/10.1016/j.biochi.2022.03.002

Purkait, B., Kumar, A., Nandi, N., Sardar, A. H., Das, S., Kumar, S., ... & Das, P. (2012). Mechanism of Amphotericin B resistance in clinical isolates of *Leishmania donovani*. *Antimicrobial Agents and Chemotherapy*, *56*(2), 1031–1041. https://doi.org/10.1128/AAC.00030-11

Rabienia, M., Mortazavidehkordi, N., Roudbari, Z., Daneshi, R., Abdollahi, A., Yousefian Langeroudi, M., ... & Farjadfar, A. (2024). Designing of a new multi-epitope vaccine against *Leishmania major* using Leish-F1 epitopes: An In-silico study. *PLoS One*, *19*(1), e0295495. https://doi.org/10.1371/journal.pone.0295495

Ramos, G. S., Vallejos, V. M., Borges, G. S., Almeida, R. M., Alves, I. M., Aguiar, M. M., ... & Frézard, F. (2022). Formulation of Amphotericin B in PEGylated liposomes for improved treatment of cutaneous leishmaniasis by parenteral and oral routes. *Pharmaceutics*, *14*(5), 989. https://doi.org/10.3390/pharmaceutics14050989

Registro Brasileiro de Ensaios Clínicos (ReBEC). (2020). RBR-4ypn69 PA GEL 0415: Open, randomized clinical trial of efficacy and safety of sequential use of a single dose of antimoniate and topical paromomycin gel compared to three intralesional applications of meglumine antimoniate in the treatment of cutaneous. https://ensaiosclinicos.gov.br/rg/RBR-4ypn69

Reguera, R. M., Pérez-Pertejo, Y., Gutiérrez-Corbo, C., Domínguez-Asenjo, B., Ordóñez, C., García-Estrada, C., ... & Balaña-Fouce, R. (2019). Current and promising novel drug candidates against visceral leishmaniasis. *Pure and Applied Chemistry*, *91*(8), 1385–1404. https://doi.org/10.1515/pac-2018-1102

Reigada, C., Valera-Vera, E. A., Sayé, M., Errasti, A. E., Avila, C. C., Miranda, M. R., & Pereira, C. A. (2017). Trypanocidal effect of isotretinoin through the inhibition of polyamine and amino acid transporters in *Trypanosoma cruzi*. *PLoS Neglected Tropical Diseases*, *11*(3), e0005472. https://doi.org/10.1371/journal.pntd.0005472

Research, D. B. M. (2024). *Global Liposomal Drugs Market Size, Share, and Trends Analysis Report – Industry Overview and Forecast to 2032*. https://www.databridgemarketresearch.com/reports/global-liposomal-drugs-market

Revvity Signals. (2024). ChemDraw (Version 23.1.2) [Computer software]. Revvity Signals. https://revvitysignals.com/products/research/chemdraw

Ritmeijer, K., Ter Horst, R., Chane, S., Aderie, E. M., Piening, T., Collin, S. M., Davidson, R. N., & Ritmeijer. (2011). Limited effectiveness of high-dose liposomal Amphotericin B (AmBisome) for treatment of visceral leishmaniasis in an ethiopian population with high HIV prevalence. *Clinical Infectious Diseases*, *53*(12). https://doi.org/10.1093/cid/cir674

Rivnay, B., Wakim, J., Avery, K., Petrochenko, P., Myung, J. H., Kozak, D., ... & Nivorozhkin, A. (2019). Critical process parameters in manufacturing of liposomal formulations of Amphotericin B. *International Journal of Pharmaceutics*, *565*, 447–457. https://doi.org/10.1016/j.ijpharm.2019.04.052

Roatt, B. M., de Oliveira Cardoso, J. M., De Brito, R. C. F., Coura-Vital, W., de Oliveira Aguiar-Soares, R. D., & Reis, A. B. (2020). Recent advances and new strategies on leishmaniasis treatment. *Applied Microbiology and Biotechnology*, *104*, 8965–8977. https://doi.org/10.1007/s00253-020-10856-w

Rogers, M., Kropf, P., Choi, B. S., Dillon, R., Podinovskaia, M., Bates, P., & Müller, I. (2009). Proteophosophoglycans regurgitated by *Leishmania*-infected sand flies target the L-arginine metabolism of host macrophages to promote parasite survival. *PLoS Pathogens*, *5*(8). https://doi.org/10.1371/journal.ppat.1000555

Romero, G. A. S., Costa, D. L., Costa, C. H. N., de Almeida, R. P., de Melo, E. V., de Carvalho, S. F. G., ... & Collaborative LVBrasil Group. (2017). Efficacy and safety of available treatments for visceral leishmaniasis in Brazil: a multicenter, randomized, open label trial. *PLoS Neglected Tropical Diseases*, *11*(6), e0005706. https://doi.org/10.1371/journal.pntd.0005706

Rossi, M., & Fasel, N. (2018). How to master the host immune system? *Leishmania* parasites have the solutions! *International Immunology*, *30*(3), 103–111. https://doi.org/10.1093/intimm/dxx075

Ruiz-Postigo, J. A., Jain, S., Madjou, S., Agua, J. F. V., Maia-Elkhoury, A. N., Valadas, S., ... & Beshah, A. (2023). Global leishmaniasis surveillance, 2022: assessing trends over the past 10 years/Surveillance mondiale de la leishmaniose, 2022: evaluation des tendances des 10 dernieres annees. *Weekly Epidemiological Record*, *98*(40), 471–488. https://www.who.int/publications/i/item/who-wer9840-471-487

Sadzuka, Y., Nakade, A., Hirama, R., Miyagishima, A., Nozawa, Y., Hirota, S., & Sonobe, T. (2002). Effects of mixed polyethyleneglycol modification on fixed aqueous layer thickness and antitumor activity of doxorubicin containing liposome. *International Journal of Pharmaceutics*, *238*(1–2), 171–180. https://doi.org/10.1016/S0378-5173(02)00075-3

Sala, M., Diab, R., Elaissari, A., & Fessi, H. (2018). Lipid nanocarriers as skin drug delivery systems: Properties, mechanisms of skin interactions and medical applications. *International journal of pharmaceutics*, *535*(1-2), 1-17. https://doi.org/10.1016/j.ijpharm.2017.10.046

Saleem, K., Khursheed, Z., Hano, C., Anjum, I., & Anjum, S. (2019). Applications of nanomaterials in leishmaniasis: A focus on recent advances and challenges. *Nanomaterials*, *9*(12), 1–18. https://doi.org/10.3390/nano9121749

Salmanpour, R., Razmavar, M. R., & Abtahi, N. (2006). Comparison of intralesional meglumine antimoniate, cryotherapy and their combination in the treatment of cutaneous leishmaniasis. *International Journal of Dermatology, 45*(9), 1115–1116. https://doi.org/10.1111/j.1365-4632.2006.02822.x

Salvioni, L., Rizzuto, M. A., Bertolini, J. A., Pandolfi, L., Colombo, M., & Prosperi, D. (2019). Thirty years of cancer nanomedicine: Success, frustration, and hope. *Cancers*, *11*(12). https://doi.org/10.3390/cancers11121855

Santiago, R. R., e Silva, K. G. D. H., dos Santos, N. D., Genre, J., de Oliveira Lione, V. F., Silva, A. L., ... & do Egito, E. S. T. (2018). Nanostructured lipid carriers containing Amphotericin B: Development, *in vitro* release assay, and storage stability. *Journal of*

Drug Delivery Science and Technology, *48*, 372-382. https://doi.org/10.1016/j.jddst.2018.10.003

Santos, D. C. M. D., de Souza, M. L. S., Teixeira, E. M., Alves, L. L., Vilela, J. M. C., Andrade, M., ... & Aguiar, M. M. G. (2018). A new nanoemulsion formulation improves antileishmanial activity and reduces toxicity of Amphotericin B. *Journal of Drug Targeting*, *26*(4), 357–364. https://doi.org/10.1080/1061186X.2017.1387787

Schettini, D. A., Ribeiro, R. R., Demicheli, C., Rocha, O. G. F., Melo, M. N., Michalick, M. S. M., & Frézard, F. (2006). Improved targeting of antimony to the bone marrow of dogs using liposomes of reduced size. *International Journal of Pharmaceutics*, *315*(1–2), 140–147. https://doi.org/10.1016/j.ijpharm.2006.01.048

Scorza, B. M., Carvalho, E. M., & Wilson, M. E. (2017). Cutaneous manifestations of human and murine leishmaniasis. *International Journal of Molecular Sciences*, *18*(6), 1296. https://doi.org/10.3390/ijms18061296

Serafim, C., Ferreira, I., Rijo, P., Pinheiro, L., Faustino, C., Calado, A., & Garcia-Rio, L. (2016). Lipoamino acid-based micelles as promising delivery vehicles for monomeric amphotericin B. *International Journal of Pharmaceutics*, *497*(1-2), 23-35. https://doi.org/10.1016/j.ijpharm.2015.11.034

Shankar, A. H., & Titus, R. G. (1995). T cell and non-T cell compartments can independently determine resistance to *Leishmania major*. *Journal of Experimental Medicine*, *181*(3), 845–855. https://doi.org/10.1084/jem.181.3.845

Srivastava, P., Prajapati, V. K., Rai, M., & Sundar, S. (2011). Unusual case of resistance to Amphotericin B in visceral leishmaniasis in a region in India where leishmaniasis is not endemic. *Journal of Clinical Microbiology*, *49*(8), 3088–3091. https://doi.org/10.1128/JCM.00173-11

Su, C., Yang, H., Sun, H., Fawcett, J. P., Sun, D., & Gu, J. (2018). Bioanalysis of free and liposomal amphotericin B in rat plasma using solid phase extraction and protein precipitation followed by LC-MS/MS. *Journal of Pharmaceutical and Biomedical Analysis*, *158*, 288-293. https://doi.org/10.1016/j.jpba.2018.06.014

Sundar, S., Rosenkaimer, F., Lesser, M. L., & Murray, H. W. (1995). Immunochemotherapy for a systemic intracellular infection: accelerated response using interferon-γ in visceral leishmaniasis. *Journal of Infectious Diseases*, *171*(4), 992–996. https://doi.org/10.1093/infdis/171.4.992

Thacker, S. G., McWilliams, I. L., Bonnet, B., Halie, L., Beaucage, S., Rachuri, S., ... & Verthelyi, D. (2020). CpG ODN D35 improves the response to abbreviated low-dose

pentavalent antimonial treatment in non-human primate model of cutaneous leishmaniasis. *PLoS Neglected Tropical Diseases*, *14*(2), e0008050. https://doi.org/10.1371/journal.pntd.0008050

Tomiotto-Pellissier, F., Bortoleti, B. T. D. S., Assolini, J. P., Gonçalves, M. D., Carloto, A. C. M., Miranda-Sapla, M. M., ... & Pavanelli, W. R. (2018). Macrophage polarization in leishmaniasis: broadening horizons. *Frontiers in Immunology*, *9*, 2529. https://doi.org/10.3389/fimmu.2018.02529

Torchilin, V. P. (2007). Micellar nanocarriers: pharmaceutical perspectives. *Pharmaceutical research*, *24*, 1-16. https://doi.org/10.1007/s11095-006-9132-0

Torrado, J. J., Espada, R., Ballesteros, M. P., & Torrado-Santiago, S. (2008). Amphotericin B formulations and drug targeting. *Journal of pharmaceutical sciences*, *97*(7), 2405-2425. https://doi.org/10.1002/jps.21179

Tuon, F. F., Dantas, L. R., de Souza, R. M., Ribeiro, V. S. T., & Amato, V. S. (2022). Liposomal drug delivery systems for the treatment of leishmaniasis. *Parasitology Research*, *121*(11), 3073–3082. https://doi.org/10.1007/s00436-022-07659-5

van Etten, E. W. M., Ten Kate, M. T., Stearne, L. E. T., & Bakker-Woudenberg, I. A. J. M. (1995a). Amphotericin B liposomes with prolonged circulation in blood: *In vitro* antifungal activity, toxicity, and efficacy in systemic candidiasis in leukopenic mice. *Antimicrobial Agents and Chemotherapy*, *39*(9), 1954–1958. https://doi.org/10.1128/AAC.39.9.1954

van Etten, E. W. M., van Vianen, W., Tijhuis, R. H. G., Storm, G., & Bakker-Woudenberg, I. A. J. M. (1995b). Sterically stabilized Amphotericin B-liposomes: toxicity and biodistribution in mice. *Journal of Controlled Release*, *37*(1–2), 123–129. https://doi.org/10.1016/0168-3659(95)00071-F

van Griensven, J., Dorlo, T. P., Diro, E., Costa, C., & Burza, S. (2024). The status of combination therapy for visceral leishmaniasis: an updated review. *The Lancet Infectious Diseases*, *24*(1), e36–e46. https://doi.org/10.1016/S1473-3099(23)00353-5

van Haute, D., Jiang, W., & Mudalige, T. (2019). Evaluation of size-based distribution of drug and excipient in Amphotericin B liposomal formulation. *International Journal of Pharmaceutics*, *569*, 118603. https://doi.org/10.1016/j.ijpharm.2019.118603

Vellozo, N. S., Pereira-Marques, S. T., Cabral-Piccin, M. P., Filardy, A. A., Ribeiro-Gomes, F. L., Rigoni, T. S., ... & Lopes, M. F. (2017). All-trans retinoic acid promotes an M1-to M2-phenotype shift and inhibits macrophage-mediated immunity to *Leishmania major*. *Frontiers in immunology*, *8*, 1560. https://doi.org/10.3389/fimmu.2017.01560

Verma, P., Kureel, A. K., Saini, S., Prakash, S., Kumari, S., Kottarath, S. K., ... & Rai, A. K. (2019). *Leishmania donovani* reduces the levels of retinoic acid–synthesizing enzymes in infected macrophages and favoring its own survival. *Parasitology research*, *118*, 63–71. https://doi.org/10.1007/s00436-018-6115-0

Voak, A. A., Harris, A., Qaiser, Z., Croft, S. L., & Seifert, K. (2017). Pharmacodynamics and biodistribution of single-dose liposomal Amphotericin b at different stages of experimental visceral leishmaniasis. *Antimicrobial Agents and Chemotherapy*, *61*(9). https://doi.org/10.1128/AAC.00497-17

Vogelsinger, H., Weiler, S., Djanani, A., Kountchev, J., Bellmann-Weiler, R., Wiedermann, C. J., & Bellmann, R. (2006). Amphotericin B tissue distribution in autopsy material after treatment with liposomal Amphotericin B and Amphotericin B colloidal dispersion. *Journal of Antimicrobial Chemotherapy*, *57*(6), 1153–1160. https://doi.org/10.1093/jac/dkl141

Volpedo, G., Pacheco-Fernandez, T., Holcomb, E. A., Cipriano, N., Cox, B., & Satoskar, A. R. (2021). Mechanisms of immunopathogenesis in cutaneous leishmaniasis and post kala-azar dermal leishmaniasis (PKDL). *Frontiers in Cellular and Infection Microbiology, 11*, 685296. https://doi.org/10.3389/fcimb.2021.685296

Vyas, S. P., & Gupta, S. (2006). Optimizing efficacy of amphotericin B through nanomodification. *International journal of nanomedicine*, *1*(4), 417-432. https://doi.org/10.2147/nano.2006.1.4.417

Vyas, S., & Gupta, S. (2006). Optimizing efficacy of Amphotericin B through nanomodification. *International Journal of Nanomedicine*, *1*, 417–432. https://doi.org/10.2147/nano.2006.1.4.417

Waghule, T., Saha, R. N., Alexander, A., & Singhvi, G. (2022). Tailoring the multi-functional properties of phospholipids for simple to complex self-assemblies. *Journal of Controlled Release*, *349*, 460-474. https://doi.org/10.1016/j.jconrel.2022.07.014

Wallace, T. L., Larson, J. L., Bazemore, S. A., Wilson, C. W., & Cossum, P. A. (2000). The nonclinical safety evaluation of the anticancer drug ATRAGEN®(Liposomal all-trans-retinoic acid). *International journal of toxicology*, *19*(1), 33-42. https://doi.org/10.1080/109158100225024

Wang, D., Zhang, W., Ju, J. X., Wang, L. J., Huang, R. Y., Xu, Y. F., ... & Qi, J. L. (2021). Gender differences in acute toxicity, toxicokinetic and tissue distribution of Amphotericin B liposomes in rats. *Toxicology Letters*, *338*, 78–84. https://doi.org/10.1016/j.toxlet.2020.12.004

Wijnant, G. J., Van Bocxlaer, K., Fortes Francisco, A., Yardley, V., Harris, A., Alavijeh, M., ... & Croft, S. L. (2018a). Local skin inflammation in cutaneous leishmaniasis as a source of variable pharmacokinetics and therapeutic efficacy of liposomal Amphotericin B. *Antimicrobial Agents and Chemotherapy*, *62*(10), 10–1128. https://doi.org/10.1128/AAC.00631-18

Wijnant, G. J., Van Bocxlaer, K., Yardley, V., Harris, A., Alavijeh, M., Silva-Pedrosa, R., ... & Croft, S. L. (2018b). Comparative efficacy, toxicity and biodistribution of the liposomal Amphotericin B formulations Fungisome® and AmBisome® in murine cutaneous leishmaniasis. *International Journal for Parasitology: Drugs and Drug Resistance*, *8*(2), 223–228. https://doi.org/10.1016/j.ijpddr.2018.04.001

Wijnant, G.-J., Van Bocxlaer, K., Yardley, V., Harris, A., Murdan, S., & Croft, S. L. (2018c). Relation between skin pharmacokinetics and efficacy in AmBisome treatment of murine cutaneous leishmaniasis. *Antimicrobial Agents and Chemotherapy*, *62*(3), 10–1128. https://doi.org/10.1128/aac.02009-17

Wilhelm, S., Tavares, A. J., Dai, Q., Ohta, S., Audet, J., Dvorak, H. F., & Chan, W. C. (2016). Analysis of nanoparticle delivery to tumours. *Nature Reviews Materials*, *1*(5), 1–12. https://doi.org/10.1038/natrevmats.2016.14

World Health Organization (WHO). (2009). *Vitamin A deficiency*. Geneva: *WHO*. https://www.who.int/data/nutrition/nlis/info/vitamin-a-deficiency

World Health Organization (WHO). (2020). Ending the neglect to attain the Sustainable Development Goals: a road map for neglected tropical diseases 2021–2030. In *Ending the neglect to attain the sustainable development goals: a road map for neglected tropical diseases 2021–2030*. Geneva: *WHO*.

World Health Organization (WHO). (2022). *WHO guideline for the treatment of visceral leishmaniasis in HIV co-infected patients in East Africa and South-East Asia*. Geneva: *WHO.*

World Health Organization (WHO). (2023a). *Determining discriminating concentrations of insecticides for monitoring resistance in sand flies: report of a multi-centre laboratory study and WHO expert consultations*. Geneva: *WHO.*

World Health Organization (WHO). (2023b). *Operational manual on leishmaniasis vector control, surveillance, monitoring and evaluation*. Geneva: *WHO.*

World Health Organization (WHO). (2023c). *WHO and Gilead Sciences extend collaborative agreement to enhance access to treatment for visceral leishmaniasis*. Geneva: *WHO.* https://www.who.int/news/item/26-01-2023-who-and-gilead-sciences-

extend-collaborative-agreement-to-enhance-access-to-treatment-for-visceral-leishmaniasis

World Health Organization (WHO). (2025). *Leishmaniasis*. Geneva: *WHO.* https://www.who.int/health-topics/leishmaniasis#tab=tab_1

Wu, D., Khan, F. A., Zhang, K., Pandupuspitasari, N. S., Negara, W., Guan, K., ... & Huang, C. (2024). Retinoic acid signaling in development and differentiation commitment and its regulatory topology. *Chemico-Biological Interactions*, *387*, 110773. https://doi.org/10.1016/j.cbi.2023.110773

Yu, Y. Q., Yang, X., Wu, X. F., & Fan, Y. B. (2021). Enhancing permeation of drug molecules across the skin via delivery in nanocarriers: novel strategies for effective transdermal applications. *Frontiers in bioengineering and biotechnology*, *9*, 646554. https://doi.org/10.3389/fbioe.2021.646554

Zhao, T., Liu, S., Zhang, R., Zhao, Z., Yu, H., Pu, L., ... & Han, L. (2022). Global burden of vitamin A deficiency in 204 countries and territories from 1990–2019. *Nutrients*, *14*(5), 950. https://doi.org/10.3390/nu14050950